Secondary Waste Form Development and Optimization—Cast Stone

SK Sundaram   C-W Chung
KE Parker   ML Kimura
ME Valenta   CA Burns
SG Pitman   W Um
J Chun   JH Westsik, Jr

July 2011

Pacific Northwest
NATIONAL LABORATORY

Proudly Operated by **Battelle** *Since 1965*

DISCLAIMER

This report was prepared as an account of work sponsored by an agency of the United States Government. Neither the United States Government nor any agency thereof, nor Battelle Memorial Institute, nor any of their employees, makes **any warranty, express or implied, or assumes any legal liability or responsibility for the accuracy, completeness, or usefulness of any information, apparatus, product, or process disclosed, or represents that its use would not infringe privately owned rights**. Reference herein to any specific commercial product, process, or service by trade name, trademark, manufacturer, or otherwise does not necessarily constitute or imply its endorsement, recommendation, or favoring by the United States Government or any agency thereof, or Battelle Memorial Institute. The views and opinions of authors expressed herein do not necessarily state or reflect those of the United States Government or any agency thereof.

Secondary Waste Form Development and Optimization— Cast Stone

SK Sundaram   C-W Chung
KE Parker   ML Kimura
ME Valenta   CA Burns
SG Pitman   W Um
J Chun   JH Westsik, Jr

July 2011

Pacific Northwest National Laboratory
Richland, Washington 99352

Executive Summary

Washington River Protection Solutions is considering the design and construction of a Solidification Treatment Unit (STU) for the Effluent Treatment Facility (ETF) at the Hanford Site. The ETF is a *Resource Conservation and Recovery Act*-permitted, multi-waste, treatment and storage unit that can accept dangerous, low-level, and mixed wastewaters for treatment. The STU needs to be operational by 2018 to receive secondary liquid wastes generated during operation of the Hanford Tank Waste Treatment and Immobilization Plant (WTP). The STU will provide the additional capacity needed for ETF to process the increased volume of secondary wastes expected to be produced by the WTP.

Pacific Northwest National Laboratory is conducting a secondary waste form screening program to support the evaluation and selection of waste forms to stabilize and solidify the liquid secondary waste stream from the WTP. The following monolith waste forms are being evaluated for immobilizing the secondary wastes: 1) Cast Stone; 2) DuraLith alkali aluminosilicate geopolymer; 3) Ceramicrete phosphate-bonded ceramic; and 4) THOR[®] fluidized bed steam reforming waste product encapsulated in geopolymer. This report documents work to further develop and characterize the Cast Stone waste form. Other reports will cover the development and characterization of the other three waste forms. Follow-on activities will address the mechanisms of radionuclide retention to support disposal-system performance assessments, and regulatory and waste acceptance testing to demonstrate the waste forms will meet requirements for disposal at the Hanford Integrated Disposal Facility.

Cast Stone (also called "Containerized Cast Stone") is a cementitious waste form that is essentially a mixture of Class F fly ash, Grade 100 or 120 blast furnace slag, and Type I/II Portland cement. CH2M Hill Hanford Group Inc. developed this waste form to solidify numerous waste streams, including secondary waste generated at the Hanford Site. The Cast Stone cementitious waste form is the current baseline for solidifying the liquid secondary wastes from the WTP. Pierce et al. (2010) demonstrated that the Cast Stone is a viable waste form for immobilizing WTP secondary wastes. This statement is based on the leachability of technetium-99 (^{99}Tc) as determined using draft U.S. Environmental Protection Agency (EPA) test methods examining contaminant diffusivity (Method 1315) and the impacts of solution pH (Method 1313) and liquid-to-solids ratio (Method 1316).[1]

The Cast Stone testing reported here focused on optimizing waste loading and evaluating the robustness of the waste form to waste stream variability. Because of the extensive work on the Cast Stone formulation and the similar Saltstone formulation used at the Savannah River Site for low-level tank waste immobilization, testing conducted as part of this current test plan relied on those previous testing studies and did not aim to optimize the dry-blend material components or mix ratios beyond what has already been accomplished.

---

[1] EPA. 2009. *Leaching Test (Liquid-Solid Partitioning as a Function of Extract pH) of Constituents in Solid Materials Using a Parallel Batch Extraction Test*. Draft EPA Method 1313, U.S. Environmental Protection Agency, Washington D.C.
EPA. 2009. *Mass Transfer Rates of Constituents in Monolith or Compacted Granular Materials Using a Semi-Dynamic Tank Leaching Test*. Draft EPA Method 1315, U.S. Environmental Protection Agency, Washington D.C.
EPA. 2009. *Leaching Test (Liquid-Solid Partitioning as a Function of Liquid to Solid Ratio) of Constituents in Solid Materials Using a Parallel Batch Extraction Test*. Draft EPA Method 1316, Washington D.C.

To optimize waste loading, a baseline secondary waste simulant composition was prepared at five different concentrations. Three additional waste compositions were defined to evaluate the robustness of the waste form to waste composition variability. Cast Stone specimens were then prepared using each of the eight simulants. After curing, the Cast Stone specimens were characterized for compressive strength, leachability, mineralogy, and pore structure. The workability of the Cast Stone was evaluated through rheology studies to characterize the stiffening and setting of Cast Stone mixtures.

The liquid secondary wastes to be treated are from the caustic scrubber at the end of the melter off-gas treatment process for low-activity waste within the WTP. These wastes are combined with evaporator condensates within the WTP pretreatment facility and then transferred to the ETF. The secondary waste simulants were developed from the G2 flow sheet model of the WTP process. The baseline simulant is the median composition for the duration of the WTP mission. Two additional simulants (S1 and S2)—one (S1) a high-nitrate, high-chloride and the other (S2) a low-nitrate, low-chloride simulant—were defined. The fourth simulant (S4) was a blended secondary baseline simulant plus 10% of a simulated low-activity waste melter-submerged bed scrubber effluent from the off-gas treatment process. Each of the simulants was prepared at 2 M sodium concentration. In addition, the baseline simulant was prepared at 4 M, 6 M, 8 M, and 10 M sodium concentration to investigate waste loading effects. The Cast Stone dry material mix is composed of 8-weight percent (wt%) Portland cement (Type I/II), 45-wt% fly ash (Class F), and 47-wt% blast furnace slag (Grade 100). The dry blend was mixed with the simulants at a water-to-solids ratio of approximately 4 parts solution to 10 parts dry materials on a weight basis. Nonradioactive samples were prepared with rhenium as the technetium surrogate for compressive strength testing and other characterization. Similar ^{99}Tc-spiked simulants were mixed with the same Cast Stone dry blend to form cylindrical monoliths of the same dimensions for leachability testing. Though the plan was to mix the waste simulants directly with the dry materials, deionized water was also added such that the adjusted sodium concentrations ranged from 0.52 M to 2.1 M rather than 2 M to 10 M. For 6-M, 8-M, and 10-M simulants, more water was added to improve the workability of the Cast Stone during mixing. The Cast Stone/waste simulant mix was poured into 2-in. × 4-in. cylinders and cured for 28 days before testing.

Average compressive strengths of the cured Cast Stone were in the range of 1330 to 2240 psi, well above the 500 psi (3.45 MPa) minimum expected for cement-based waste forms. There were no significant trends in the compressive strength with changes in simulant composition or concentration.

Leaching of ^{99}Tc from the Cast Stone was evaluated using the EPA Draft Method *Mass Transfer Rates of Constituents in Monolith or Compacted Granular Materials Using a Semi-Dynamic Tank Leaching Test*.[1] This test is similar to the American National Standards Institute/American Nuclear Society (ANSI/ANS) 16.1 method but is conducted for 63 days rather than 90 days. Diffusivities for ^{99}Tc typically decreased several orders of magnitude over the first 2 weeks of the test and then stabilized for the duration of the testing. From 14 to 63 days, the ^{99}Tc diffusivities were less than 2.3×10^{-11} cm^2/s for the Cast Stone prepared with the 2-M and 4-M baseline (S1), S2, and S3 simulants. Most of the leachate concentrations were below analytical detection limits, so the calculated diffusivities were less-than values. For Cast Stone prepared with the 6 M, 8 M, and 10 M sodium simulants, the ^{99}Tc diffusivity increased

---

[1] EPA. 2009. *Mass Transfer Rates of Constituents in Monolith or Compacted Granular Materials Using a Semi-Dynamic Tank Leaching Test*. Draft EPA Method 1315, U.S. Environmental Protection Agency, Washington, D.C.

with increasing simulant concentration, ranging from 1.4×10^{-11} to 3.9×10^{-11} to 1.4×10^{-10} cm^2/s, respectively. The S4 Cast Stone had a diffusivity of 6.5×10^{-13} cm^2/s. These compare favorably with a target diffusivity of less than 1×10^{-9} cm^2/s.

To fully understand the chemistry effect and control the waste performance, the phase, microstructure, and pore-size distribution were characterized for the Cast Stone specimens. Three of the most notable phases—calcite, quartz, and ettringite—were observed in all the Cast Stone specimens. However, both calcite and quartz originated from the dry blend solids, so ettringite can be considered as the main crystalline phase formed in the hydrated Cast Stone. Another notable phase observed in the XRD pattern was carbonated AFm phases. Hemicarbonate AFm (AFm$_{0.5C}$) and monocarbonate AFm (AFM$_C$) were observed in the hydrated Cast Stone waste forms made with all secondary waste simulants. The XRD peak intensity of AFM$_C$ was very small but the XRD peak intensity of the AFm$_{0.5C}$ was quite noticeable in the Cast Stone solids made with simulants S1, S2, and S3. The Cast Stone made with simulant S4 exhibited a significantly decreased XRD intensity peak for AFm$_{0.5C}$ and showed a more prominent nitrate-based AFm (AFm$_N$) XRD peak instead. The most characteristic features of SEM microstructural images of the Cast Stone samples were needle-like ettringite and hexagonal AFms. Ettringite and AFms were observed in the open area where these crystals had grown without any restrictions. Ettringite was observed to grow from the surfaces of AFm crystals and fly ash, easily recognized by its round shape in the background of the images. The microstructural images validate the earlier observations from XRD patterns that ettringite and AFms are the main hydration phases in Cast Stone.

Rheology, stiffening, and setting studies of the Cast Stone using undisturbed yield stress, dynamic yield stress, and ultrasonic wave reflection techniques show the Cast Stone has a workability range from less than 1 hour for the most concentrated baseline simulant at an adjusted sodium concentration of 2.1 M (10 M unadjusted) to 5 to 6 hours for the more dilute simulants.

Test results show the optimum waste loading is approximately 6-M sodium concentration (target), corresponding to 1.42-M corrected sodium concentration. This approximation is based on the workability range in addition to the general performance of Cast Stone. From a ^{99}Tc leachability perspective, the Cast Stone performance was very good over the entire range of simulant concentrations and composition studies. For Cast Stone prepared with the 6-M, 8-M, and 10-M sodium simulants, the ^{99}Tc diffusivity increased with increasing simulant concentration, ranging from 1.4×10^{-11} to 3.9×10^{-11} to 1.4×10^{-10} cm^2/s, respectively, from 14 to 63 days. The S4 Cast Stone had a diffusivity of 6.5×10^{-13} cm^2/s. These compare favorably with a target diffusivity of less than 1×10^{-9} cm^2/s. From a processing perspective, the stiffening and setting studies showed that, before the 6-M sodium region, the lower sloping region is about 300 minutes (6 hours). Beyond 6 M sodium, workability becomes a practical issue, probably providing less than an hour of working time. Ideally, at least an hour of work time is needed to facilitate full-scale production. Although not tested, adding a superplasticizer may also help attain the workability window without lowering the waste loading.

With ^{99}Tc diffusivities below 2×10^{-10} cm^2/s at an adjusted sodium concentration in the waste at 2 M, there is the potential to increase the sodium concentration above the currently demonstrated range to 3 M to 5 M sodium for secondary waste blended with the dry materials without additional water. Testing at these concentrations will need to address both the leaching performance and the stiffening and setting behavior of the Cast Stone. These studies may include steps such as adding superplasticizers or set

retarders to improve the workability and reduce the pH of the waste stream to slow the hydration reactions.

The authors of this report have made several recommendations based on Phase 2 results. If Cast Stone is selected as the secondary waste form, these recommendations will be implemented in preparing the Cast Stone samples for Phase 3. Phase 3 will provide the results of product acceptance testing needed to support a final down-selection to a waste form for the secondary wastes. After a final waste form is selected, secondary waste form testing will be directed toward testing to support 1) a detailed design of the supplemental treatment unit for the ETF; 2) data collection to support risk assessments and long-term performance assessments; and 3) as appropriate, further optimization of the waste form to reduce costs and improve performance.

Acknowledgments

Acronyms and Abbreviations

AFm	calcium monosulfoaluminate
AFt	ettringite
ANS	American Nuclear Society
ANSI	American National Standards Institute
ASTM	ASTM International (formerly the American Society for Testing and Materials)
BET	Brunauer-Emmett-Teller (method)
BFS	blast furnace slag
BJH	Barrett, Joyner, and Halenda (method)
C_3A	tricalcium aluminate
C_4AF	tetracalcium aluminoferrite
CCS	containerized Cast Stone
COC	constituents of concern
C_2S	dicalcium silicate
C_3S	tricalcium silicate
C-S-H	calcium silicate hydrate
DIW	deionized water
DOE	U.S. Department of Energy
DLVO	Derjaguin-Landau-Verwey-Overbeek (theory)
EC	electrical conductivity
EDS	energy dispersive X-ray spectroscopy
Eh	oxidation-reduction potential
EPA	U.S. Environmental Protection Agency
EQL	estimated quantitation limit
ETF	Effluent Treatment Facility
EVA	Evaluation (graphics program)
HEPA	high-efficiency particulate air
HIPS	high impact polystyrene (polymer)
ICP	inductively coupled plasma
IDF	Integrated Disposal Facility
IS	impedance spectroscopy
LAW	low-activity waste
LI	leachability index
NIST	National Institute of Standards and Technology
NRC	U.S. Nuclear Regulatory Commission
OM	optical microscopy
PNNL	Pacific Northwest National Laboratory

PSD	particle-size distribution
RCRA	*Resource Conservation and Recovery Act*
RHA	rice husk ash
SBS	submerged bed scrubber
SEM	scanning electron microscopy
STU	Solidification Treatment Unit
TCLP	Toxicity Characteristic Leach Procedure
TEM	transmission electron microscopy
UWR	ultrasonic wave reflection
WAC	Washington State Administrative Code
WRPS	Washington River Protection Solutions
WTP	Hanford Tank Waste Treatment and Immobilization Plant
XRD	X-ray diffraction

Units of Measure

θ	angle of incidence (Bragg angle)
Å	angstrom (10^{-10} m or 10^{-1} nm)
°C	temperature in degrees Celsius [$T(°C) = T(K) - 273.15$]
cm	centimeter
g	gram
μ	micro (prefix, 10^{-6})
μm	micrometer
mS/cm	millisiemens per centimeter (electrical conductance)
M	molarity, mol/L
mL	milliliter
rpm	revolutions per minute
λ	wavelength
wt%	weight percent

Contents

Figures

Tables

1.0   Introduction

Washington River Protection Solutions (WRPS), a prime contractor to the U.S. Department of Energy (DOE), is responsible for the Effluent Treatment Facility (ETF) upgrades that need to be operational by 2018 to receive secondary liquid wastes from the Hanford Tank Waste Treatment and Immobilization Plant (WTP) at the Hanford Site. The WTP is being constructed for treating and immobilizing radioactive waste currently stored in underground tanks onsite. Wastes retrieved from the tanks will be separated into a low-volume, high-level waste stream and a large-volume, low-activity waste (LAW) stream. Both streams will be vitrified into glass waste forms for disposal. Secondary wastes, including routine solid wastes and liquid process effluents, will be generated during the separations and vitrification processes. The liquid wastes will be transferred to the ETF for treatment and solidification before disposal at the onsite Integrated Disposal Facility (IDF). Technetium-99 (^{99}Tc), a long-lived fission product, presents a challenge in managing these tank wastes. In the thermal processes used to convert radioactive tank wastes to a glass waste form, much of the ^{99}Tc volatilizes in the high temperatures of the glass melters and is collected in off-gas scrubber systems within the vitrification plants. Although the off-gas scrubber solutions containing the ^{99}Tc are recycled back to the melters, some technetium ultimately leaves the vitrification facilities as a secondary waste stream to the ETF. A performance assessment (PA) of the IDF will benefit from a high retention of constituents of concern (COCs) in the solidified secondary liquid waste. To this end, areas related to the capability of the solidified secondary waste form to retain COCs that need to be investigated are 1) changes to waste form composition (chemistry); 2) process conditions (e.g., temperature of the mixture, humidity during curing); and 3) impacts on other COCs on the release of key COCs. The ETF is a *Resource Conservation and Recovery Act* (RCRA) permitted multi-waste treatment and storage unit and can accept liquid secondary wastes (low-level and mixed waste waters) for treatment, treated effluent under the ETF State Wastewater Discharge Permit, and solidified liquid effluents under the Washington State Department of Ecology Dangerous Waste Permit.

A formal decision on which waste form(s) is preferred for solidifying the secondary liquid wastes, including agreement with the Washington State Department of Ecology, will be made by 2012. Pacific Northwest National Laboratory (PNNL) is conducting a secondary waste form testing program to support the evaluation and selection of waste forms for stabilizing and solidifying the liquid secondary waste stream from the WTP. This report summarizes the progress made in Phase 2 testing of Cast Stone as a robust waste form.

Cast Stone (also called "Containerized Cast Stone" [CCS]) is a cementitious waste form that is essentially a mixture of Class F fly ash, Grade 100 or 120 blast furnace slag (BFS), and Type I and II Portland cement. CH2M Hill Hanford Group, Inc. developed this waste form to solidify numerous waste streams, including secondary waste generated at the Hanford Site. Several reports[1] (Lockrem 2005; Lockrem et al. 2003, 2008; Cooke and Lockrem 2005; Cooke et al. 2003, 2006a, 2006b, 2006c, 2006d, 2009; Duncan et al. 2009; Duncan and Burke 2008; Clark et al. 2005, 2006) exist on this topic. After

---

[1] Aromi ES and KD Boomer. 2003. Memo to RJ Schepens (DOE Office of River Protection) from ES Aromi and KD Boomer (CH2M Hill Hanford Group, Inc.), "The Application of the Incidental Waste Requirements to Cast Stone & Steam Reforming," CH2M-0302577, dated July 14, 2003, Richland, Washington.
Aromi ES and RE Raymond. 2009. Memo to RJ Schepens (DOE Office of River Protection) from ES Aromi and KD Boomer (CH2M Hill Hanford Group, Inc.), "Final Test Reports for Bulk Vitrification & Cast Stone Technologies Demonstrations for Treatment & Disposal of K Basin Sludge," CH2M-0304811, dated December 22, 2009, Richland, Washington.

conducting screening tests on four different formulations, two of the formulations were selected by CH2M Hill Hanford Group, Inc. for further testing as shown in Table 1.1. A picture of a Cast Stone monolith is shown in Figure 1.1.

Table 1.1. Dry Reagent Compositions Used in CCS (Cooke et al. 2003)

Ingredient	DRF2 (wt %)	DRF4 (wt %)
Portland cement, Type I, II[a]	8	20
Fly ash, Class F	45	66
BFS, Grade 100	47	--
Attapulgite clay	--	14

(a) Type I is a more general purpose Portland cement, whereas Type II is a general purpose Portland cement that has better sulfate resistance. Hence, the properties of these two cements are not very different. If the cement conforms to both Type I and II, a cement vendor may designate its product as either Type I, Type II, or Type I/II depending on its commercial purpose. Cast Stone is produced using cement conforming to both Type I and II; therefore, either Type I or II can be used to produce Cast Stone.

Figure 1.1. A Cast Stone Monolith (Cooke et al. 2009; Pierce et al. 2010a)

The formulations shown in Table 1.1 were tested by CH2M Hill Hanford Group, Inc. with a LAW simulant at waste loadings of 8.2 to 24.2% (by weight); results are discussed in Lockrem et al. (2008). The results demonstrate that Cast Stone made from a DRF2 mix met both the U.S. Nuclear Regulatory Commission (NRC 1991) and the *Washington State Administrative Code*, "Land Disposal" (WAC 173-303-140) regulatory requirements. As a result of the testing, the DRF2 formulation was recommended for the Containerized Cast Stone (Cooke et al. 2003).

In addition, Cast Stone has also been tested with various getters (inorganic materials that selectively adsorb radionuclides and hazardous contaminants) as a waste form for treating the Basin 43 waste stream of the Liquid Effluent Retention Facility concentrated to achieve 28.9% solids (Duncan et al. 2008; Cooke et al. 2009). Getters can be used to immobilize permanently as well as just retard contaminant release. Getters interact both physically and chemically with the encapsulating matrix and COCs in the

liquid waste stream. Studies by Lockrem et al. (2005) and Cooke et al. (2009) have demonstrated that including BFS as an integral component as well as a getter in the Cast Stone does not degrade the performance of this cement- and fly ash-based waste form. Bone char, bone ash, bone black, synthetic apatites, iron powder, iron phosphate, tin apatites, and two ion-exchange resins (Cooke et al. 2009; Lockrem 2005b) are some examples of getters that have been tested (see also Harbour et al. 2004). Typically, each getter is added to the solid mix (at about 10% by mass). In the case of tin apatite, only 1% by mass of tin apatite, previously loaded with technetium, was incorporated into the mix. The resins and tin apatite have shown the best ANSI/ANS-16.1-2003 leach performance with oxidation reduction potential adjustment. The highest leach index (LI = 12.7) has been obtained by tin(II)apatite reacting with the pertechnetate and then incorporating the mixture into the cementitious waste form. In addition, getters can also be deployed in near-field barriers of repositories to adsorb and attenuate the release of any long-lived radionuclides (Mattigod et al. 2003; Pierce et al. 2010).

1.1 Summary of Phase 1 Activities and Results

The Cast Stone cementitious waste form is the current baseline for solidifying the liquid secondary wastes from WTP. A literature survey has identified other noncementitious materials as candidate alternative waste forms: DuraLith alkali-alumino-silicate geopolymer, Fluidized Bed Steam Reforming granular product encapsulated in a geopolymer matrix, and Ceramicrete phosphate-bonded ceramics. These alternative waste forms have met waste disposal acceptance criteria, including compressive strength and universal treatment standards for RCRA metals (as measured by the U.S. Environmental Protection Agency [EPA] *Toxicity Characteristic Leaching Procedure* [EPA 1992]), making them acceptable for land disposal. Some formulation issues remain unresolved, and optimization of composition versus performance has not yet been tested.

Pierce et al. (2010a) summarized the Phase 1 project results of screening tests on cementitious as well as one of the noncementitious waste forms (the DuraLith alkali-alumino-silicate geopolymers) for immobilizing secondary liquid wastes from the WTP. Ceramicrete phosphate-bonded ceramic and encapsulated fluidized bed steam reformed material were not available then for screening. In Phase 1, 50-mm -diameter $\times$ 100-mm-length cylindrical samples of the Cast Stone and DuraLith geopolymer materials were spiked with ^{99}Tc to better understand how the waste forms retained the COCs. The waste loading in both waste forms was at a prescribed 8 wt% solids on a dry basis using a simulant at 2 M sodium. The simulant composition was representative of the secondary liquid wastes to be treated and solidified in the ETF. Draft EPA leach test methods were used for the screening tests, including the following:

- EPA Draft Method 1313: *Leaching Test (Liquid-Solid Partitioning as a Function of Extract pH) of Constituents in Solid Materials Using a Parallel Batch Extraction Test* (EPA 2009a)

- EPA Draft Method 1315: *Mass Transfer Rates of Constituents in Monolith or Compacted Granular Materials Using a Semi-Dynamic Tank Leaching Test* (EPA 2009b)

- EPA Draft Method 1316: *Leaching Test (Liquid-Solid Partitioning as a Function of Liquid-to-Solid Ratio) of Constituents in Solid Materials Using a Parallel Batch Extraction Test* (EPA 2009c).

The results and major conclusions of the screening study are as follows:

- Cast Stone and DuraLith geopolymer would qualify as viable waste forms for solidifying the secondary liquid wastes to be treated in the ETF. The diffusivity range calculated for the release of technetium from Cast Stone as determined by EPA Draft Method 1315 (EPA 2009b) was 1.2×10^{-11} to 2.3×10^{-13} cm^2/s through the 63-day test. The diffusivity for technetium from the DuraLith geopolymer was in the range of 1.7×10^{-10} to 3.8×10^{-12} cm^2/s for the 63-day test. These values compare with a target of 1×10^{-9} cm^2/s or less. The DuraLith geopolymer continues to show some fabrication issues with the diffusivities, ranging from 1×10^{-9} to 2×10^{-13} cm^2/s for the better-performing batch to from 4×10^{-9} to 7×10^{-11} cm^2/s for the poorer-performing batch. However, throughout 49 days of immersion testing, the samples did not show the breakup into several smaller pieces observed for some DuraLith geopolymer samples in an earlier study of low-temperature immobilization technologies.

- In the EPA Draft Methods 1313 and 1316 on leach tests (EPA 2009a and 2009c), the Cast Stone and DuraLith geopolymers show similar leaching behavior. For both waste forms, the natural solution pH after soaking in deionized water (DIW) is approximately 12. The alkaline solutions that result from leaching Cast Stone and DuraLith suggest these waste forms may be suitable for a subsurface environment that has alkaline pore water, similar to the IDF in which leaching of the co-disposed immobilized low activity waste glass is expected to control the pH of the infiltrating water at a pH around 10 over geologic times.

- Based on the fractions leached, technetium, mercury, and arsenic are more leachable than sodium and potassium, which are more leachable than the waste form matrix materials silicon and aluminum. These results suggest the most leachable species reside predominantly in the pore water and that sodium and potassium, while partly in the pore water, are also bound within the structural matrix of the waste forms. As such, relatively high-fraction releases for the technetium from the crushed waste from samples would be expected because of the large surface area and exposed pores. In the intact monoliths, the releases would be much slower because of the tortuosity factor between interconnected pores, the lower porosity, and small pore throat sizes. Both materials are largely amorphous. The Cast Stone is >88 wt% amorphous with ettringite and calcite as the identified crystalline phases. The DuraLith is >70 wt% amorphous with quartz from the sand and fumed silica components as the identified crystalline phases.

- Dry materials (fly ash and BFS in the Cast Stone and silica fume in the DuraLith geopolymers) contain significant quantities of the hazardous RCRA metals, and for some COCs, dry materials are the largest contributor to the overall inventory.

In summary, the conclusions of the Phase 1 report identified Cast Stone as a worthy candidate waste form that needs to be further evaluated and optimized. Besides optimizing the composition of final Cast Stone formulation, the compatibility of various effective getter materials needs to be investigated to better understand and exploit this waste form. The reader is referred to Pierce et al. (2010a) for more details in the literature and all aspects of secondary waste forms, including getter selection criteria.

1.2 Objectives and Purpose

Laboratory testing to be performed at PNNL is being conducted to support the selection of a final waste form for immobilizing the WTP liquid secondary wastes under task 2 of *Waste Form Development and Optimization*. The objectives of the experimental work include the following:

1. Support down-selection to a final waste form for the WTP secondary liquid wastes to be treated in ETF

2. Begin testing to support long-term waste form performance evaluations

3. Support the conceptual design of the ETF solidification treatment unit.

During Phase 1, the Cast Stone cementitious waste form and DuraLith alkali alumino-silicate geopolymer were shown to be viable candidates for immobilizing the WTP secondary liquid wastes (Pierce et al. 2010). For consistency, the waste loading in both waste forms was at a single prescribed 8 wt% solids on a dry basis using a simulant at a 2-M sodium concentration. To support a final waste form selection, the Phase 2 testing focused on optimizing waste loading and evaluating the robustness of the waste form to waste variability. Activities that are being conducted on the selected waste forms include the following efforts:

- Optimize the quantities of binder materials to improve waste loading. This may include removing water to concentrate the secondary liquid wastes to be immobilized, thereby increasing the waste solids-to-binder ratio.

- Evaluate the robustness of the waste form to waste-stream composition variability.

  – Test waste forms using a range of simulants.

  – Identify key (most impactful) waste and binder parameters that impact waste loading.

  – Identify impacts of process upsets, such as variation in waste-to-binder ratios and dry binder materials ratios.

  – Impacts will be assessed in terms of waste form properties such as free liquids, cure time, flowability, compressive strength, and leach resistance.

  – Define formulation adjustment strategy.

- Examine other binder materials that may be less costly.

- Examine waste form porosity control during fabrication, including starting materials and starting material size.

- To date, the use of getter materials for secondary wastes has not been investigated beyond that inherent in the normal materials used in the solidification process (i.e., the BFS). Previous work by Lockrem (2005), Duncan et al. (2008), and Cooke et al. (2009) has investigated getters for other waste streams with Cast Stone.

Because of the extensive past research on the Cast Stone formulation (Lockrem 2005; Cooke et al. 2003, 2009; Lockrem et al. 2003, 2008; Cooke and Lockrem 2005; Cooke et al. 2006a, 2006b, 2006c, 2006d; Duncan et al. 2009; Duncan and Burke 2008; Clark et al. 2005, 2006) and the similar Saltstone formulation used at the Savannah River Site to immobilize low-level tank wastes (Orebaugh 1992; Harbour et al. 2006, 2007, 2009; Harbour and Aloy 2007; Harbour and Williams 2008; Dixon et al. 2008; Harbour and Edwards 2009), testing reported in this report relied on those previous works and did not include optimization of the dry blend material components or mix ratios beyond the research that has already been accomplished.

1.3   Report Content and Layout

Section 2.0 of this report describes the secondary waste simulants used in the Cast Stone development and optimization. Section 3.0 provides background information on cement chemistry and some of the dry materials used in preparing cements. In Section 4.0, the characteristics of the dry materials used in the Cast Stone testing are described. Section 5.0 describes the preparation of the Cast Stone specimens to be used for testing. Section 6.0 describes the waste form characterization methods and provides the results of the testing, including compressive strength; leachability using EPA Draft Methods 1313, 1315, and 1316 (EPA 2009a, 2009b, 2009c); phase assemblage and microstructure; and surface area and porosity. Section 7.0 presents the rheology of the Cast Stone as it is prepared and the results of ultrasonic wave reflection testing and impedance analysis to characterize Cast Stone as it cures. Section 8.0 provides conclusions and recommendations, and Section 9.0 lists the references cited in the report.

2.0 Secondary Waste Simulants Preparation and Characterization

This section describes the basis for the compositions of the secondary waste selected for the Cast Stone development and optimization and the preparation of the simulants used in the testing.

2.1 Target Compositions of Secondary Waste Simulants

Three simulant compositions (S1, S2, and S3) were used to represent the variability in the composition of the caustic scrubber secondary waste stream. The caustic scrubber is downstream of the primary LAW vitrification off-gas treatment system and is expected to capture volatile iodine and technetium not removed earlier in the process. Further, as part of the overall secondary off-gas treatment system, the caustic scrubber is downstream of the high-efficiency particulate air (HEPA) filters used for particulate removal, the carbon beds for mercury removal, and the selective catalytic reduction beds for oxidizing volatile organic compounds SO_x and carbon monoxide and for NO_x reduction. The caustic scrubber liquid effluents are returned to the pretreatment plant where they are combined with the pretreatment evaporator condensates and sent to the Liquid Effluent Retention Facility/ETF, becoming the source of the secondary wastes requiring treatment. In addition, this report used another (a fourth) simulant to represent the blended caustic scrubber/submerged bed scrubber (SBS)/wet electrostatic precipitator liquid waste stream.

The target compositions shown in Table 2.1 are adapted from an analysis of a G2 flow sheet model run (MRQ 09-0019 Scenario 5.0.22a). The compositions are based on the spreadsheet "Secondary Waste Expected Liquid Waste Composition, rev 1.xlsx" provided to PNNL by WRPS.[1] This spreadsheet provides estimates of the caustic scrubber composition for 241 monthly times. The projected compositions include 32 components (not counting sodium and ones that only had zero values), but only 11 of them plus sodium represent more than 99.9% of the nonaqueous molar content of the waste. These 11 components are OH^-, NO_3^-, Al, CO_3^{-2}, Cl^-, NO_2^-, PO_4^{-3}, SO_4^{-2}, Si, K, and F^-. Other components, such as RCRA metals and ^{99}Tc, are relevant to waste form performance and were included in the simulants. Before selecting the simulant compositions, the compositions for each of the 241 monthly times was charge balanced for the 11 components using sodium and then normalized to a constant sodium concentration (moles per mole Na).

The S1 simulant composition is the median composition (Table 2.1). The composition was developed by taking the monthly composition estimates from the G2 model over the 241 dates provided and determining the median value for each species over the data set provided. This yielded the concentrations for OH^-, NO_3^-, CO_3^{-2}, Cl^-, F^-, NO_2^-, PO_4^{-3}, SO_4^{-2}, Si, K, Al, and NH_4^+.

The RCRA metals, technetium, and iodine concentrations chosen were based on their maximum concentrations (moles per mole Na) over the 241 dates. In a few cases, it was still necessary to increase the concentrations of selected species to facilitate reasonable analytical detection limits in the testing.

---

[1]Josephson GB, GF Piepel, and JH Westsik, Jr. 2010. *Selection of Secondary Waste Test Compositions*. Pacific Northwest National Laboratory, Richland, Washington.

Table 2.1. Composition of WTP Secondary Waste Simulants Proposed for Phase 2 Testing

Constituent (mole/liter)	S1[a] Caustic Scrubber Median	S2[a] Statistical – Cluster 1 3/16/2038	S3[a] Statistical – Cluster 2 05/28/2024	S4[a] Caustic Scrubber /10% of SBS Blend	Phase 1 Simulant	Target Russell et al. (2006)
Na	1	1	1	1	2.0	2.0
Al(OH)$_3$	9.39E-02	1.14E-01	9.22E-02	4.24E-02	0.23	0.011
Si	1.88E-03	2.04E-03	7.74E-04	1.39E-02	-	-
K	5.82E-04	6.51E-04	2.18E-03	2.87E-02	-	-
NH$_4^+$ (total)	---	---	---	4.41E-01	-	-
OH$^-$	3.98E-01	3.98E-01	3.98E-01	1.02E-08	1.2	0.094
NO$_3^-$	3.28E-01	1.90E-01	3.97E-01	1.13E+00	0.69	0.018
CO$_3^{-2}$	2.28E-02	4.66E-02	3.94E-02	1.04E-02	1.5E-6	0.96
Cl$^-$	2.25E-02	2.17E-02	2.91E-02	1.04E-02	-	-
NO$_2^-$	1.20E-02	1.05E-02	3.83E-02	4.31E-02	-	-
PO$_4^{-3}$	6.87E-03	4.85E-03	6.03E-03	5.10E-03	1.7E-2	-
SO$_4^{-2}$	4.41E-03	5.81E-03	5.14E-03	4.36E-02	9.7E-3	-
F$^-$	5.57E-04	3.75E-04	4.42E-04	1.02E-08	-	-
Cr	2.03E-04	2.03E-04	2.03E-04	1.09E-03	8.43E-3	2.8E-04 (100x) [b]
Ag	6.27E-06	6.27E-06	6.27E-06	2.35E-05	2.5E-4 (100x) [b]	2.2E-04 (100x) [b]
As	3.48E-05	3.48E-05	3.48E-05	1.61E-05	-	-
Cd	1.57E-06	1.57E-06	1.57E-06	2.16E-05	5.0E-5 (100x) [b]	1.4E-05 (100x) [b]
Hg	1.13E-05	1.13E-05	1.13E-05	5.30E-06	3.3E-5 (1x) [b]	2.4E-06
Pb	8.99E-06	8.99E-06	8.99E-06	8.28E-06	7.9E-4 (100x) [b]	1.5E-04 (100x) [b]
Tc	1.81E-05	1.81E-05	1.81E-05	5.59E-04	7.7E-06	-
^{99}Tc (Ci/Liter)	3.05E-05	3.05E-05	3.05E-05	9.41E-04	1.3E-5 Ci/L	
Re	1.81E-05	1.81E-05	1.81E-05	5.59E-04	-	6.00E-07 (Re)
I	4.62E-06	4.62E-06	4.62E-06	6.29E-05	2.9E-6	2.90E-06
^{129}I (Ci/Liter)	9.53E-08	9.53E-08	9.53E-08	1.30E-06		
TOC (as oxalate)	9.39E-02	1.14E-01	9.22E-02	4.24E-02	0.23	0.18

(a) Simulant compositions shown at 1 M Na. Actual target compositions were in the range of 2 M to 10 M Na.
(b) Indicates increase in concentration above nominal concentration for analytical sensitivity.

The two "cluster" compositions (S2 and S3) are based on a statistical analysis of the same G2 model set after charge balancing and were normalized to a constant sodium concentration. In this case, seven dates and corresponding data points were removed as apparent outliers, and the analysis was conducted on the remaining 234 compositions. A cluster analysis of the data showed that the compositions appear to fall into one of two clusters. Two waste compositions were selected from the 234 "realistic" G2 model compositions, one from each cluster. The two representative clusters were selected to maximize the range in concentrations of nitrate plus chloride.

- Simulant S2 is from Cluster 1 and represents a low nitrate plus chloride concentration for that cluster. This is the 3/16/2038 projected composition in the G2 CS data set.

- Simulant S3 is from Cluster 2 and represents a high nitrate plus chloride concentration for that cluster. This is the 5/28/2024 projected composition in the G2 CS data set.

Because of the need to increase the analytical sensitivity for some of the RCRA metals (namely Ag, As, Cd, and Pb), the concentrations of these COCs were spiked at 10 to 100 times their maximum expected concentration. The concentration of Cr and Hg were not increased because the simulant concentration for these is sufficient to achieve the analytical sensitivity required to obtain quantitative information from these leach experiments. The same maximum RCRA metal concentrations were used for the three caustic scrubber simulants (S1, S2, and S3). One batch of simulant was prepared and used to make samples of the Cast Stone waste. The three caustic scrubber waste simulants were prepared by mixing 18 MΩ-cm DIW with reagent-grade chemicals.

The fourth simulant (S4) represents the caustic scrubber blended with a bleed stream from the SBS condensate tank, which will receive liquids from the low-activity waste melter SBS and wet electrostatic precipitator. For this simulant, it was assumed that 10% of the SBS recycle stream is purged to prevent a buildup of species, such as chlorides or sulfates. Table 2.1 shows the four simulants used for the Cast Stone testing. The table also shows the simulant used in the Phase 1 testing (Pierce et al. 2010b) as well as an earlier secondary waste simulant used in an earlier low-temperature immobilization study (Russell et al. 2006). Components that cannot be detected within the detection limits will be reported as "below the limit." The technetium concentrations used in each simulant were kept above 10^{-5} mole/liter regardless of the calculated target concentrations to facilitate detecting technetium in the leachates. All four simulants were analyzed using wet chemical analysis to verify how close they were to the target compositions.

2.2   Simulant Preparation

The simulants specified in Table 2.2 were identified by the recipe number, S1, S2, S3, or S4, and then the various concentrations used by the sodium concentration, such as -2 M, -4 M, etc. Table 2.2 shows the simulant test matrix for the Cast Stone testing. To prepare the five S1 simulants with different sodium concentrations, the recipe for S1-2 M was developed (see following paragraph), and then the amount of each chemical compound was increased proportionally to yield the specified sodium concentration.

Details on the chemical compounds used and order of dissolution for the simulant recipes are shown in Table 2.3 and Table 2.4. Anions and cations were paired to balance the ionic charges and help identify the most soluble chemical compounds that could be used to prepare the simulant solutions. Next, chemical compatibility was reviewed and the order of addition determined. To obtain the proper sodium concentrations, various sodium compounds were used. For example, sodium di-hydrogen orthophosphate was used in simulants S1 and S3, and sodium orthophosphate was used in simulant S2. In simulant S3, oxalate was added using two different compounds—oxalic acid and sodium oxalate—to obtain the correct oxalate and sodium concentration. When the mass of a chemical compound was less than 0.01 g, a concentrated stock solution was prepared, and aliquots of the stock solution were added to the simulant. After each chemical compound was added, the solution was stirred until the compound dissolved before adding another one. Table 2.3 shows the chemical compounds and the order in which they were added to prepare S1 simulant solutions at 2 M, 4 M, 6 M, 8 M, and 10 M Na. Table 2.4 shows the chemical compounds used to prepare simulants S2 and S3 at 2 M sodium. While preparing simulant solutions S1, S2, and S3, no precipitates were observed until the oxalate compounds were added. After adding 2 M sodium oxalate, simulant S1 remained cloudy even after mixing the solution overnight. Finally, gibbsite, a compound that is difficult to dissolve, was added to the cloudy simulants S1 through S3. Simulant solutions without precipitates were not required because the actual wastes can be expected to form

precipitates as they are concentrated and treated in the ETF. The simulant solutions were shaken vigorously before extracting the quantities of simulant needed for preparing the waste form specimens.

Table 2.2. Simulant Test Matrix

Nominal Sodium Concentration	S1 Median	S2 Cluster 1	S3 Cluster 2	S4 Caustic Scrubber/SBS Condensate Blend
2 M	X	X	X	X
4 M	X	-	-	-
6 M	X	-	-	-
8 M	X	-	-	-
10 M	X	-	-	-

Table 2.4 also shows the chemical compounds and the order in which they were added to prepare simulant solution S4. This simulant solution contains ammonia, which required modification of the recipe. To obtain the proper concentration of ammonia and sodium, some sodium compounds were replaced with ammonium compounds, such as ammonium nitrate, ammonium carbonate, and ammonium sulfate. No sodium hydroxide was added to simulant S4. When the sodium nitrate was added, the solution became slightly cloudy. It was mixed for ~1 hour, but the amount of cloudiness did not appear to change. The rest of the chemical compounds were added in the order specified, and the amount of cloudiness did not change until oxalate and gibbsite were added. The solution became very cloudy and looked like the other three simulant recipes. The cloudy simulant was used as such without filtering.

The technetium was obtained in two different solution matrices. For simulants S1, S2, and S3, the technetium, as pertechnetate, was in a potassium hydroxide matrix. For simulant S4, the technetium was in an ammonium hydroxide matrix. Aliquots of each simulant that were to include the technetium were obtained, and the technetium was added to the solutions as specified by the test plan.

The specific gravity for each of the eight simulants was measured and is shown in Table 2.5. As expected, the simulants with 2 M sodium had similar specific gravities. The waste loadings were calculated on a wet basis (since the technetium solution and the DIW were included in the total weight as in appropriate samples). As the sodium concentration in a given simulant increased, the specific gravity also increased.

Table 2.3. Chemical Makeup for Simulants S1 at 2M, 4M, 6M, 8M, and 10M Na

S1 Median Simulant	Chemical Compound	2 M	4 M	6 M	8 M	10 M
Sodium meta silicate	Na_2SiO_3	0.2285	0.4591	0.6894	0.9205	1.1491
Potassium nitrate	KNO_3	0.0587	0.118	0.1772	0.2365	0.2954
Sodium nitrate	$NaNO_3$	27.7917	55.586	83.3738	111.1672	138.9998
Silver nitrate	$AgNO_3$	0.0011[a]	0.0021[a]	0.0032[a]	0.0043[a]	0.0053[a]
Sodium monohydrogen orthoarsenate	$Na2HAsO_4 \cdot 7H2O$	0.0109[a]	0.0217[a]	0.0326[a]	0.0434[a]	0.0543[a]
Cadmium nitrate tetrahydrate	$Cd(NO_3)_2 \cdot 4H_2O$	0.0005[a]	0.0010[a]	0.0015[a]	0.0019[a]	0.0024[a]
Mercury (II) nitrate	$Hg(NO_3)_2 \cdot 1.5\ H_2O$	0.0040[a]	0.0079[a]	0.0119[a]	0.0159[a]	0.0199[a]
Lead nitrate	$Pb(NO_3)_2$	0.0030[a]	0.0060[a]	0.0089[a]	0.0119[a]	0.0149[a]
Sodium carbonate	$Na_2CO_3 \cdot H_2O$	0.5734	1.1421	1.7141	2.2848	2.8515
Sodium chloride	$NaCl$	1.3167	2.6296	3.9489	5.2598	6.5742
sodium nitrite	$NaNO_2$	0.8286	1.659	2.4865	3.3183	4.145
Sodium dihydrogen orthophosphate	$NaH_2PO_4 \cdot 6H_2O$	2.1568	4.3199	6.473	8.6313	10.7912
Sodium sulfate	Na_2SO_4	0.5835	1.1678	1.7507	2.3349	2.916
Sodium fluoride	NaF	0.0268	0.0498	0.0724	0.0954	0.1172
Sodium dichromate	$Na_2Cr_2O_7 \cdot 2H_2O$	0.0328	0.0608	0.0905	0.1217	0.1521
Sodium iodide	NaI	0.0007[a]	0.0014[a]	0.0021[a]	0.0028[a]	0.0035[a]
Sodium perrhenate	$NaReO_4$	0.0049[a]	0.0097[a]	0.0146[a]	0.0194[a]	0.0243
Sodium hydroxide	$NaOH$	15.9567	31.7868	47.7011	63.5076	79.4784
Sodium oxalate	$Na_2C_2O_4$	12.5838	25.1652	37.7458	50.3348	62.9129
Gibbsite	$Al(OH)_3$	7.3229	14.6491	21.9756	29.294	36.6166
Technetium in potassium hydroxide		1.7919[b]	3.5838[b]	5.3757[b]	7.1676[b]	8.9595[b]

(a) Added as a spike solution.
(b) In mg; added as a spike solution.

Table 2.4. Chemical Makeup for Simulants S2, S3, and S4 at 2M Na

	Chemical Compound	S2	S3	S4
Sodium meta silicate	Na_2SiO_3	0.2500	0.0957	1.7037
Potassium nitrate	KNO_3	0.0660	0.2207	2.9014
Ammonium nitrate	NH_4NO_3	—	—	26.5587
Sodium nitrate	$NaNO_3$	16.0639	33.5734	65.3621
Silver nitrate	$AgNO_3$	0.0011[a]	0.0011[a]	0.0040[a]
Sodium monohydrogen orthoarsenate	$Na_2HAsO_4 \cdot 7H_2O$	0.0109[a]	0.0109[a]	0.0050[a]
Cadmium nitrate tetrahydrate	$Cd(NO_3)_2 \cdot 4H_2O$	0.005[a]	0.005[a]	0.0067[a]
Mercury (II) nitrate	$Hg(NO_3)_2 \cdot 1.5\ H_2O$	0.0040[a]	0.0040[a]	0.0019[a]
Lead nitrate	$Pb(NO_3)_2$	0.0030[a]	0.0030[a]	0.0027[a]
Sodium carbonate	$Na_2CO_3 \cdot H_2O$	5.3194	—	—
Sodium bicarbonate	$NaHCO_3$	—	4.4971	—
Ammonium carbonate	$(NH_4)_2CO_3 \cdot H_2O$	—	—	1.1917
Sodium chloride	$NaCl$	1.2642	1.7012	0.6157
sodium nitrite	$NaNO_2$	0.726	2.6428	2.9710
Sodium dihydrogen orthophosphate	$NaH_2PO_4 \cdot 6H_2O$	—	1.8977	—
Sodium orthophosphate	$Na_3PO_4 \cdot 12\ H2O$	1.8472	—	1.9447
Sodium sulfate	Na_2SO_4	0.7683	0.6817	—
Ammonium sulfate	$(NH_4)_2SO_4$	—	—	5.7623
Sodium fluoride	NaF	0.0165	0.0184	—
Sodium dichromate	$Na_2Cr_2O_7 \cdot 2H_2O$	0.0316	0.0325	0.1630
Sodium iodide	NaI	0.0007[a]	0.0007[a]	0.0094[a]
Sodium perrhenate	$NaReO_4$	0.0049[a, b]	0.0049[a]	0.1520
Sodium hydroxide	$NaOH$	16.0106[b]	15.9398	—
Oxalic Acid	$H_2C_2O_4$	—	4.6110	—
Sodium oxalate	$Na_2C_2O_4$	15.2776	5.4962	5.6819
Gibbsite	$Al(OH)_3$	8.8925	7.1918	3.3138
Technetium in potassium hydroxide		1.7919[c]	1.7919[c]	—
Technetium in ammonium hydroxide		—	—	55.34[c]

(a) Added as a spike solution
(b) Sodium hydroxide was added before sodium perrhenate for simulant S2.
(c) In mg; added as a spike solution

Table 2.5. Simulant Specific Gravity

Simulant	Specific Gravity
S1-2 M	1.08
S1-4 M	1.17
S1-6 M	1.27
S1-8 M	1.34
S1-10 M	1.40
S2-2 M	1.09
S3-2 M	1.11
S4-2 M	1.13

3.0   Chemistry of Cementitious Materials

As background, this section describes some of the fundamentals of the chemistry of cement-based materials. Chemical formulae in the cement literature are often abbreviated using single letters for convenience. The abbreviations most widely used are $C = CaO$, $S = SiO_2$, $A = Al_2O_3$, $F = Fe_2O_3$, $M = MgO$, $K = K_2O$, $\bar{S} = SO_3$, $\bar{N} = Na_2O$, $H = H_2O$, $\bar{C} = CO_2$. Therefore, C_3S is used for $3CaO \cdot SiO_2$ (Ca_3SiO_5), C_2S is used for $2CaO \cdot SiO_2$ (Ca_2SiO_4), C_3A is used for $3CaO \cdot Al_2O_3$ ($Ca_3Al_2O_6$), and C_4AF is used for $4CaO \cdot Al_2O_3 \cdot Fe_2O_3$ ($Ca_4Al_2Fe_2O_{10}$).

Hydration of Cement Paste: Ordinary Portland cement consists of four main phases: tricalcium silicate (C_3S), dicalcium silicate (C_2S), tricalcium aluminate (C_3A), and tetracalcium aluminoferrite (C_4AF). Because the amount of C_3S is about 60% or higher, C_3S hydration is mainly affecting the behavior of Portland cement paste. Properties of the hydration products of Portland cement compounds are summarized in Table 3.1. Hydration stoichiometry is presented in Equation (3.1) (Mindess et al. 2003):

$$2C_3S + 11H \rightarrow C_3S_2H_8 \text{ (mostly described as C-S-H)} + 3CH \tag{3.1}$$
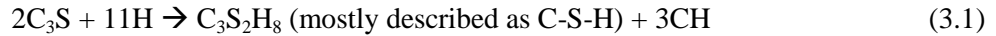
where C-S-H indicates poorly crystalline or amorphous calcium silicate hydrate of unspecified composition (Taylor 1997), and CH is calcium hydroxide. The calcium/silicate ratio typically varies around 1.5 ~ 2.0 in normal concrete.

Table 3.1. Summary of Properties of the Hydration Products of Portland Cement Compounds (Mindess et al. 2003)

Compound	Specific Gravity	Crystallinity	Morphology in Pastes	Typical Crystal Dimensions in Pastes	Resolved by
C-S-H	2.3-2.6 (depends on water content)	Very poor	Spines; unresolved morphology	1×0.1 μm (less than 0.01 μm thick)	SEM,[a] TEM[b]
CH	2.24	Very good	Nonporous striated material	0.01– 0.1 mm	OM,[c] SEM
Ettringite	~1.75	Good	Long slender prismatic needles	10×0.5 μm	OM, SEM
Monosulfo-aluminate	1.95	Fair-good	Thin hexagonal plates; irregular "rosettes"	$1 \times 1 \times 0.1$ μm	SEM

(a)   SEM = scanning electron microscopy
(b)   TEM = transmission electron microscopy
(c)   OM = optical microscopy

This reaction is often disregarded because the hydration of C_2S is very similar to the C_3S hydration, but slower. This reaction is because heat evolution of C_2S hydration is smaller than C_3S and the amount of C_2S phases in ordinary Portland cement is also smaller than the amount of C_3S. Hydration stoichiometry is given in Equation (3.2) (Mindess et al. 2003):

$$2C_2S + 9H \rightarrow C_3S_2H_8 + CH \tag{3.2}$$

To produce Portland cement, clinker is interground with a few percent of gypsum. The role of gypsum is to prevent the rapid hydration of C_3A by forming protective ettringite layers at the surface of C_3A, which hinders the dissolution rate of C_3A (Mindess et al. 2003). When gypsum is not present in the cement, flash set occurs by rapid AFm formation (C_4AH_{13}: hydroxyl AFm), which is an irrecoverable stiffening process of the mixture with a large evolution of heat due to rapid reaction of C_3A (Taylor 1997). The reaction stoichiometry causing flash set is given by Equation (3.3) (Mindess et al. 2003):

$$2C_3A + 21H \rightarrow C_4AH_{13} + C_2AH_8 \tag{3.3}$$

When gypsum is present, C_3A hydrates to form ettringite. The reaction stoichiometry of C_3A to form ettringite is shown in Equation (3.4) (Mindess et al. 2003):

$$C_3A + 3C\overline{S}H_2 + 26H \rightarrow C_6A\overline{S}_3H_{32} \text{ (ettringite, AFt)} \tag{3.4}$$

Normally, sulfate is consumed before the C_3A has completely hydrated. When gypsum is depleted, further C_3A hydration causes the pH to increase, and ettringite becomes unstable and transforms to calcium monosulfoaluminate. The reaction stoichiometry of calcium monosulfoaluminate formation is shown in Equation (3.5) (Mindess et al. 2003):

$$2C_3A + C_6A\overline{S}_3H_{32} + 4H \rightarrow 3C_4A\overline{S}H_{12} \text{ (calcium monosulfoaluminate, AFm)} \tag{3.5}$$
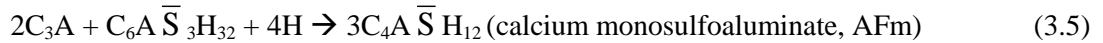
From this point, the diffusion barrier afforded by the ettringite is broken, and remaining C_3A reacts rapidly. In ordinary Portland cements, the molar ratio of $\overline{S}$ to C_3A ranges from 0.7 to 1.2, suggesting that the final hydration product will not be ettringite, but mainly calcium monosulfatoaluminate or some other form of AFm. The term AFm (Al_2O_3-Fe_2O_3-Mono) and AFt (Al_2O_3-Fe_2O_3-tri) indicates the composition of this phase. In this report, the terms "mono" and "tri" relate to the number of molecules in each phase (Taylor 1997). For example, C_4AH_{13} and $3C_4A\overline{S}H_{12}$ contain single hydroxide and sulfate, respectively, so it is referred to as mono. Because hydroxyl ion (OH-) is substituted in the phase structure, it is often referred to as hydroxyl AFm. Similarly, $3C_4A\overline{S}H_{12}$ is referred to as sulfate AFm because SO_4^{2-} ion is substituted in the phase structure. Many different anions can substitute for sulfate in AFm; the most important ones are OH^-, Cl^-, and CO_3^{2-}. Under favorable conditions, AFm forms hexagonal plates. Some AFm in Portland cement paste is of these types, but much is poorly crystalline and intimately mixed with C-S-H (Taylor 1997). However, $C_6A\overline{S}_3H_{32}$ contains three $\overline{S}$ in its structure, so it is referred to as trisulfate. AFt usually indicates ettringite because this is the most common phase in the cement.

C_4AF forms similar hydration products to C_3A, with or without gypsum (Mindess et al. 2003), and C_4AF hydrates much slower than C_3A; thus, it is less likely to cause flash set. In addition, gypsum retards C_4AF hydration much more significantly than it does to C_3A. Therefore, C_4AF hydration is less important than C_3A hydration with respect to stiffening and set.

Calcium Silicate Hydrate (C-S-H): Because of its amorphous character, compositional variability, and poorly resolved morphology, C-S-H is a very difficult material to study (Mindess et al. 2003). C-S-H makes up over one half of the volume of hydrated paste, and therefore it is the most important component. It is generally understood that C-S-H is the strongest material in concrete; thus, more production of C-S-H is always preferable.

During early hydration, C-S-H grows out from the particle surface into the surrounding water-filled space in the form of low-density thin sheets. Once hydration has become diffusion controlled, C-S-H forms primarily as a denser coating around the hydrating cement grains, referred to as either late or inner product. These coatings form the diffusion barrier during later hydration and thicken with time, growing inwards as well as outwards. The coatings maintain the shape of the original cement grains.

Calcium Hydroxide (CH): Unlike C-S-H, CH is a well crystallized material that has a distinctive hexagonal morphology. Unlike C-S-H, CH is crystallized in the pore solution during hydration. It occupies about 20 to 25% of the paste solid volume, so it also plays an important role. Normally, it provides the source of hydroxide to protect the stability of C-S-H in the cement paste. However, CH is not a strong material, so it does not contribute so much to the strength and durability of cement paste.

Ettringite and Monosulfoaluminate: These products are relatively minor constituents of hydrated cement paste, making up only 10 to 15% by solid volume. Considering that most of the hydration products consist of C-S-H and CH, these two phases play a relatively minor role in the microstructural development of hydrated cement paste. Ettringite has a sharp, needle-like microstructure, and monosulfoaluminate has hexagonal plates. These phases are metastable, which means that the phase can change according to surrounding conditions, especially with ingress of sulfates. The phase change from monosulfate (AFm) to trisulfate (AFt) occurs accordingly and generates the expansive forces, which is known to cause serious cracking in the paste (Taylor 1997; Mehta et al. 2006). The cause of expansion pressure is still in debate, but one of two hypotheses are generally agreed upon: 1) directly caused by the crystal growth of ettringite, or 2) swelling due to adsorption of water in alkaline environment by poorly crystalline ettringite.

Pozzalanic Reaction: A pure pozzolanic reaction can be represented as the consumption of CH by S to produce C-S-H. Such a conversion is done by adding amorphous or reactive silica in the cement paste as shown in Equation (3.6) (Mindess et al. 2003).

$$CH + S + H = C\text{-}S\text{-}H \tag{3.6}$$
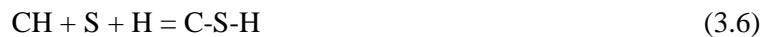
In a normal case, the composition of C-S-H is not very different from the composition of C-S-H from cement hydration. However, with very reactive pozzolans of high silica content (silica fume and rice husk ash [RHA]), the calcium/silicate ratio is significantly different, being close to 1.0, and the hydrogen silicate ratio is slightly lower. This indicates that a secondary pozzolanic reaction with C-S-H is occurring. Thus, the overall reaction can be written as Equation (3.7) (Mindess et al. 2003)

$$C_3S + 2S + 13.5H \rightarrow 3(CSH3.5) + 3CH \tag{3.7}$$

Small quantities of reactive alumina in a pozzolan generally substitute for silica as part of the C-S-H. When a pozzolan has appreciable quantities of reactive alumina (e.g., natural pozzolans or calcined clay-like metakaolin), a separate set of secondary reactions can occur, leading to the formation of calcium aluminate hydrates Equation (3.8) and Equation (3.9) (Mindess et al. 2003).

$$C\text{-}S\text{-}H + A \rightarrow C\text{-}A\text{-}S\text{-}H \tag{3.8}$$

$$CH + A + H \rightarrow C\text{-}A\text{-}H \tag{3.9}$$

The exact composition of calcium aluminate silicate hydrates or calcium aluminate hydrates depends on the particular pozzolan, such as C_2AH_8, C_2ASH_8, or monosulfoaluminate.

Since the pozzolanic reaction consumes physically weaker CH and produces physically stronger C-S-H, C-A-H, or C-A-S-H, pozzolanic materials are often incorporated into the concrete to improve strength and durability. Pozzolans include fly ash, silica fume, ground granulated BFS and other calcined natural pozzolanic materials, such as rice husk ash (RHA) and metakaolin (Mindess et al. 2003). All of these materials are waste by-products of industry (except metakaolin).

Fly Ash: The most typical pozzolanic material is fly ash. This is a glassy round-shaped by-product that is produced from burning coal in electricity-generating power plants. It is known that round-shape particles enhance the workability of the concrete mixtures. Fly ash particle sizes vary around a mean of 10~15 μm. According to ASTM C-618, the *Standard Specification for Coal Fly Ash and Raw or Calcined Natural Pozzolan for Use in Concrete*, by-product fly ashes are classified into C and F types. To be Class F, the sum of SiO_2, Al_2O_3, and Fe_2O_3 should be higher than 70%.

Typically, Class F is produced from bituminous or subbituminous coal, and Class C is produced from lignitic coal. Class C contains a higher level of calcium oxide, which corresponds quite well with the sum of other oxides. Many of these constituents are present in the glass fraction. Class F fly ash has a low CaO content around 3~5% (aluminosilicate glass) whereas Class C fly ash has a high CaO content around 20~30% (calcium aluminosilicate glass). Generally, the CaO content of 10% is understood as a guideline to distinguish between high-calcium and low-calcium fly ash. Although the ASTM International specifies to use total oxide contents to classify fly ashes, many researchers tend to use the term "high calcium" and "low calcium" fly ash rather than Class C and Class F fly ash (Mindess et al. 2003; Taylor 1997; Hewlett 1998; Mehta and Monteiro 2006). This is because they are completely different in the pozzolanic properties, depending on CaO content. If the amount of CaO in the fly ash is higher, the fly ash is going to hydrate, although it still has pozzolanic activity.

Silica Fume: Silica fume is one of the most powerful pozzolanic materials. It is an amorphous silica (90% or higher), a by-product in the manufacture of silicon metal and alloys. The mean particle size of silica fume is around 0.1 μm. Considering the particle sizes of cement (10~15 μm), the silica fume particles can effectively fill the empty space in between cement particles, which will eventually lead to a faster pozzolanic reaction. In addition, this smaller-sized, particle packing effect reduces bleeding, lowers the mean size of the capillary pores (Mindess et al. 2003), and therefore develops a better microstructure to provide higher durability and strength. Because of these properties, silica fume is used to produce high-strength concrete. Due to the higher surface area associated with the smaller particle-size distribution (PSD) of silica fume, concrete using silica fume is not workable, so a superplasticizer is used to obtain workability of the mixture.

Blast Furnace Slag: Slags are residues from metallurgical processes, either from producing metals from ore or refining impure metals. They are derived from lime-based inorganic fluxes used to extract impurities from metals, which solidify on cooling. The cooling rate determines the crystallinity of the slag (faster: amorphous; slower: crystalline). The slags used in concrete typically come from the blast furnace production of iron from ore. Steel-making slags (from the conversion of iron to steel) or those used to produce nickel or copper are rich in iron, so they are not used as additives in concrete. BFSs are rich in lime, silica, and alumina. Typical mass percentages are CaO = 35~45%, SiO_2 = 32~38%, Al_2O_3 = 8~16%, MgO = 5~15%, Fe_2O_3 < 2%, and sulfur = 1~2% (Mindess et al. 2003). Since the CaO

content is high, slag can hydrate in the presence of water. Slags are ground to achieve about the same particle size as cement (10~15 μm).

Rice Husk Ash: RHA is high in amorphous SiO_2 (90% or higher), and that makes it become a very reactive pozzolanic material. The microstructural characteristics of RHA are very different from that of silica fume. Because RHA maintains the original cellular structure of the rice husk, it contains a large amount of empty spaces. Such empty spaces lead to higher water demand, but the pore solution is allowed to access inside the husk structure, which is a place for CH crystallization. A large amount of such spaces promotes the pozzolanic reaction.

For this reason, RHA can be comparable or is even more strongly pozzolanic than the silica fume (Taylor 1997). Research regarding the preparation, properties, and applications of RHA to concrete has been extensively performed since the 1960s, but actual application of the RHA has been somewhat limited because the properties of RHA are greatly affected by its preparation. This includes burning conditions etc. and, more importantly, it demands a large amount of water in the concrete mix because of its high surface area. An acidic treatment on rice husk is known to enhance its pozzolanic activity by removing metallic ions in the husk structure (Salas et al. 2009).

Metakaolin: Metakaolin is produced from aluminosilicate clay, mainly kaolinite clay. Aluminosilicate clay is calcined under controlled temperature (700~900 ºC) for the transformation from kaolin to metakaolin. Such a process produces highly reactive pozzolanic material by removing water and by leaving an amorphous aluminosilicate with a high internal porosity that exhibits strong pozzolanic activity (Dunster et al. 1993; Badogiannis et al. 2005). This material is known to consume the highest amount of CH among other pozzolanic materials. The pozzolanic activity of metakaolin is often compared with that of silica fume, and it is known to be similar or higher than silica fume.

Cast Stone: Cast Stone is composed of cement, fly ash, and slag. The hydration of Cast Stone will therefore follow the significant characteristics of these materials as explained above. However, it should be noted that the current Cast Stone recipe uses 8% cement, 45% Class F fly ash, and 47% grade 100 slag by weight. Therefore, the effect of cement hydration is minimized, and the effect of fly ash and slag reaction is more dominant with Cast Stone. As mentioned above, the major reaction of the fly ash and slag in the cement rich paste is pozzolanic. Since the production of CH in Cast Stone is limited due to the smaller quantity of cement, the reaction by fly ash and slag should be enhanced by adding a high level of hydroxide on purpose. In case of Cast Stone, the high level of OH^- concentration is achieved by using the secondary waste solution.

4.0   Cast Stone Dry Materials Characterization

The Cast Stone dry materials include Portland cement (Type I/II), fly ash (Class F), and BFS (Type 100). This section describes the characteristics of the dry materials used in preparing the secondary waste Cast Stone specimens, including chemical composition, mineralogy, and particle-size distribution.

4.1   Dry Materials Chemical Composition and Mineralogy

The chemical compositions of cement, Class F fly ash, and grade 100 BFS are presented in Table 4.1. X-ray diffraction (XRD) patterns of raw materials are presented in Figure 4.1 to Figure 4.3. The phase compositions shown in Table 4.1 indicate the phase composition of typical Type I or II Portland cement.

The cement powder contained C_3S, C_2S, C_3A, and C_4AF (brownmillerite). Two forms of calcium sulfate, gypsum, and calcium sulfate hemihydrates (bassanite) were observed from the XRD pattern. Unless hemihydrates are incorporated on purpose to control the reactivity of C_3A, the presence of two different sulfate polymorphs indicates the grinding process elevated the temperature of the material within the mill so that gypsum was dehydrated to form the hemihydrate. Calcite was also observed in the XRD pattern. Calcite was recently added in the cement because the generation of CO_2 from the plant has been a serious issue for the cement industry. Therefore, some amount of cement is replaced with calcite. Although adding calcite to the cement is not known to be beneficial for the performance concrete, it was reported that calcite can be a site for nucleation of the hydration product (Taylor 1997) so that it does not hurt the general performance unless a significant amount is added.

XRD patterns of ASTM Class F fly ash are presented in Figure 4.2. Fly ash showed a broad amorphous band with many crystalline peaks, which is quite unlikely for normal Class F fly ash. The cooling process in the coal power plant from which this material was obtained seems not to be fast enough to prevent aluminosilicate phases from crystallizing. An interesting finding is that three main phases in cement, C_3S, C_3A, and C_4AF, were also observed in this fly ash. Although the phase composition of fly ash varies quite a bit, it is unusual to see these phases in Class F fly ash. Free lime, periclase, gypsum, anhydrite, and quartz were also observed. The presence of periclase is expected considering the amount of MgO shown in Table 2.2. However, the presence of gypsum, hemihydrates, and anhydrite is surprising because the SO_3 content in the fly ash is only 0.8%.

As shown from Table 2.2, the calcium oxide content of fly ash is 14.1%. When calculating the total oxide contents—excluding CaO, which is 71.4%—it is recognized that this fly ash barely passed the requirement of Class F fly ash (ASTM C-618), which is 70%. As discussed in Section 3.0, the CaO content of Class F fly ash is normally around 3~5%. The CaO content in this fly ash is considered rather high, so it is possible to hydrate in the presence of water. In addition, the differences between high (typically Class C fly ash) and low-calcium fly ash (typically Class F fly ash) can be detected by the shifting of the amorphous band in XRD patterns. The center of the amorphous band with this fly ash was observed at around 29°, which is characteristic of high-calcium fly ash (Class C fly ash) (Diamond 1986).

Table 4.1. Properties of Dry Materials Used to Produce Cast Stone

Chemical Analysis (wt %)	Cement	Fly ash	Slag
SiO_2	20.2	49.0	32.4
Al_2O_3	4.8	16.1	12.2
Fe_2O_3	3.4	6.2	0.9
CaO	64.0	14.1	43.4
$Na_2O^{(a)}$	0.5	4.24	0.88
K_2O [b]	-	-	-
MgO	0.8	4.6	4.9
$CaCO_3$	3.2	-	-
SO_3	2.7	0.8	4.9
Phase Composition			
C_3S	62.22	-	-
C_2S	10.98	-	-
C_3A	6.97	-	-
C_4AF	10.35	-	-
Specific Gravity (g/cm^3)	3.15	2.58	2.89
Specific Surface area (m^2/g)	1.05	-	0.515
Average Particle Size (μm)	19		
Color	Grey	Light brown	White

(a) Usually an equivalent content of Na_2O is used to represent the alkali contents in cement. An equivalent content of Na_2O can be calculated using the Na_2O content + 0.658 × K_2O content.

(b) The K_2O content is not specified from the manufacturer because it is already included in the equivalent Na_2O content.

XRD patterns of the Grade 100 BFS used in the Cast Stone waste form generation are presented in Figure 4.3. The slag shows a quite sharp amorphous band, centered at about 31°. The amorphous band is not as broad as that of fly ash, indicating the slag is more crystalline than fly ash. Slag also shows many crystalline phases, such as C_2S, calcite, quartz, gypsum, hemihydrates (bassanite), and anhydrite. With the presence of C_2S, the slag will hydrate as cement does, but at a slower rate. Calcite, gypsum, bassanite, and anhydrite were also observed. These are not commonly observed phases in slag, which indicates this slag was likely mixed and milled with limestone and gypsum at the time of production.
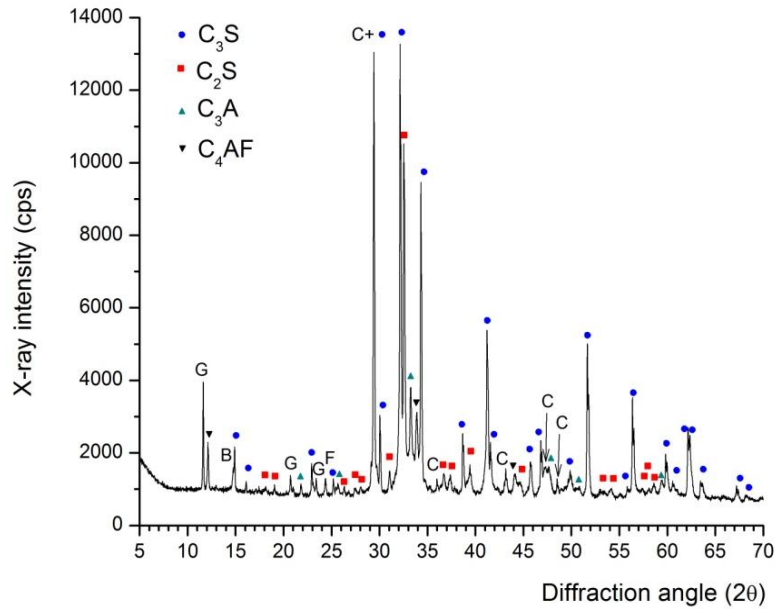
Figure 4.1. XRD Patterns of Unhydrated Type II Portland Cement. Note that B indicates calcium sulfate hemihydrates (bassanite), C indicates calcite, and G indicates gypsum. Also note that C_3S, C_2S, C_3A, and C_4AF are noted with blue round, red square, dark cyan triangle, and black reverse triangle symbols, respectively.
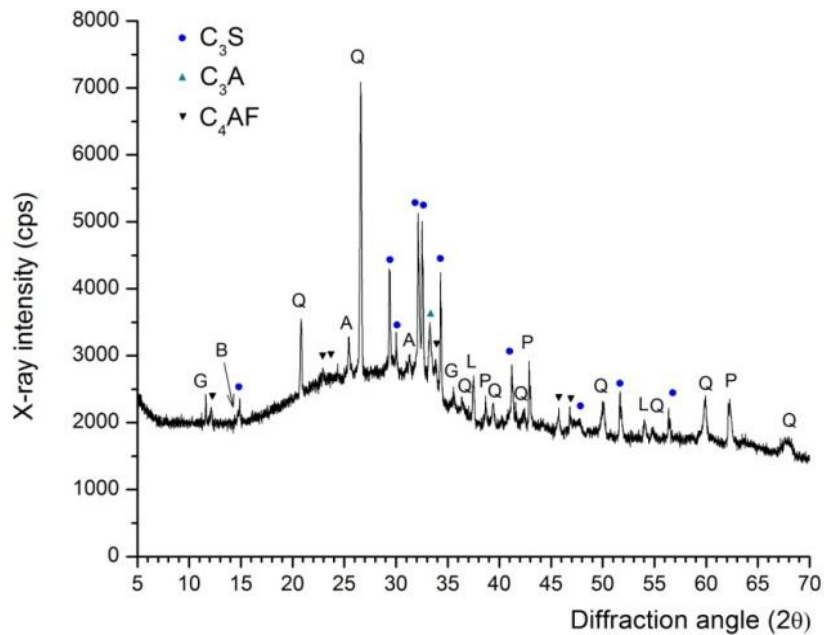
Figure 4.2. XRD Patterns of Class F Fly Ash. Note that A indicates calcium sulfate anhydrite, B indicates calcium sulfate hemihydrates (bassanite), C indicates calcite, G indicates gypsum, and Q indicates quartz. Also note that C_3S, C_3A, and C_4AF are noted with the blue round, dark cyan triangle, and black reverse triangle symbols, respectively.
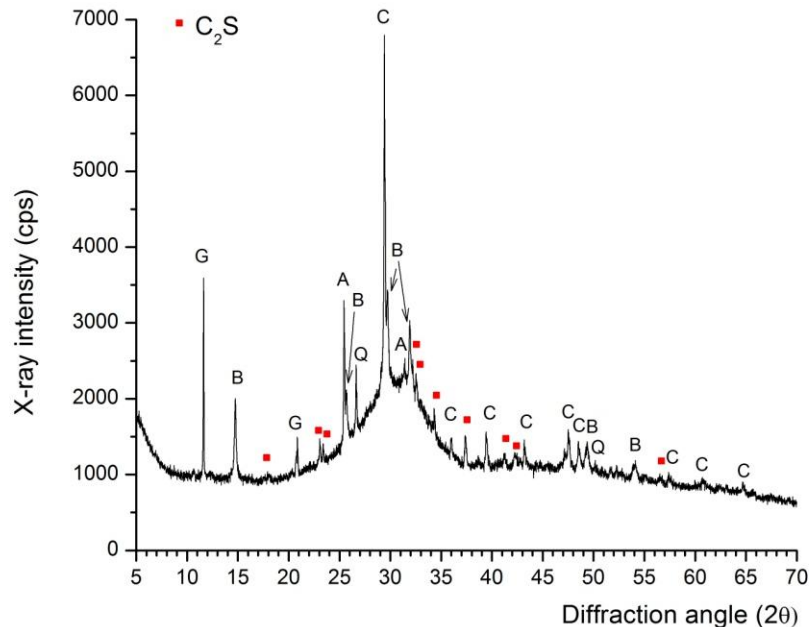
Figure 4.3. XRD Patterns of BFS. Note that A indicates calcium sulfate anhydrite, B indicates calcium sulfate hemihydrates (bassanite), C indicates calcite, G indicates gypsum, L indicates free lime, P indicates periclase, and Q indicates quartz. Also note that C_2S is indicated with a red square symbol.

4.2   Particle-Size Distribution

Particle-size characterization of the dry blend materials used to form the Cast Stone was performed with a Mastersizer 2000[1] with a Hydro G wet dispersion accessory (equipped with a continuously variable and independent pump, stirrer, and ultrasound). The instrument uses a focused laser beam (He-Ne laser and solid-state light source) and subsequent scattering light by the motion of particles. The angular intensity of the scattered light is then measured by a series of photosensitive detectors. The Mastersizer has a nominal size measurement range of 0.02 to 2000 μm. The actual range is dependent on the accessory used as well as the properties of the solids being analyzed. When coupled with the Hydro G wet dispersion accessory, the nominal measuring range is effectively 0.02 to 2000 μm (also dependent on material density). A performance check of the particle-size analyzer was performed using a National Institute of Standards and Technology (NIST)-traceable particle-size standard before any particle-size analysis was undertaken.

Small aliquots (~ 0.2 to 1 g) of the Cast Stone blend reagents were submerged in degassed DIW in the Hydro G dispersion unit with the pump and stirrer speed set at 2500 and 1000 rpm, respectively, for 60 seconds before making the particle-size measurements. The total volume of the dispersion unit is ~800 mL. Appropriate dilutions were determined by the amount of light passing through the diluted material (obscuration), which was measured by the particle-size analyzer. Samples were analyzed on the same aliquot initially without sonication and then during sonication (100%, 20 W) after an initial sonication period of 60 seconds. Duplicate samples were measured to confirm the mixing and sub-sampling technique to ensure a representative PSD of the material was obtained.

---

[1]Malvern Instruments, Inc., Southborough, Massachusetts.

Data with and without sonication are reported in Table 4.2. Agglomeration upon sonication was observed for the fly ash, which resulted in an increase in the d(95) and d(99) in Table 2.1. Sonication had no effect on the PSD for both the cement and the slag aliquots that were analyzed. The PSD and the cumulative % volume plots given in Figure 4.4 and Figure 4.5 are for the unsonicated materials measured after a 1-minute recirculation time.

As observed from Figure 4.4, the PSD of fly ash was wider than those of cement and slag. This is because the particle size of fly ash is not controlled for the use. The cement and BFS are ground in a mill before being used for civil engineering purposes because the original product is in much larger sizes.

Table 4.2. Summary Table of Estimated Size of Particles in Selected Percentile Values for Measurements Taken at 1-Minute Recirculation Time and with Sonication

Percentiles	Fly Ash[a]		Cement[a]		Slag[a]	
	1 min recirculation	Sonicated	1 min recirculation	Sonicated	1 min recirculation	Sonicated
	Percentile Size, µm					
d(0.01)	0.37	0.38	0.41	0.41	0.42	0.41
d(0.05)	0.77	0.76	1.4	1.4	0.96	0.94
d(0.10)	1.5	1.4	3.2	3.0	1.9	1.9
d(0.50)	15	15	17	16	13	13
d(0.90)	114	115	39	38	38	37
d(0.95)	175	184	47	45	48	47
d(0.99)	348	421	63	58	72	69

(a) Based on the average of six PSD measurements generated (three each) from two sub-aliquots.
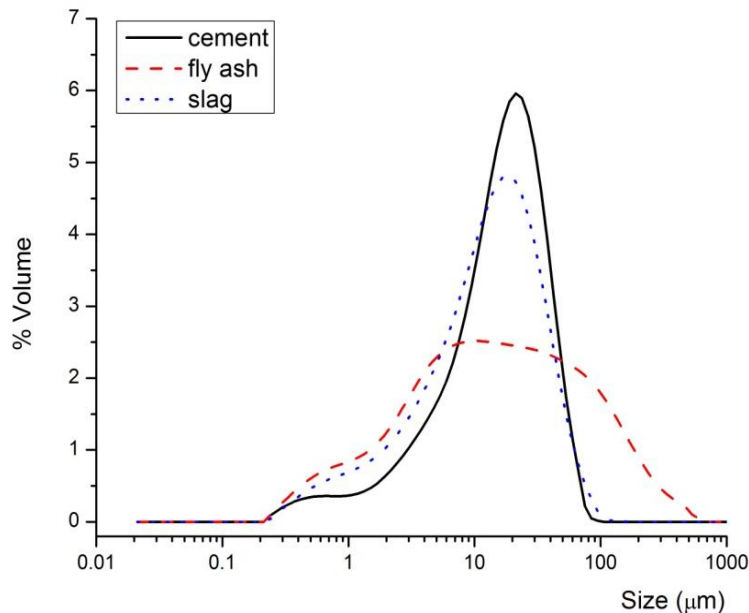
Figure 4.4. PSD at 1-Minute Recirculation Time, No Sonication
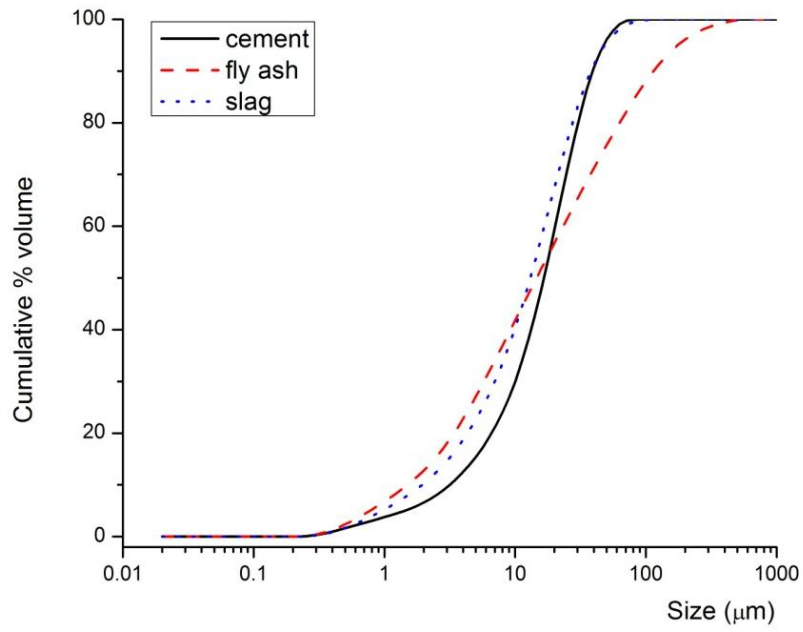
Figure 4.5. Cumulative % Volume at 1-Minute Recirculation Time, No Sonication

5.0   Cast Stone Monolith Preparation and Characterization

To characterize the Cast Stone as a waste form for secondary wastes, 2-in. × 4-in. cylinders were prepared from the eight simulant formulations discussed in Section 2.0. This section describes the preparation of the cylinders and measurement of the heat generated during curing. Additional studies of the curing process are described in Section 7.0.

5.1   Cast Stone Monolith Preparation

Using the Cast Stone formulation developed in Phase 1, monoliths were made using the eight simulant recipes. As described in Section 1.0 and Table 1.1, a dry materials blend of 8 wt% Portland cement (Type I/II), 45 wt% Class F fly ash, and 47 wt% BSF (Grade 100) was selected to develop and optimize the Cast Stone formulation for the secondary waste form. For each of the waste simulants described in Section 2.0, nonradioactive monoliths were prepared for compressive strength and phase characterization, and monoliths spiked with ^{99}Tc were prepared for leaching studies. Table 5.1 shows the recipes for making the Cast Stone specimens with the ^{99}Tc spike, and Table 5.2 shows the recipes for the nonradioactive Cast Stone specimens.

Cement, fly ash, and BFS were hand-mixed in a large bowl until the dry mixture appeared to be homogenous. A simulant with or without technetium along with a specified amount of simulant and DIW (26% simulant with 74% DIW) was added to the dry mix. Note that adding water beyond that in the simulant has the effect of reducing the sodium concentration as shown in Table 5.3. The mixture was then stirred until a homogeneous paste was developed. The slurry was then transferred to plastic molds. When each mold was approximately half full, it was vibrated using a hand-held vibrator until no bubbles were observed on the surface. The mold was then filled, and a small 0.5-cm-diameter rod was inserted into the paste. The rod was moved up and down until the interface between the two pours disappeared. Next, the entire mold was vibrated until no bubbles were observed at the surface. A perforated cap was placed on the mold. Finally, the molds were transferred to a room-temperature, 100% humidity chamber.

Various steps involved are shown in

Figure 5.1.

Table 5.1. Makeup of Cast Stone Specimens Containing Technetium

	2 M	4 M	6 M	8 M	10 M
S1-Median			Grams		
Portland Cement Type I, II	134.47	134.61	134.78	134.46	134.5
Fly Ash, Class F	756.4	756.55	756.47	756.43	756.09
Blast Furnace Slag, Grade 100	789.81	789.94	789.82	790.15	789.67
Waste Simulant	183.76	199.2	216.86	233.21	236.54
Water	484.74	483.3	549.71	574	636.97
Tc-mL	0.627[a]	1.254[a]	1.885[a]	2.564[a]	3.135[a]
S2 – Cluster 1					
Portland Cement Type I, II	134.59	—	—	—	—
Fly Ash, Class F	756.54	—	—	—	—
Blast Furnace Slag, Grade 100	789.99	—	—	—	—
Waste Simulant	184.05	—	—	—	—
Water	484.47	—	—	—	—
Tc-mL	0.627[a]	—	—	—	—
S3 – Cluster 2					
Portland Cement Type I, II	134.84	—	—	—	—
Fly Ash, Class F	756.44	—	—	—	—
Blast Furnace Slag, Grade 100	789.79	—	—	—	—
Waste Simulant	187.25	—	—	—	—
Water	484.45	—	—	—	—
Tc-mL	0.627[a]	—	—	—	—
S4 – Caustic Scrubber / SBS Condensate Blend					
Portland Cement Type I, II	134.77	—	—	—	—
Fly Ash, Class F	756.51	—	—	—	—
Blast Furnace Slag, Grade 100	789.85	—	—	—	—
Waste Simulant	192.41	—	—	—	—
Water	470.17	—	—	—	—
Tc-mL	19.370[b]	—	—	—	—

(a) Prepared with a 60.6 ppm Tc in a potassium hydroxide solution. The volume added was based on a 1000 ppm solution. Later analysis revealed that the spike solution was only 60.6 ppm Tc.
(b) Prepared with a 1000 ppm Tc in ammonium hydroxide solution.

Table 5.2. Makeup of Non-Radioactive Cast Stone Specimens

	2M	4M	6M	8M	10M
S1-Median			Grams		
Portland Cement Type I, II	96	96.31	96.64	96.33	96.23
Fly Ash, Class F	540.01	540.16	540.35	540.74	540.16
Blast Furnace Slag, Grade 100	564.02	564.85	564.64	564.2	564.36
Waste Simulant	121.04	142.21	154.25	161.97	169.05
Water	346.02	346.18	355.59	356.75	382.52
S2 – Cluster 1					
Portland Cement Type I, II	96.17	--	--	--	--
Fly Ash, Class F	540.57	--	--	--	--
Blast Furnace Slag, Grade 100	564.49	--	--	--	--
Waste Simulant	131.9	--	--	--	--
Water	346.84	--	--	--	--
S3 – Cluster 2					
Portland Cement Type I, II	96.13	--	--	--	--
Fly Ash, Class F	540.3	--	--	--	--
Blast Furnace Slag, Grade 100	564.15	--	--	--	--
Waste Simulant	133.84	--	--	--	--
Water	346.04	--	--	--	--
S4 – Caustic Scrubber/SBS Condensate Blend					
Portland Cement Type I, II	96.27	--	--	--	--
Fly Ash, Class F	540.4	--	--	--	--
Blast Furnace Slag, Grade 100	564.08	--	--	--	--
Waste Simulant	137.43	--	--	--	--
Water	346.31	--	--	--	--

Table 5.3. Waste Simulant Adjusted Sodium Concentration Based on Water Additions in Cast Stone Preparation

Simulant	Adjusted Na Concentration	Waste Loading (wt%, wet basis)	Dry Solids Loading (wt %)
S1-2 M	0.518 M	7.8	1.01
S1-4 M	1.039 M	8.5	2.01
S1-6 M	1.420 M	8.9	2.93
S1-8 M	1.866 M	9.5	3.92
S1-10 M	2.100 M	9.4	4.65
S2-2 M	0.518 M	7.9	0.96
S3-2 M	0.518 M	8.0	1.11
S4-2 M	0.518 M	9.0	1.89

Figure 5.1. Steps Involved in Cast Stone Monolith Preparation

When preparing monoliths using simulants S1-6 M, -8 M, -10 M, and S4-2 M, it was necessary to add more water than the simulant recipe called for to obtain a workable paste. Monoliths made from simulants S1-6 M, -8 M, and -10 M required an additional of 7, 10, and 14 mL of DIW for each monolith, respectively. For example, an additional 50 mL of DIW was added to the total slurry mix used for the seven monoliths made from simulant S1-6 M. A dispersing agent, such as a superplasticizer, could have been added to enhance the workability, but it was not included at this stage because adding a dispersing agent may change the leaching capability of technetium, which is one of the most important characteristics in the waste form.

While mixing the S4-2-M simulant with the dry materials, a very strong ammonia odor was detected. NH_3 gas is expected to evolve when the pH is raised in a solution containing significant NH_4^+ concentrations. All mixing and pouring activities were transferred to a ventilated hood. Initially, the paste made using simulant S4-2 M was very workable. However, after standing for less than a minute, the paste became very stiff, and an additional 5 mL of DIW had to be added. To keep the paste from getting stiff while the half-full molds were being vibrated, the paste was continually mixed.

The monoliths were checked periodically while they were curing. During the 28-day curing period, nothing unusual was observed except for the molds containing monoliths made from the S4-2-M simulant. Sometime during the first 24 to 48 hours, the molds for both the radioactive and nonradioactive monoliths cracked as shown in Figure 5.2. Based on how the molds cracked, it appears that the paste expanded a small amount, increasing the pressure on the mold walls and causing them to crack.
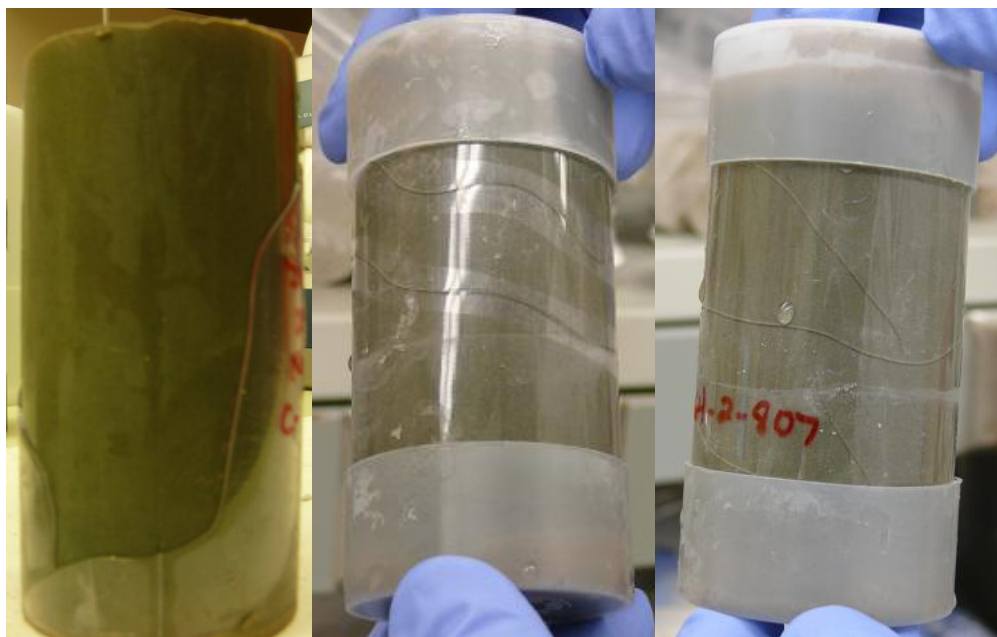
Figure 5.2. Cracked Molds from Simulant 4 Cast Stone Preparation

The monoliths made from the S4-2-M simulant initially were placed with the other monoliths in the humidity chambers to cure. When the humidity chambers were opened, a strong ammonia odor was detected. After a few days, the monoliths made from the S4-2-M simulant were removed and placed in their own humidity chamber. The chamber was only opened in a ventilation hood.

The two sets of monoliths were made over a period of several weeks. After the 28-day cure, the monoliths (Figure 5.3) were removed from the molds, placed into buckets with lids, and stored at room temperature. The nontechnetium monoliths were compression tested 13 days after they were removed from the molds. The monoliths with technetium were sent for leach testing 4 days after they were removed from the molds. Two Cast Stone monoliths from each simulant were broken to make smaller size fractions of samples. The powder samples of Cast Stone were prepared by separately breaking each monolith into large chunks with a hammer and placing the chunks into a ball mill to further reduce the particle size. The powdered material was then sieved to a less than 0.3-mm-diameter size fraction using U.S. sieve # 50 mesh. The <0.3-mm size fraction was subsequently used to determine the moisture

content and specific surface area. The powdered samples of a less than 0.3-mm size fraction were also used for EPA Draft Methods 1313 and 1316 (EPA 2009a, 2009c) described in Section 6.0.

Figure 5.3. Cast Stone Monoliths

5.2   Heat Generation During Curing

One monolith from each simulant without the ^{99}Tc spike was selected after pouring, and a digital thermometer was inserted into the top of the mold (Figure 5.3, left panel). The tip of the thermometer was centered and inserted approximately 50 mm into the Cast Stone slurry from the top. The temperature was initially monitored every day, except for the weekend, until a constant temperature was observed. The changes in temperature are shown in Figure 5.4. The data in Figure 5.4 show a temperature rise of about 2 to 5°C within a day or two at the beginning of the curing, but the temperature returned back to about room temperature within about 10 days and stayed more or less constant through the rest of the curing time. The measured temperature rise is low, given the small cylinder size. A higher temperature rise would be expected for larger blocks of Cast Stone. Harbour et al. (2007) provides heats of hydration measured for Saltstone that may be of value in modeling the cooling of cement waste form blocks.
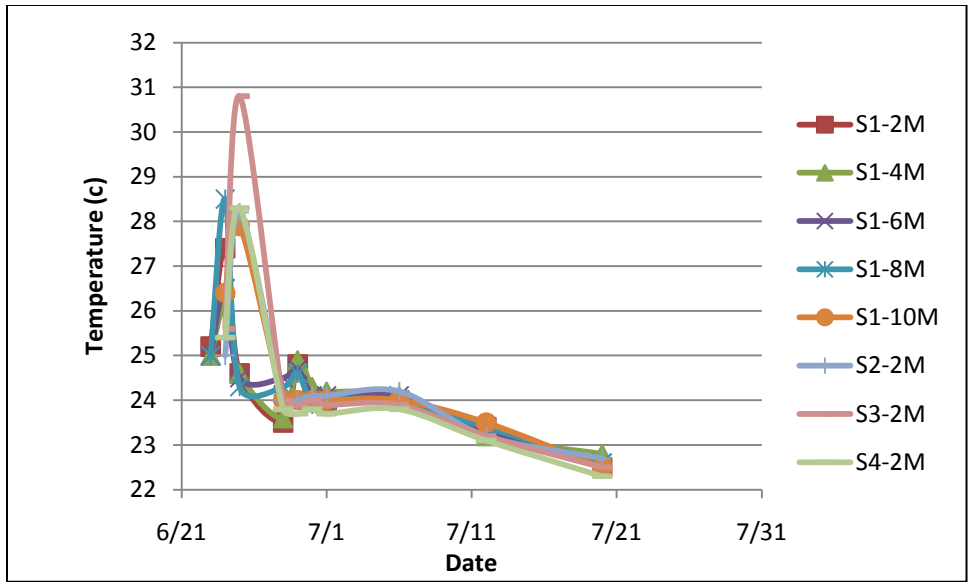
Figure 5.4. Curing Temperatures of 2-in. Diameter by 4-in. Cast Stone Cylinders

6.0   Cast Stone Waste Form Characterization

The Cast Stone specimens prepared with the range of secondary waste simulants were characterized with respect to their compressive strength, leachability, phase assemblage and microstructure, and pore structure. For each of these properties and characteristics, this section provides a description of the methodology used followed by the results.

6.1   Compressive Strength

Radioactive waste disposal facilities, such as the IDF, typically include requirements with respect to the structural stability of the waste or waste package to be disposed of. These requirements are derived from the need to minimize the subsidence of the disposal area to maintain the integrity of closure caps and barriers. The Nuclear Regulatory Commission's *Technical Position on Waste Form* (NRC 1991) recommends that cement-based waste forms have a compressive strength of at least 3.45 MPa (500 psi).

6.1.1   Compressive Strength Measurement

Selected nonradioactive Cast Stone monoliths (right cylinders with 50-mm diameter by 100-mm [2-in. $\times$ 4-in.] length) were prepared for compressive strength tests. At 28 days, compressive strength tests were conducted by placing the cylindrical test specimens between parallel platens in a servohydraulic test machine and applying a compressive load until fracture occurred. The tests were run under displacement control, with a crosshead rate of 2.5 mm/min, and load and displacement were recorded during the tests. Three specimens for each waste simulant condition were tested and averaged.

6.1.2   Compressive Strength Results

The compressive strength of Cast Stone specimens at 28 days of hydration is presented in Figure 6.1 and Figure 6.2. From Figure 6.1, small changes in compressive strength were noted with changes in simulant type. Although these data showed some variation, the actual differences in the compressive strength are within the range of their standard deviations. Therefore, the difference in compressive strength between Cast Stone monoliths made with the various secondary waste simulants at their overall 2-M sodium concentrations are not great enough to be used as a criterion to rank the performance of the Cast Stone specimens. Further, all the Cast Stone monoliths prepared with 2 M sodium (and their respective other constituent concentrations normalized to the sodium) exhibited compressive strengths well above the IDF disposal requirement of 3.45 MPa.
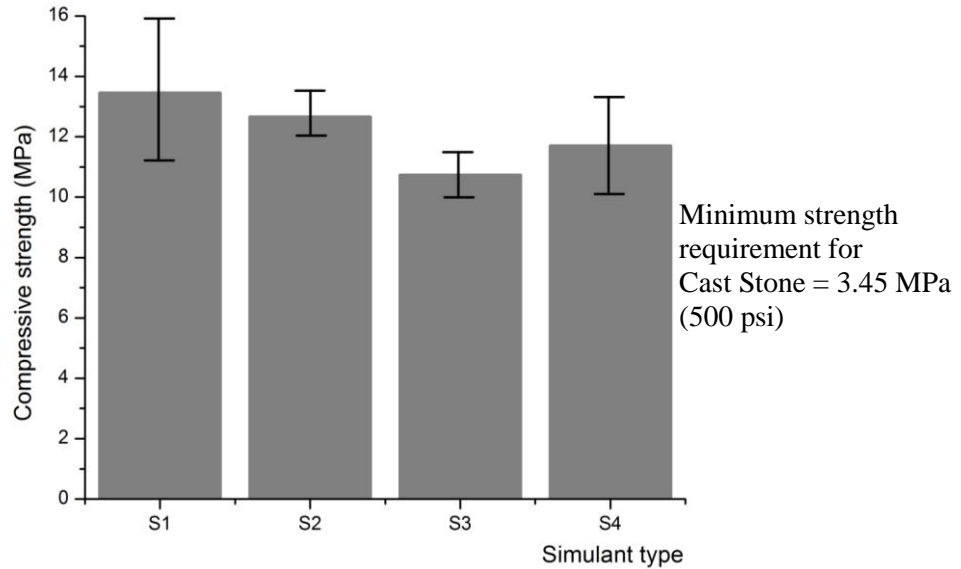
Figure 6.1. Compressive Strength of Cast Stone for Simulants S1, S2, S3, and S4

The effect of S1 simulant solution concentration on the compressive strength of the Cast Stone monoliths is presented in Figure 6.2. The compressive strength for S1 monoliths was maximized at the 4-M-sodium solution, and the compressive strength started to decrease as the simulant solution concentration increased above 4 M sodium. However, it should be noted that a lower compressive strength of Cast Stone monoliths made with the S1-6-M, 8-M, and 10-M solutions is mainly attributed to the increase in water content to facilitate workability at the time of mixing. Excluding the Cast Stone monoliths from 6-M, 8-M, and 10-M sodium simulant solutions, the compressive strength seems to be affected by the increase of concentration. However, it is difficult to correlate the development of kanemite in the Cast Stone made at the higher sodium concentrations with the decrease in compressive strength because of the lack of supporting data.
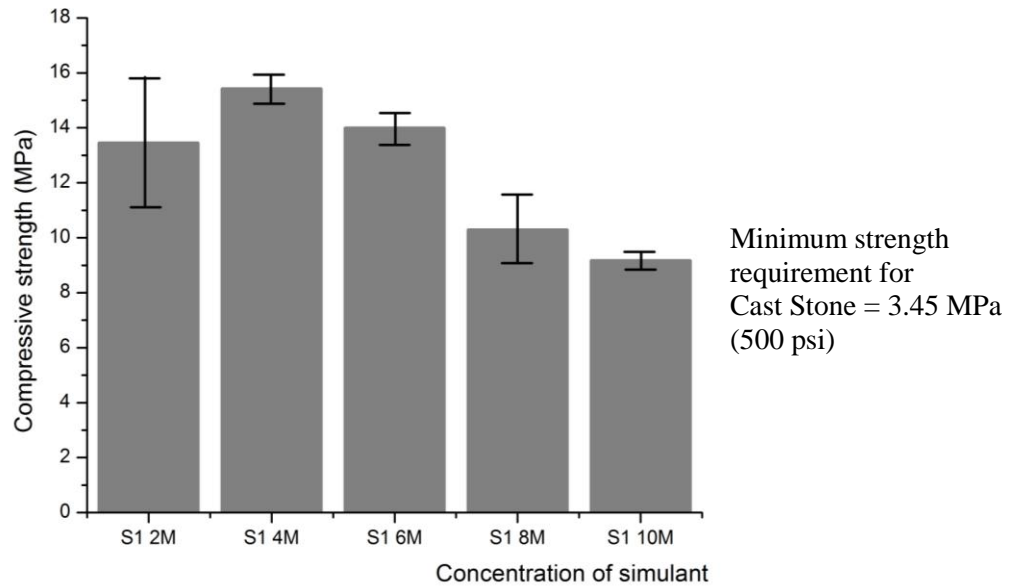
Figure 6.2. Compressive Strength of Cast Stone for Range of S1 Simulant Concentrations

6.2 Cast Stone Leach Testing

To evaluate the effects of the waste composition on the leachability of the Cast Stone, the three EPA draft methods used in the Phase 1 Cast Stone and DuraLith geopolymer waste form were used as discussed below. EPA Draft Method 1315 (EPA 2009b) is similar to ANSI/ANS-16.1-2003 and is intended to measure the diffusivity of radioactive and hazardous constituents as they leach out of the waste form. EPA Draft Method 1313 (EPA 2009a) is a leach test designed to provide extracts for the generation of a liquid-solid partitioning (LSP) curve as a function of pH for inorganic compounds. EPA Draft Method 1316 (EPA 2009c) is a leach test designed to evaluate the effect of differing liquid-solid ratio of constituent release rates. The results from three EPA methods provide detailed information on the amount and release behavior of key COCs and provide insight into the processes and mechanisms controlling element release. Two of the leach methods, EPA Draft Methods 1313 and 1316, used powdered Cast Stone samples (less than 0.3-mm size fraction) while the EPA Draft Method 1315 (EPA 2009b) used intact Cast Stone monoliths.

The EPA leaching test methods and results are described in the sections below. Common to all tests is the need to characterize the waste forms and leachate solutions. The analytical methods used are described first.

6.2.1   Analytical Methods

Analytical methods to characterize the leachate from the various leach tests, the chemical composition of the Cast Stone waste form, and the moisture content of the crushed Cast Stone used in the EPA Draft Methods 1313 (EPA 2009a) and 1316 (EPA 2009c) are described in this report.

6.2.1.1   Leachate Characterization

All leachate solutions collected from the three EPA methods were monitored for pH, oxidation-reduction potential (Eh), electrical conductivity (EC), alkalinity, major anions, major cations, technetium, iodide, and RCRA metals. The pH of the solution samples was measured with a solid-state pH electrode and a pH meter (Hanna, model HI 4521). Before measuring the pH, the probe was calibrated with NIST-traceable buffers (pH = 2.00, 4.00, 7.00, 10.00, and/or 12.00 at 25°C). The precision of the pH measurement was ±0.1 pH units. The Eh of the leachate solutions was measured with an Eh probe (Hanna, 3131B) also connected to the Hanna model HI 4521 meter. The Eh probe was calibrated using a pH buffer solution (pH = 4.00 and 7.00 at 25°C) mixed with 0.5 g of quinhydrone. The EC of leachate solutions was measured with a Pharmacia Biotech conductivity sensor. The sensor was calibrated with a range of freshly prepared potassium chloride standard solutions, ranging from 0.001 M to 1.0 M. The conductivity was measured with approximately 2 mL to 3 mL of filtered leachate. The alkalinity (mg/L as $CaCO_3$) was measured with a standard acid titration method (total alkalinity at pH = 4.5). The alkalinity procedure is equivalent to the U.S. Geological Survey method in the *National Field Manual for the Collection of Water-Quality Data*.

The concentrations of nitrate (NO_3^-), phosphate (PO_4^{-3}), and sulfate (SO_4^{-2}) in leachate solutions were determined using ion chromatography with a Dionex AS17 column. This methodology is based on EPA Method 300.0A (EPA 1984), with the exception of using the gradient elution of sodium hydroxide. The concentration of major cations was measured with inductively coupled plasma optical emission

spectroscopy (ICP-OES) using high-purity calibration standards to generate calibration curves and verify continuing calibration during the analysis run. Because of the differences in the leachate cation concentration, a number of dilutions, ranging from 100 to 1.01 times, were used to obtain reliable measurements of the concentrations of the cations of interest. Details of this method are found in EPA Method 6010B (EPA 2000a). Inductively coupled plasma mass spectrometry (ICP-MS) was used to measure RCRA metals concentrations, including iodine, mercury, and [99]Tc. These measurements were performed following the PNNL-AGG-415 method (PNNL 1998), which is similar to EPA Method 6020 (EPA 2000b).

6.2.1.2   Chemical Composition of Cast Stone Specimens

Each waste simulant Cast Stone type is being characterized with a suite of techniques that includes chemical composition by digestion followed by ICP-MS, ICP-OES, XRD, and SEM/transmission electron microscopy (TEM). Chemical digestion results provide the elemental composition of each waste form and information needed to normalize the release results obtained in the leach tests. XRD analyses were performed on pre- and post-leach test samples to determine the mineralogy and evaluate any phase changes that occur during the leach testing. Electron microscopy is being performed on pre- and post-leach test samples to gain insight into the distribution of elements and potential phase changes the waste form undergoes during testing.

Aliquots of the <0.3 mm crushed 28-day cured Cast Stone samples were chemically digested to determine the elemental composition. Microwave-assisted strong acid digestions were conducted using 16 M HNO_3 (~17 wt%), 12 M HCl (7 wt%), 32 M HF (3.3 wt%), and DIW (72.7%). About 0.5 grams of H_3BO_3 were added to the acid leachate later before analysis. The powdered Cast Stone samples were prepared following the PNNL AGG-MARS-001 (PNNL 2009b), which is modified from EPA Method 3052 (EPA 1996). The solid was reacted with the acid mixture (0.1 g/10 mL) for 1 hour at $180 \pm 5°C$. The reaction time was extended due to the presence of undissolved solids. Upon dissolution of the sample, the resulting solution was transferred to a centrifuge tube using DIW and the original solid-to-final solution ratio was increased by the addition of DIW to result in a 0.1 g/30 mL final solid-to-solution ratio. The final solution was filtered through a 0.45-µm membrane and was analyzed for ^{99}Tc and trace metals using ICP-MS and major cations using ICP-OES. This method cannot be used to measure anion concentrations due to the strong acids, which contain the anions like nitrate, chloride, and fluoride, which are used in the dissolution procedure. A separate alkaline chemical digestion is necessary to determine the iodide concentrations in the samples because iodide can oxidize and volatilize at low pH. For the alkaline digestion, Cast Stone powder was mixed with a KOH-KNO_3 fusion solution in a crucible and heated at about 550°C for 1 hour. Sodium bisulfate was also added to prevent oxidation of iodide to elemental iodine in the final solution. The final fusion melt was cooled and acidified with HNO_3. The solution was filtered using a 0.45-µm membrane and submitted for iodide analysis using ICP-MS. A surfactant, Spectrasol CFA-C[1], was used to remove the memory effect when going from one sample analysis to the next (Brown et al. 2005, 2007). Because technetium and iodine concentrations were so low in the final Cast Stone specimens, reliable analytical results were not obtained. Therefore, theoretical concentrations were calculated based on the chemical makeup of the simulants and the waste forms. These theoretical concentrations were used in the leach test results calculations.

Because concentrations of technetium and iodine were so low, reliable concentrations in the Cast Stone specimens were not obtained by the analytical methods used. For the leach test results reported

---

[1] Spectrasol Inc., Warwick, New York.

below, initial technetium and iodine concentrations in the specimens are calculated based on the simulant and waste form recipes. Table 6.1 lists these initial calculated concentrations plus the measured concentration of sodium in the waste forms.

Table 6.1. Concentration of Tc, I, and Na in Cast Stone Specimens

Simulant	Calculated Tc Concentration μg/g (wet)	Calculated I Concentration μg/g (wet)	Measured Na Concentration μg/g (dry)
S1-2 M	0.0162	0.0847	18000
S1-4 M	0.0321	0.1683	21000
S1-6 M	0.0466	0.2425	25600
S1-8 M	0.0625	0.3323	28400
S1-10 M	0.0743	0.3882	31700
S2-2 M	0.0162	0.0846	19100
S3-2 M	0.0161	0.0844	18900
S4-2 M	8.20	1.5319	18000

6.2.1.3   Moisture Content

To determine the moisture content of the <0.3-mm size fraction, a 10-gram aliquot of the Cast Stone powder was placed into a pre-tared container and dried in an oven at 105°C until constant weight was achieved for a minimum of 24 hours (ASTM D4442-07). Each container was removed from the oven, sealed, cooled, and reweighed. At least two weighings were conducted after a 24-hour heating period to verify that constant weight had been achieved. To verify the weights, all gravimetric measurements were performed with a calibrated balance. The gravimetric water content was computed as the percent weight change of the powder sample before and after oven drying (i.e., [{wet weight - dry weight}/dry weight]). The oven-dried sample used for moisture content was also used for surface-area measurement and discarded.

6.3   Contaminant Diffusivity – EPA Draft Method 1315

6.3.1   EPA Draft Method 1315 Methodology

EPA Draft Method 1315, *Mass Transfer Rates of Constituents in Monolith or Compacted Granular Materials Using a Semi-Dynamic Tank Leaching Test* (EPA 2009b) is a 63-day semi-dynamic leach experiment that consists of submerging a monolithic sample (with a fixed geometry) in water at a fixed liquid volume-to-solid surface area ratio and sampling at fixed periods of time (EPA 2009c). The total leaching time was extended up to 90 days, and the data collected at 90 days were used to determine the effective diffusivity of select constituents in this report. The geometric surface area is used in this test method and calculated based on the cylindrical dimensions of the Cast Stone monolith. At each of the nine predetermined leaching intervals, the sample mass is recorded, and the leaching solution is changed. This method is similar to ANSI/ANS-16.1-2003, but the leaching intervals are modified, and the process of mass transfer can be interpreted by more complex release models that account for physical retention of the porous medium and chemical retention at the pore wall through geochemical speciation modeling. A schematic of this process is shown in Figure 6.3.

Each Cast Stone cylindrical monolith (2-in. diameter by 4-in. height) was placed into the center of a leaching vessel and mixed with DIW to maintain a solid-to-solution ratio of 9 ±1 mL of leachant per cm^2 of sample. The sample stand and holder were used to maximize the contact area of the Cast Stone monolith with the leaching solution. In between the sampling/replacement intervals, the experimental vessels were covered with a lid. An example of the experimental setup and sample specimens in the leaching vessels is shown in Figure 6.4. The leaching intervals used for these experiments were 2 hours and 1, 2, 7, 14, 28, 42, 49, and 63 days. Samples collected during these intervals were used to measure pH, electrical conductivity, and redox potential. Before being submitted for chemical analyses, the leachates were also filtered with a 0.45-μm syringe filter.
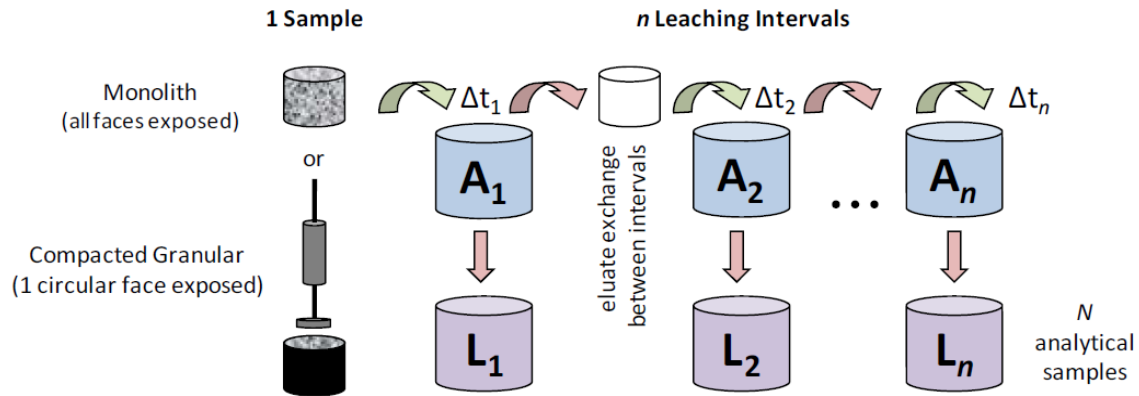
Figure 6.3. Schematic of 1315 Test Method
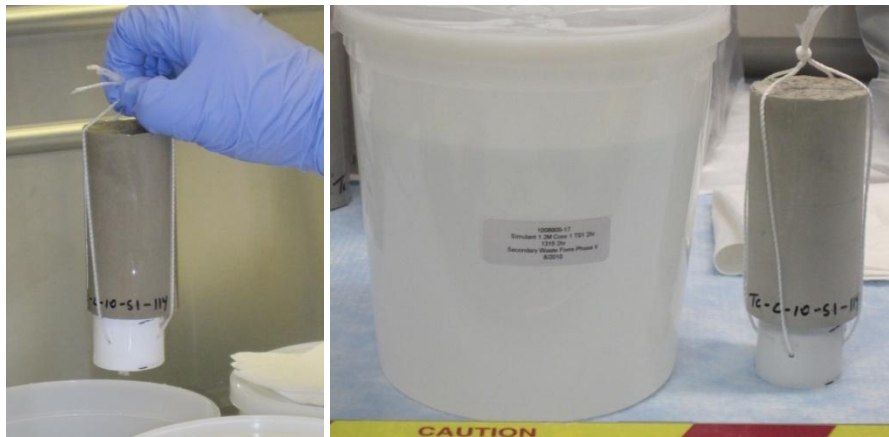
Figure 6.4. Cast Stone Monoliths Submerged into DIW in the Leaching Vessels with the Lids

The observed effective diffusivity for each constituent was calculated using the analytical solution, Equation (6.1), for simple radial diffusion from a cylinder into an infinite bath as presented by Crank (1986).

$$D_i = \pi \left[\frac{M_{t_i}}{2\rho C_o \left(\sqrt{t_i} - \sqrt{t_{i-1}} \right)} \right]^2$$

(6.1)

where D_i =observed diffusivity of constituent for leaching interval, i [m^2/s]

M_{ti} =, mass released during leaching interval i [mg/m^2]

t_i = cumulative contact time after leaching interval, i [s]

t_{i-1} = cumulative contact time after leaching interval, $i-1$ [s]

C_o = initial leachable content [mg/Kg]

ρ = sample density [Kg/m^3].

The mean observed effective diffusivity for each constituent can be determined by taking the average of the interval observed diffusivity with the standard deviation. A leachability index (LI) can then be calculated as the negative logarithm of the observed diffusivity in cm^2/s (ANSI/ANS 16.1 2003). A low diffusivity means a larger LI.

6.3.2   Contaminant Diffusivity Results

For EPA Draft Method 1315 (EPA 2009b) , the monolith samples containing the different simulated waste recipes were suspended in DIW at a liquid volume-to-specimen geometric surface area of 9 ± 1 mL per cm^2. At each sampling time, the Cast Stone cylinder was removed from the leachate and placed in a fresh leaching solution. The leachate was sampled and characterized. The pH, EC, Eh, and alkalinity that were measured for each leaching solution are displayed in Table 6.2. The measured pH values for each leachate of the Cast Stone monoliths made with various simulants were between 10 and 12 with a slight initial increase that leveled out as the contact time for each monolith increased. A near steady-state of the pH value of ~11.5 that was achieved at contact times longer than 1 day suggests that equilibrium conditions were reached. The conductivity, Eh, and alkalinity results all display an initial increase in the measurements followed by a decrease in the measured values starting from the 14- to 49-days of cumulative leaching.

Table 6.2. pH, EC, Eh, and Alkalinity Results for Cast Stone by EPA Draft Method 1315

Simulant	Cumulative Leach Time (days)	Interval Label	pH	EC (mS/cm)	Eh (mV)	Alkalinity (mg/L as CaCO$_3$)
	0.08	T01	10.6	0.236	340	41.7
	0.08	T01	10.5	0.192	336	41.5
	1	T02	11.3	0.601	268	130
	1	T02	11.4	0.671	262	138
	2	T03	11.2	0.402	218	95.5
	2	T03	11.1	0.363	218	75.1
	7	T04	11.6	1.02	172	208
Simulant 1, 2M	7	T04	11.6	1.04	168	215
	14	T05	11.7	0.941	93.3	191
	14	T05	11.6	0.899	90.1	183
	28	T06	11.7	0.948	249	222
	28	T06	11.7	0.975	242	221
	42	T07	11.5	0.872	103	197
	42	T07	11.5	0.869	131	196
	49	T08	11.3	0.488	213	125

Simulant	Cumulative Leach Time (days)	Interval Label	pH	EC (mS/cm)	Eh (mV)	Alkalinity (mg/L as CaCO$_3$)
	49	T08	11.3	0.454	211	113
	63	T09	11.4	0.598	162	144
	63	T09	11.3	0.538	163	133
	0.08	T01	10.5	0.213	329	41.5
	0.08	T01	10.6	0.251	318	45.7
	1	T02	11.5	1.02	253	189
	1	T02	11.6	0.974	254	183
	2	T03	11.3	0.593	220	110
	2	T03	11.3	0.569	211	119
	7	T04	11.6	1.12	230	206
	7	T04	11.6	1.09	226	209
Simulant 1, 4M	14	T05	11.7	1.12	86.5	219
	14	T05	11.7	1.06	85.8	205
	28	T06	11.7	1.14	236	242
	28	T06	11.7	1.11	238	241
	42	T07	11.5	0.988	101	223
	42	T07	11.6	1.02	88.5	219
	49	T08	11.4	0.573	117	140
	49	T08	11.4	0.555	117	140
	63	T09	11.4	0.695	166	151
	63	T09	11.5	0.680	161	166

Table 6.2 (contd)

Simulant	Cumulative Leach Time (days)	Interval Label	pH	EC (mS/cm)	Eh (mV)	Alkalinity (mg/L as CaCO$_3$)
	0.08	T01	10.5	0.478	308	47.3
	0.08	T01	10.4	0.383	304	37.8
	1	T02	11.6	1.50	275	238
	1	T02	11.6	1.50	260	233
	2	T03	11.3	0.723	214	143
	2	T03	11.4	0.925	227	172
Simulant 1, 6M	7	T04	11.8	1.64	205	304
	7	T04	11.8	1.95	209	346
	14	T05	11.8	1.36	85.4	257
	14	T05	11.8	1.44	85.0	268
	28	T06	11.8	1.28	149	275
	28	T06	11.8	1.38	141	292
	42	T07	11.6	1.10	149	229
	42	T07	11.6	1.27	127	265

Table 6.2 (contd)

Simulant	Cumulative Leach Time (days)	Interval Label	pH	EC (mS/cm)	Eh (mV)	Alkalinity (mg/L as $CaCO_3$)
	49	T08	11.5	0.720	115	173
	49	T08	11.5	0.760	115	183
	63	T09	11.5	0.858	158	197
	63	T09	11.6	0.884	159	203
	0.08	T01	10.9	0.684	291	78.4
	0.08	T01	10.9	0.733	283	78.4
	1	T02	11.6	1.51	254	240
	1	T02	11.6	1.58	251	250
	2	T03	11.4	0.876	204	136
	2	T03	11.4	0.793	208	133
	7	T04	11.7	1.56	215	281
	7	T04	11.6	1.28	222	221
Simulant 1, 8M	14	T05	11.8	1.29	86.0	238
	14	T05	11.3	1.36	85.5	245
	28	T06	11.8	1.22	248	256
	28	T06	11.8	1.34	149	280
	42	T07	11.6	1.00	121	211
	42	T07	11.6	1.08	93.2	232
	49	T08	11.4	0.572	123	142
	49	T08	11.3	0.460	117	112
	63	T09	11.4	0.695	158	165
	63	T09	11.4	0.696	159	163
	0.08	T01	10.9	0.983	273	82.6
	0.08	T01	10.9	0.970	270	82.2
	1	T02	11.7	1.98	246	283
	1	T02	11.6	1.99	239	282
	2	T03	11.5	1.15	208	192
	2	T03	11.5	1.05	196	187
	7	T04	11.7	1.68	208	288
Simulant 1, 10M	7	T04	11.8	1.85	208	315
	14	T05	11.3	1.49	97.8	264
	14	T05	11.8	1.51	95.9	269
	28	T06	11.8	1.46	127	300
	28	T06	11.8	1.40	127	284
	42	T07	11.6	1.15	96.0	232
	42	T07	11.6	1.11	93.5	227
	49	T08	11.4	0.662	118	156
	49	T08	11.5	0.665	117	154

Table 6.2 (contd)

Simulant	Cumulative Leach Time (days)	Interval Label	pH	EC (mS/cm)	Eh (mV)	Alkalinity (mg/L as $CaCO_3$)
	63	T09	11.5	0.824	222	183
	63	T09	11.6	0.844	229	193
	0.08	T01	10.8	0.236	330	49.9
	0.08	T01	10.8	0.256	315	51.5
	1	T02	11.4	0.677	247	147
	1	T02	11.4	0.707	242	147
	2	T03	11.2	0.373	211	79.0
	2	T03	11.1	0.345	221	72.4
	7	T04	11.5	0.738	211	146
	7	T04	11.6	0.993	205	206
Simulant 2, 2M	14	T05	11.6	0.848	108	173
	14	T05	11.6	0.808	100	169
	28	T06	11.6	0.841	224	195
	28	T06	11.5	0.672	247	158
	42	T07	11.5	0.760	115	178
	42	T07	11.5	0.794	112	184
	49	T08	11.2	0.406	118	107
	49	T08	11.2	0.346	124	87.8
	63	T09	11.3	0.481	194	123
	63	T09	11.3	0.489	198	123
	0.08	T01	10.8	0.236	307	47.8
	0.08	T01	10.6	0.223	304	47.8
	1	T02	11.3	0.596	245	123
	1	T02	11.3	0.590	249	129
	2	T03	11.2	0.402	225	77.4
	2	T03	11.2	0.385	223	77.0
	7	T04	11.5	0.827	206	165
	7	T04	11.6	0.945	206	192
Simulant 3, 2M	14	T05	11.5	0.761	98.9	160
	14	T05	11.5	0.763	97.6	157
	28	T06	11.6	0.692	221	171
	28	T06	11.5	0.652	222	154
	42	T07	11.4	0.692	110	163
	42	T07	11.4	0.711	107	165
	49	T08	11.1	0.327	116	94.5
	49	T08	11.0	0.269	119	71.1
	63	T09	11.2	0.416	189	110
	63	T09	11.2	0.398	194	101
Simulant 4,	0.08	T01	10.7	0.228	293	42.5

Table 6.2 (contd)

Simulant	Cumulative Leach Time (days)	Interval Label	pH	EC (mS/cm)	Eh (mV)	Alkalinity (mg/L as $CaCO_3$)
2M	0.08	T01	10.6	0.211	289	42.3
	1	T02	11.3	0.588	271	98.5
	1	T02	11.3	0.593	257	111
	2	T03	11.1	0.370	216	75.1
	2	T03	11.1	0.373	217	55.5
	7	T04	11.5	0.758	204	148
	7	T04	11.5	0.812	213	162
	14	T05	11.4	0.631	102	133
	14	T05	11.4	0.612	101	130
	28	T06	11.5	0.561	217	145
	28	T06	11.5	0.572	217	148
	42	T07	11.3	0.514	109	123
	42	T07	11.2	0.493	105	119
	49	T08	11.0	0.282	123	79.3
	49	T08	11.0	0.237	121	65.9
	63	T09	11.1	0.354	177	95.1
	63	T09	11.0	0.302	175	74.3

The cation concentrations in EPA Draft Method 1315 (EPA 2009b) leachates are shown in Table 6.3. The leachates show that sodium, and to a lesser extent potassium, released more quickly (within the first day to the first 7 days), and the divalent alkaline-earth cation calcium leached more slowly with the maximum concentrations occurring after 28 to 42 days of cumulative leaching. Magnesium concentrations in the leachates were considerably lower (maximum in the tenths of mg/L) than the other cations. The timing of the maximum release of aluminum and silicon is dependent on the simulant used to make the Cast Stone monoliths, and for S1, which had the waste recipe varying from 2 to 10 M sodium, the concentrations of aluminum released increased with the concentration of the simulant used. For the 2-M Na-based simulants, 2 to 3 mg/L Al were the maximum concentrations observed. Maximum silicon concentrations in the leachates varied from about 7 to 11 mg/L regardless of the simulant type or the concentration used for S1. The dominant anions measured in the Method 1315 leachate are displayed in Table 6.3 and Table 6.4. The dominant anion in the solutions from the different waste simulants is alkalinity (combination of inorganic carbon [carbonate and bicarbonate] and hydroxyl) in Table 6.3, with lesser amounts of nitrate and sulfate as shown in Table 6.4. The nitrate release from the monoliths was highest in the first day of leaching and then the concentrations in the leachates slowly dropped with time.

Table 6.3. The Concentrations of Major Cations in Leachate Solutions from EPA Draft Method 1315

Simulant	Cumulative Leaching Time (days)	Na (mg/L)	Ca (mg/L)	K (mg/L)	Al (mg/L)	Si (mg/L)	Mg (mg/L)	S (mg/L)	Fe (mg/L)
	0.08	1.93E+01	ND	ND	6.89E-01	ND	ND	5.16E+00	ND
	0.08	2.66E+01	8.74E-01	ND	1.26E+00	ND	ND	7.43E+00	ND
	1	5.66E+01	6.73E+00	5.22E+00	2.97E+00	4.90E+00	4.12E-02	4.64E+00	ND
	1	6.06E+01	7.20E+00	5.89E+00	2.94E+00	5.51E+00	4.33E-02	3.80E+00	ND
	2	2.48E+01	1.42E+01	3.29E+00	1.66E+00	4.50E+00	1.65E-01	ND	ND
	2	2.66E+01	1.33E+01	3.59E+00	1.64E+00	4.37E+00	1.41E-01	ND	ND
	7	4.50E+01	4.40E+01	6.49E+00	2.86E+00	1.03E+01	9.86E-02	ND	ND
	7	4.77E+01	4.30E+01	6.46E+00	3.00E+00	1.05E+01	9.39E-02	ND	ND
Simulant 1, 2M	14	2.81E+01	4.83E+01	4.83E+00	2.34E+00	8.62E+00	7.34E-02	ND	ND
	14	2.81E+01	4.39E+01	4.64E+00	2.13E+00	7.80E+00	6.72E-02	ND	ND
	28	2.55E+01	5.79E+01	3.92E+00	2.61E+00	9.88E+00	4.77E-02	ND	ND
	28	2.75E+01	5.62E+01	4.31E+00	2.57E+00	9.64E+00	4.42E-02	ND	ND
	42	1.67E+01	5.71E+01	3.26E+00	2.62E+00	9.38E+00	4.72E-02	ND	ND
	42	1.79E+01	5.52E+01	3.23E+00	2.71E+00	9.36E+00	5.32E-02	ND	ND
	49	6.74E+00	3.81E+01	ND	2.12E+00	7.45E+00	5.90E-02	ND	ND
	49	7.23E+00	3.61E+01	ND	2.10E+00	7.28E+00	5.62E-02	ND	ND
	63	1.04E+01	4.49E+01	ND	2.48E+00	9.07E+00	4.51E-02	ND	ND
	63	1.05E+01	4.16E+01	ND	2.43E+00	8.73E+00	5.70E-02	ND	ND

Table 6.3 (contd)

Simulant	Cumulative Leaching Time (days)	Na (mg/L)	Ca (mg/L)	K (mg/L)	Al (mg/L)	Si (mg/L)	Mg (mg/L)	S (mg/L)	Fe (mg/L)
Simulant 1, 4M	0.08	3.36E+01	5.25E-01	ND	8.39E-01	ND	ND	7.96E+00	ND
	0.08	3.07E+01	6.46E-01	ND	6.51E-01	ND	1.20E-01	5.80E+00	ND
	1	9.71E+01	5.92E+00	5.42E+00	3.65E+00	6.69E+00	ND	6.92E+00	ND
	1	1.01E+02	6.16E+00	5.60E+00	3.82E+00	6.79E+00	3.50E-02	6.59E+00	ND
	2	4.68E+01	1.32E+01	3.28E+00	2.00E+00	5.32E+00	1.09E-01	ND	ND
	2	4.61E+01	1.31E+01	3.38E+00	2.18E+00	5.64E+00	1.19E-01	ND	ND
	7	7.62E+01	3.09E+01	6.09E+00	2.57E+00	8.31E+00	6.69E-02	ND	ND
	7	7.37E+01	3.00E+01	5.86E+00	2.50E+00	8.13E+00	4.97E-02	ND	ND
	14	4.63E+01	4.54E+01	4.56E+00	2.41E+00	8.36E+00	6.09E-02	ND	ND
	14	4.50E+01	4.33E+01	4.71E+00	2.28E+00	7.91E+00	7.09E-02	ND	ND
	28	4.28E+01	5.58E+01	4.14E+00	2.59E+00	9.16E+00	5.36E-02	ND	ND
	28	4.21E+01	5.71E+01	4.30E+00	2.63E+00	9.40E+00	5.23E-02	ND	ND
	42	2.72E+01	5.76E+01	3.02E+00	2.80E+00	9.80E+00	4.18E-02	ND	ND
	42	2.68E+01	5.78E+01	ND	2.86E+00	1.01E+01	4.31E-02	ND	ND
	49	1.12E+01	4.14E+01	ND	2.23E+00	8.03E+00	5.92E-02	ND	ND
	49	1.08E+01	4.07E+01	ND	2.22E+00	8.13E+00	6.64E-02	ND	ND
	63	1.61E+01	4.62E+01	ND	2.62E+00	9.48E+00	3.84E-02	ND	ND
	63	1.57E+01	4.53E+01	ND	2.65E+00	9.69E+00	3.74E-02	ND	ND
Simulant 1, 6M	0.08	5.73E+01	9.93E-01	ND	8.42E-01	ND	ND	1.29E+01	ND
	0.08	4.70E+01	5.80E-01	ND	5.35E-01	ND	ND	9.67E+00	ND
	1	1.70E+02	3.80E+00	6.31E+00	5.58E+00	7.50E+00	ND	1.94E+01	ND
	1	1.85E+02	3.78E+00	6.81E+00	5.44E+00	7.79E+00	ND	1.97E+01	ND
	2	8.11E+01	4.52E+00	4.06E+00	3.17E+00	6.67E+00	1.05E-01	3.90E+00	ND
	2	9.19E+01	8.03E+00	4.59E+00	3.33E+00	7.20E+00	6.26E-02	4.95E+00	ND
	7	1.30E+02	3.17E+01	7.92E+00	4.21E+00	1.27E+01	4.33E-02	6.25E+00	ND
	7	1.67E+02	3.32E+01	9.23E+00	4.77E+00	1.42E+01	3.83E-02	9.83E+00	ND
	14	7.25E+01	4.54E+01	5.72E+00	2.89E+00	9.15E+00	5.44E-02	ND	ND

Table 6.3 (contd)

Simulant	Cumulative Leaching Time (days)	Na (mg/L)	Ca (mg/L)	K (mg/L)	Al (mg/L)	Si (mg/L)	Mg (mg/L)	S (mg/L)	Fe (mg/L)
	14	8.08E+01	4.54E+01	6.09E+00	2.99E+00	9.57E+00	5.14E-02	3.94E+00	ND
	28	5.87E+01	5.62E+01	4.71E+00	2.81E+00	9.16E+00	4.32E-02	ND	ND
	28	6.94E+01	6.05E+01	5.37E+00	2.97E+00	9.87E+00	ND	3.99E+00	ND
	42	3.72E+01	5.61E+01	3.53E+00	2.45E+00	8.37E+00	3.93E-02	ND	ND
	42	4.09E+01	6.47E+01	3.77E+00	3.07E+00	1.03E+01	4.86E-02	3.56E+00	ND
	49	1.58E+01	4.97E+01	ND	2.48E+00	9.14E+00	4.91E-02	ND	ND
	49	1.76E+01	5.33E+01	ND	2.54E+00	9.59E+00	4.48E-02	ND	ND
	63	2.08E+01	5.35E+01	ND	2.76E+00	1.05E+01	ND	ND	ND
	63	2.20E+01	5.50E+01	ND	2.79E+00	1.08E+01	ND	ND	ND
	0.08	9.98E+01	5.77E-01	ND	2.23E+00	ND	ND	2.40E+01	ND
	0.08	1.05E+02	1.41E+00	ND	2.74E+00	ND	ND	2.64E+01	ND
	1	1.80E+02	3.99E+00	7.45E+00	6.12E+00	5.64E+00	3.61E-02	1.94E+01	ND
	1	1.88E+02	3.60E+00	7.44E+00	6.42E+00	5.40E+00	ND	2.19E+01	ND
	2	7.99E+01	1.35E+01	3.77E+00	3.03E+00	4.90E+00	8.38E-02	6.14E+00	ND
	2	7.90E+01	1.07E+01	3.96E+00	2.76E+00	4.28E+00	7.98E-02	5.48E+00	ND
	7	1.22E+02	3.79E+01	5.38E+00	4.43E+00	9.09E+00	5.86E-02	9.28E+00	ND
	7	1.04E+02	2.50E+01	4.85E+00	3.26E+00	6.26E+00	3.87E-02	7.75E+00	ND
Simulant 1, 8M	14	6.88E+01	4.21E+01	3.75E+00	3.11E+00	7.12E+00	4.89E-02	5.22E+00	ND
	14	7.63E+01	4.32E+01	4.07E+00	3.35E+00	7.59E+00	6.14E-02	5.99E+00	ND
	28	6.41E+01	4.92E+01	3.56E+00	3.28E+00	8.09E+00	3.88E-02	5.09E+00	ND
	28	6.95E+01	5.55E+01	3.74E+00	3.84E+00	1.00E+01	ND	5.53E+00	ND
	42	4.25E+01	4.58E+01	ND	2.95E+00	7.55E+00	5.78E-02	3.86E+00	ND
	42	4.61E+01	5.17E+01	3.03E+00	3.55E+00	9.17E+00	5.14E-02	4.49E+00	ND
	49	1.76E+01	3.58E+01	ND	2.63E+00	7.36E+00	7.65E-02	ND	ND
	49	1.76E+01	2.79E+01	ND	2.23E+00	6.33E+00	4.47E-02	ND	ND
	63	2.50E+01	3.81E+01	ND	3.12E+00	8.59E+00	4.31E-02	3.50E+00	ND
	63	2.67E+01	3.96E+01	ND	3.17E+00	8.86E+00	3.91E-02	3.71E+00	ND

Table 6.3 (contd)

Simulant	Cumulative Leaching Time (days)	Na (mg/L)	Ca (mg/L)	K (mg/L)	Al (mg/L)	Si (mg/L)	Mg (mg/L)	S (mg/L)	Fe (mg/L)
	0.08	1.35E+02	1.17E+00	3.81E+00	2.38E+00	ND	ND	2.92E+01	ND
	0.08	1.54E+02	1.20E+00	3.97E+00	2.98E+00	ND	ND	3.46E+01	ND
	1	2.48E+02	3.32E+00	8.46E+00	7.79E+00	5.46E+00	ND	3.50E+01	ND
	1	2.49E+02	3.20E+00	8.40E+00	7.69E+00	5.08E+00	ND	3.59E+01	ND
	2	1.16E+02	1.14E+01	4.59E+00	4.17E+00	5.95E+00	1.01E-01	1.17E+01	ND
	2	1.16E+02	9.89E+00	4.49E+00	3.82E+00	4.97E+00	5.56E-02	1.09E+01	ND
	7	1.47E+02	3.01E+01	5.47E+00	4.76E+00	8.45E+00	5.00E-02	1.47E+01	ND
	7	1.65E+02	2.86E+01	5.99E+00	5.02E+00	8.49E+00	5.59E-02	1.74E+01	ND
Simulant 1, 10M	14	9.36E+01	3.77E+01	4.23E+00	3.68E+00	6.62E+00	4.13E-02	8.27E+00	ND
	14	9.62E+01	3.74E+01	4.18E+00	3.65E+00	6.68E+00	3.74E-02	8.98E+00	ND
	28	8.77E+01	5.19E+01	3.91E+00	3.87E+00	8.63E+00	3.48E-02	7.46E+00	ND
	28	8.97E+01	4.66E+01	3.73E+00	3.50E+00	7.53E+00	6.32E-02	9.01E+00	ND
	42	5.55E+01	4.38E+01	3.30E+00	2.96E+00	6.13E+00	5.01E-02	5.69E+00	ND
	42	5.04E+01	4.30E+01	3.18E+00	2.69E+00	5.56E+00	6.70E-02	3.99E+00	ND
	49	2.42E+01	3.97E+01	ND	2.75E+00	7.44E+00	5.03E-02	ND	ND
	49	2.39E+01	3.86E+01	ND	2.84E+00	7.65E+00	6.03E-02	ND	ND
	63	3.29E+01	4.20E+01	ND	3.29E+00	8.72E+00	3.55E-02	4.42E+00	ND
	63	3.30E+01	4.47E+01	ND	3.41E+00	8.99E+00	ND	4.53E+00	ND
	0.08	2.73E+01	1.11E+00	ND	1.02E+00	ND	ND	6.65E+00	ND
	0.08	2.66E+01	9.09E-01	ND	9.55E-01	ND	ND	5.90E+00	ND
	1	5.10E+01	1.04E+01	6.20E+00	2.28E+00	5.23E+00	6.80E-02	ND	ND
	1	5.43E+01	1.02E+01	6.77E+00	2.36E+00	5.16E+00	5.59E-02	ND	ND
Simulant 2, 2M	2	2.23E+01	1.65E+01	3.00E+00	1.37E+00	4.04E+00	1.42E-01	ND	ND
	2	2.37E+01	1.28E+01	3.04E+00	1.47E+00	4.23E+00	1.44E-01	ND	ND
	7	3.25E+01	3.04E+01	4.11E+00	1.75E+00	5.76E+00	7.35E-02	ND	ND
	7	4.02E+01	4.28E+01	5.35E+00	2.59E+00	8.76E+00	9.42E-02	ND	1.17E-01
	14	2.31E+01	4.40E+01	3.62E+00	2.03E+00	7.28E+00	6.20E-02	ND	ND

Table 6.3 (contd)

Simulant	Cumulative Leaching Time (days)	Na (mg/L)	Ca (mg/L)	K (mg/L)	Al (mg/L)	Si (mg/L)	Mg (mg/L)	S (mg/L)	Fe (mg/L)
	14	2.35E+01	4.21E+01	3.26E+00	1.98E+00	6.80E+00	8.35E-02	ND	ND
	28	2.24E+01	5.19E+01	ND	2.34E+00	8.70E+00	4.08E-02	ND	ND
	28	2.21E+01	3.96E+01	ND	1.56E+00	5.77E+00	4.72E-02	ND	ND
	42	1.40E+01	4.97E+01	ND	2.60E+00	7.78E+00	6.18E-02	ND	ND
	42	1.43E+01	5.19E+01	ND	2.63E+00	7.89E+00	5.77E-02	ND	ND
	49	5.74E+00	3.28E+01	ND	2.05E+00	6.11E+00	9.17E-02	ND	ND
	49	5.53E+00	2.86E+01	ND	2.08E+00	6.43E+00	8.90E-02	ND	ND
	63	8.57E+00	3.71E+01	ND	2.42E+00	7.36E+00	7.57E-02	ND	ND
	63	8.56E+00	3.75E+01	ND	2.49E+00	7.62E+00	7.48E-02	ND	ND
	0.08	2.76E+01	8.26E-01	ND	1.41E+00	ND	ND	6.44E+00	ND
	0.08	2.89E+01	1.21E+00	ND	1.57E+00	ND	ND	6.42E+00	ND
	1	4.80E+01	9.55E+00	6.12E+00	2.51E+00	4.82E+00	6.72E-02	ND	ND
	1	4.87E+01	9.78E+00	6.39E+00	2.54E+00	4.76E+00	5.89E-02	ND	ND
	2	2.07E+01	1.68E+01	ND	1.42E+00	3.62E+00	1.35E-01	ND	ND
	2	1.95E+01	1.54E+01	ND	1.25E+00	3.27E+00	1.25E-01	ND	ND
	7	3.38E+01	4.06E+01	4.47E+00	2.38E+00	7.79E+00	1.32E-01	ND	ND
	7	3.91E+01	4.35E+01	5.39E+00	2.62E+00	8.67E+00	9.60E-02	ND	ND
Simulant 3, 2M	14	2.12E+01	4.12E+01	3.33E+00	2.08E+00	7.19E+00	7.89E-02	ND	ND
	14	2.15E+01	3.96E+01	3.35E+00	1.94E+00	6.81E+00	7.20E-02	ND	ND
	28	2.01E+01	4.67E+01	ND	2.27E+00	8.22E+00	6.48E-02	ND	ND
	28	2.13E+01	4.11E+01	ND	1.69E+00	6.35E+00	3.57E-02	ND	ND
	42	1.26E+01	4.48E+01	ND	2.59E+00	7.73E+00	5.82E-02	ND	ND
	42	1.34E+01	4.84E+01	ND	2.63E+00	8.26E+00	5.48E-02	ND	1.93E-01
	49	4.80E+00	2.80E+01	ND	1.97E+00	5.64E+00	8.86E-02	ND	ND
	49	5.19E+00	2.31E+01	ND	2.03E+00	5.96E+00	8.99E-02	ND	ND
	63	7.31E+00	3.14E+01	ND	2.39E+00	6.70E+00	9.06E-02	ND	ND
	63	7.36E+00	3.02E+01	ND	2.40E+00	6.89E+00	8.26E-02	ND	ND

Table 6.3 (contd)

Simulant	Cumulative Leaching Time (days)	Na (mg/L)	Ca (mg/L)	K (mg/L)	Al (mg/L)	Si (mg/L)	Mg (mg/L)	S (mg/L)	Fe (mg/L)
Simulant 4, 2M	0.08	2.46E+01	2.33E+00	3.21E+00	7.20E-01	ND	ND	ND	ND
	0.08	2.52E+01	2.84E+00	3.32E+00	7.81E-01	ND	ND	3.56E+00	ND
	1	4.16E+01	1.81E+01	6.67E+00	1.87E+00	3.36E+00	8.52E-02	ND	ND
	1	4.02E+01	1.84E+01	6.69E+00	1.85E+00	3.41E+00	9.37E-02	ND	ND
	2	1.68E+01	1.76E+01	ND	1.10E+00	2.75E+00	1.60E-01	ND	ND
	2	1.69E+01	1.92E+01	ND	1.21E+00	3.20E+00	1.72E-01	ND	ND
	7	2.87E+01	3.99E+01	4.04E+00	2.30E+00	6.71E+00	1.46E-01	ND	ND
	7	2.98E+01	4.25E+01	4.31E+00	2.47E+00	7.55E+00	1.49E-01	ND	ND
	14	1.64E+01	3.72E+01	ND	2.00E+00	5.99E+00	1.05E-01	ND	ND
	14	1.60E+01	3.63E+01	ND	1.91E+00	5.83E+00	1.03E-01	ND	ND
	28	1.60E+01	4.13E+01	ND	2.39E+00	7.01E+00	7.83E-02	ND	ND
	28	1.58E+01	4.33E+01	ND	2.39E+00	7.13E+00	7.82E-02	ND	ND
	42	1.03E+01	3.55E+01	ND	2.26E+00	5.95E+00	6.40E-02	ND	ND
	42	1.00E+01	3.53E+01	ND	2.29E+00	5.86E+00	7.38E-02	ND	ND
	49	4.14E+00	2.44E+01	ND	2.13E+00	4.43E+00	1.15E-01	ND	ND
	49	4.20E+00	2.21E+01	ND	2.15E+00	ND	ND	ND	ND
	63	6.30E+00	2.85E+01	ND	2.54E+00	5.49E+00	1.11E-01	ND	ND
	63	6.15E+00	2.64E+01	ND	2.50E+00	5.41E+00	1.46E-01	ND	ND

Table 6.4. The Concentrations of Major Anions and ^{99}Tc and [127]I in Leachates from EPA Draft Method 1315

Simulant	Cumulative leaching time (days)	NO_3^- (mg/L)	PO_4^{3-} (mg/L)	PO_4^{3-} (mg/L)[a]	SO_4^{2-} (mg/L)	SO_4^{2-} (mg/L)[a]	I^- (µg/L)	Tc (µg/L)
Simulant 1, 2M	0.08	ND	ND	ND	ND	1.55E+01	ND	1.03E-02
	0.08	ND	ND	ND	1.57E+01	2.23E+01	ND	1.69E-02
	1	1.74E+01	ND	ND	ND	1.39E+01	1.52E+00	3.93E-02
	1	2.03E+01	ND	ND	ND	1.14E+01	2.18E+00	4.98E-02
	2	ND	ND	ND	ND	ND	5.89E-01	1.88E-02
	2	ND	ND	ND	ND	ND	7.34E-01	1.93E-02
	7	1.66E+01	ND	ND	ND	ND	1.45E+00	1.83E-02
	7	1.88E+01	ND	ND	ND	ND	1.58E+00	1.11E-02
	14	1.50E+01	ND	ND	ND	ND	ND	ND
	14	1.12E+01	ND	ND	ND	ND	ND	ND
	28	9.60E+00	ND	ND	1.68E+00	ND	ND	ND
	28	ND	ND	ND	ND	ND	1.11E+00	ND
	42	5.81E+00	ND	ND	1.63E+00	ND	ND	ND
	42	6.24E+00	ND	ND	1.57E+00	ND	ND	ND
	49	2.20E+00	ND	ND	ND	ND	ND	ND
	49	2.36E+00	ND	ND	ND	ND	ND	ND
	63	3.57E+00	ND	ND	ND	ND	ND	ND
	63	3.28E+00	ND	ND	ND	ND	ND	ND
Simulant 1, 4M	0.08	2.43E+01	ND	ND	1.70E+01	2.39E+01	1.02E+00	3.19E-02
	0.08	1.98E+01	ND	ND	ND	1.74E+01	ND	3.04E-02
	1	6.03E+01	ND	ND	1.57E+01	2.08E+01	3.15E+00	1.30E-01
	1	5.66E+01	ND	ND	1.54E+01	1.98E+01	3.25E+00	1.22E-01
	2	2.68E+01	ND	ND	ND	ND	1.22E+00	6.14E-02
	2	2.53E+01	ND	ND	ND	ND	1.17E+00	5.46E-02
	7	4.48E+01	ND	ND	ND	ND	2.26E+00	5.81E-02
	7	4.28E+01	ND	ND	ND	ND	2.18E+00	5.35E-02
	14	2.63E+01	ND	ND	ND	ND	ND	4.70E-03
	14	2.51E+01	ND	ND	ND	ND	ND	6.46E-03
	28	2.00E+01	ND	ND	ND	ND	1.47E+00	7.91E-03
	28	1.90E+01	ND	ND	ND	ND	1.33E+00	8.34E-03
	42	ND	ND	ND	ND	ND	ND	4.79E-03
	42	ND	ND	ND	ND	ND	ND	5.18E-03
	49	3.98E+00	ND	ND	ND	ND	ND	ND
	49	3.71E+00	ND	ND	ND	ND	ND	ND
	63	5.43E+00	ND	ND	1.66E+00	ND	ND	ND
	63	5.05E+00	ND	ND	ND	ND	ND	ND

Table 6.4 (contd)

Simulant	Cumulative Leaching Time (days)	NO_3^- (mg/L)	PO_4^{3-} (mg/L)	PO_4^{3-} (mg/L)[a]	SO_4^{2-} (mg/L)	SO_4^{2-} (mg/L)[a]	I^- (μg/L)	Tc (μg/L)
Simulant 1, 6M	0.08	6.32E+01	ND	ND	3.35E+01	3.87E+01	2.29E+00	1.10E-01
	0.08	5.26E+01	ND	ND	2.35E+01	2.90E+01	1.63E+00	8.37E-02
	1	1.42E+02	ND	ND	4.80E+01	5.82E+01	5.72E+00	3.15E-01
	1	1.53E+02	2.72E+01	ND	7.74E+01	5.91E+01	6.50E+00	3.46E-01
	2	5.13E+01	ND	ND	ND	1.17E+01	2.25E+00	1.16E-01
	2	6.13E+01	ND	ND	ND	1.49E+01	3.07E+00	1.38E-01
	7	8.84E+01	ND	ND	ND	1.88E+01	3.81E+00	1.07E-01
	7	1.11E+02	ND	ND	1.98E+01	2.95E+01	4.87E+00	1.57E-01
	14	4.13E+01	ND	ND	ND	ND	ND	1.80E-02
	14	4.79E+01	ND	ND	ND	1.18E+01	ND	1.81E-02
	28	2.78E+01	ND	ND	ND	ND	1.62E+00	1.88E-02
	28	3.25E+01	ND	ND	ND	1.20E+01	1.97E+00	1.87E-02
	42	1.24E+01	ND	ND	ND	ND	ND	1.25E-02
	42	1.44E+01	ND	ND	ND	1.07E+01	ND	1.44E-02
	49	4.88E+00	ND	ND	2.20E+00	ND	ND	4.75E-03
	49	5.39E+00	ND	ND	2.57E+00	ND	ND	4.48E-03
	63	6.20E+00	ND	ND	3.34E+00	ND	ND	8.27E-03
	63	6.76E+00		ND	3.88E+00	ND	ND	7.60E-03
Simulant 1, 8M	0.08	9.81E+01	ND	ND	6.26E+01	7.20E+01	3.20E+00	9.34E-02
	0.08	1.10E+02	ND	ND	6.77E+01	7.92E+01	4.06E+00	1.18E-01
	1	1.48E+02	ND	ND	4.96E+01	5.82E+01	6.11E+00	1.88E-01
	1	1.51E+02	ND	ND	5.50E+01	6.57E+01	6.16E+00	2.07E-01
	2	6.11E+01	ND	ND	ND	1.84E+01	2.60E+00	6.78E-02
	2	5.73E+01	ND	ND	ND	1.64E+01	2.27E+00	6.74E-02
	7	7.88E+01	ND	ND	2.17E+01	2.78E+01	3.11E+00	5.18E-02
	7	6.96E+01	ND	ND	1.73E+01	2.33E+01	2.71E+00	4.75E-02
	14	3.53E+01	ND	ND	ND	1.57E+01	ND	3.06E-02
	14	3.93E+01	ND	ND	ND	1.80E+01	ND	3.44E-02
	28	2.41E+01	ND	ND	ND	1.53E+01	ND	3.98E-02
	28	2.65E+01	ND	ND	ND	1.66E+01	1.36E+00	4.28E-02
	42	1.20E+01	ND	ND	ND	1.16E+01	ND	3.14E-02
	42	1.30E+01	ND	ND	ND	1.35E+01	ND	3.13E-02
	49	5.33E+00	ND	ND	4.28E+00	ND	ND	1.26E-02
	49	4.80E+00	ND	ND	4.03E+00	ND	ND	1.15E-02
	63	6.96E+00	ND	ND	7.28E+00	1.05E+01	ND	2.27E-02
	63	7.31E+00	ND	ND	7.82E+00	1.11E+01	ND	2.28E-02
Simulant 1, 10M	0.08	1.72E+02	ND	ND	7.95E+01	8.76E+01	5.72E+00	1.96E-01
	0.08	1.93E+02	ND	ND	9.30E+01	1.04E+02	6.45E+00	2.30E-01

Table 6.4 (contd)

Simulant	Cumulative Leaching Time (days)	NO_3^- (mg/L)	PO_4^{3-} (mg/L)	PO_4^{3-} (mg/L)[a]	SO_4^{2-} (mg/L)	SO_4^{2-} (mg/L)[a]	I^- (µg/L)	Tc (µg/L)
	1	2.26E+02	ND	ND	9.35E+01	1.05E+02	1.01E+01	3.01E-01
	1	2.32E+02	ND	ND	9.56E+01	1.08E+02	9.45E+00	3.27E-01
	2	8.24E+01	ND	ND	3.05E+01	3.51E+01	3.05E+00	9.95E-02
	2	7.82E+01	ND	ND	2.82E+01	3.27E+01	2.77E+00	9.42E-02
	7	9.30E+01	ND	ND	3.77E+01	4.41E+01	3.44E+00	9.90E-02
	7	9.21E+01	ND	ND	3.71E+01	5.22E+01	3.75E+00	1.11E-01
	14	4.72E+01	ND	ND	2.25E+01	2.48E+01	ND	7.26E-02
	14	4.77E+01	ND	ND	2.33E+01	2.69E+01	ND	7.48E-02
	28	3.45E+01	ND	ND	2.06E+01	2.24E+01	ND	8.59E-02
	28	3.40E+01	ND	ND	2.07E+01	2.70E+01	ND	9.23E-02
	42	1.89E+01	ND	ND	ND	1.71E+01	1.11E+00	6.41E-02
	42	1.54E+01	ND	ND	ND	1.20E+01	1.16E+00	5.47E-02
	49	7.60E+00	ND	ND	6.27E+00	ND	ND	2.80E-02
	49	ND	ND	ND	ND	ND	ND	2.86E-02
	63	1.05E+01	ND	ND	1.05E+01	1.33E+01	ND	4.45E-02
	63	1.03E+01	ND	ND	1.10E+01	1.36E+01	ND	4.84E-02
	0.08	ND	ND	ND	ND	2.00E+01	ND	9.93E-03
	0.08	ND	ND	ND	ND	1.77E+01	ND	1.06E-02
	1	ND	ND	ND	ND	ND	7.12E-01	3.35E-02
	1	ND	ND	ND	ND	ND	8.90E-01	3.49E-02
	2	ND	ND	ND	ND	ND	ND	1.60E-02
	2	ND	ND	ND	ND	ND	ND	1.64E-02
	7	ND	ND	ND	ND	ND	ND	8.87E-03
	7	ND	ND	ND	ND	ND	5.58E-01	1.18E-02
Simulant 2, 2M	14	ND	ND	ND	ND	ND	ND	ND
	14	ND	ND	ND	ND	ND	ND	ND
	28	3.69E+00	ND	ND	1.62E+00	ND	ND	ND
	28	4.36E+00	ND	ND	1.70E+00	ND	ND	ND
	42	2.24E+00	ND	ND	1.65E+00	ND	ND	ND
	42	2.48E+00	ND	ND	1.54E+00	ND	ND	ND
	49	ND	ND	ND	ND	ND	ND	ND
	49	ND	ND	ND	ND	ND	ND	ND
	63	1.24E+00	ND	ND	1.80E+00	ND	ND	ND
	63	1.29E+00	ND	ND	1.79E+00	ND	ND	ND
	0.08	ND	ND	ND	ND	1.93E+01	1.04E+00	2.79E-02
	0.08	ND	ND	ND	ND	1.93E+01	ND	2.24E-02
Simulant 3, 2M	1	1.82E+01	ND	ND	ND	ND	1.35E+00	6.98E-02
	1	1.77E+01	ND	ND	ND	ND	1.24E+00	6.11E-02
	2	ND	ND	ND	ND	ND	ND	2.56E-02

Table 6.4 (contd)

Simulant	Cumulative Leaching Time (days)	NO_3^- (mg/L)	PO_4^{3-} (mg/L)	PO_4^{3-} (mg/L)[a]	SO_4^{2-} (mg/L)	SO_4^{2-} (mg/L)[a]	I^- (µg/L)	Tc (µg/L)
	2	ND	ND	ND	ND	ND	ND	2.12E-02
	7	1.57E+01	ND	ND	ND	ND	8.55E-01	9.49E-03
	7	1.77E+01	ND	ND	ND	ND	1.01E+00	8.52E-03
	14	ND	ND	ND	ND	ND	ND	ND
	14	1.02E+01	ND	ND	ND	ND	ND	ND
	28	8.37E+00	ND	ND	ND	ND	ND	6.52E-03
	28	8.60E+00	ND	ND	ND	ND	ND	4.21E-03
	42	4.85E+00	ND	ND	ND	ND	2.32E+00	5.79E-03
	42	5.15E+00	ND	ND	ND	ND	2.61E+00	4.37E-03
	49	1.78E+00	ND	ND	ND	ND	ND	ND
	49	1.90E+00	ND	ND	ND	ND	ND	ND
	63	2.50E+00	ND	ND	1.66E+00	ND	ND	ND
	63	2.58E+00	ND	ND	1.70E+00	ND	ND	ND
	0.08	2.66E+01	ND	ND	ND	ND	3.50E+00	1.77E+00
	0.08	2.51E+01	ND	ND	ND	1.07E+01	3.25E+00	1.54E+00
	1	4.69E+01	ND	ND	ND	ND	6.62E+00	6.31E+00
	1	4.38E+01	ND	ND	ND	ND	6.30E+00	5.29E+00
	2	1.85E+01	ND	ND	ND	ND	4.50E+00	9.22E-01
	2	1.88E+01	ND	ND	ND	ND	3.41E+00	7.52E-01
	7	3.41E+01	ND	ND	ND	ND	4.36E+00	1.04E+00
	7	3.47E+01	ND	ND	ND	ND	4.61E+00	1.02E+00
Simulant 4, 2M	14	2.01E+01	ND	ND	ND	ND	ND	6.69E-01
	14	1.86E+01	ND	ND	ND	ND	ND	5.92E-01
	28	1.68E+01	ND	ND	ND	ND	2.01E+00	6.87E-01
	28	1.58E+01	ND	ND	ND	ND	1.59E+00	6.23E-01
	42	1.04E+01	ND	ND	ND	ND	3.30E+00	4.83E-01
	42	ND	ND	ND	ND	ND	3.26E+00	4.30E-01
	49	4.61E+00	ND	ND	2.25E+00	ND	ND	2.08E-01
	49	4.41E+00	ND	ND	2.35E+00	ND	ND	2.02E-01
	63	6.63E+00	ND	ND	3.31E+00	ND	6.94E-01	3.75E-01
	63	6.41E+00	ND	ND	3.42E+00	ND	6.57E-01	3.37E-01

(a) PO_4^{3-} and SO_4^{2-} were also calculated based on P and S concentrations analyzed by ICP-OES. ND indicates "not detected" below quantification level.

The effective diffusivity and LI of technetium for all eight different waste simulants used in Cast Stone prepared with different simulants are shown in Figure 6.5 through Figure 6.8. The diffusivity showed a sharp decrease over time for all of the different waste simulants up to 14 days followed by a slow decreasing trend up to 63 days. The diffusivity for Cast Stone specimens prepared with simulants S1 (2M), S2, and S3 were calculated to be $< 2.3 \times 10^{-11}$ cm^2/s for 14 through 63 days. The leachate

concentrations were below the estimated quantitation limit (EQL) so the diffusivities were calculated based on the EQL and are reported as less than values. For the S1 (4 M) Cast Stone specimens, the diffusivities were $<1.5 \times 10^{-11}$ cm^2/s for 49 and 63 days. The Cast Stone specimens prepared with the S1 simulant 6 M, 8 M, and 10 M showed technetium diffusivities (1.4×10^{-11} cm^2/s, 3.9×10^{-11} cm^2/s, and 1.4×10^{-10} cm^2/s, respectively over 14-63 days) that increased with increasing simulant concentration. Interestingly, the Cast Stone specimens prepared with the higher ionic strength S4 simulant showed the lowest technetium diffusivity, averaging 6.5×10^{-13} cm^2/s from 14 to 63 days.

The increase in the diffusivity as the S1 simulant concentrations increased or waste loadings increased is consistent with the results for the major cations, EC, and anions. Similarly, the percentage of technetium leached into solution increased as the S1 simulant concentration increased. An increasing technetium effective diffusivity or a decrease in the LI for technetium was found as the concentration of simulant S1 increased from 2 M to 10 M sodium (Figure 6.7and Figure 6.8), which is similar to the results found in EPA Draft Methods 1313 and 1316 (EPA 2009a, 2009c) leachates after 24 hours of contact between the powdered Cast Stone and DIW. Most of the calculated LI values for technetium based on the 63-day leach samples resulted in LI values higher than 10.0, suggesting that Cast Stone is a viable waste form candidate for the secondary liquid waste streams based on past performance assessment predictions for how well waste forms disposed into the IDF must perform (see Mann et al. 2003 for details).
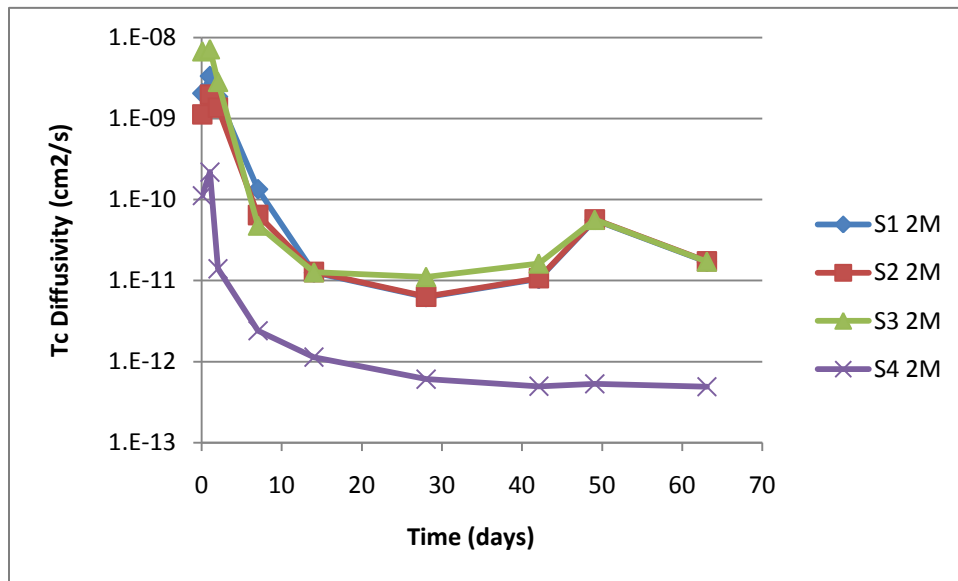

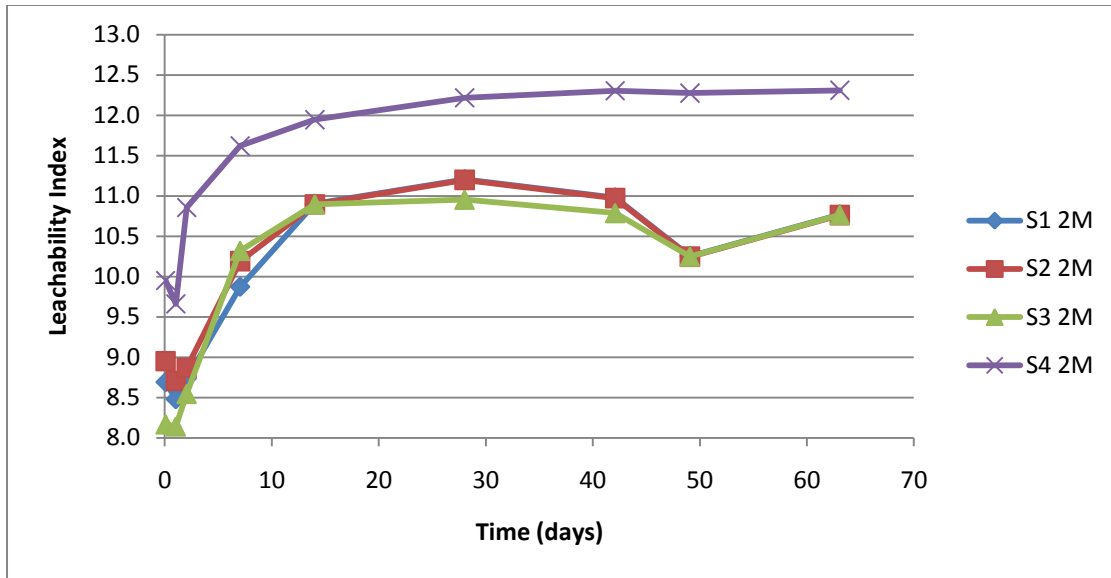**Figure 6.5.** Technetium Diffusivity of Simulants S1 to S4

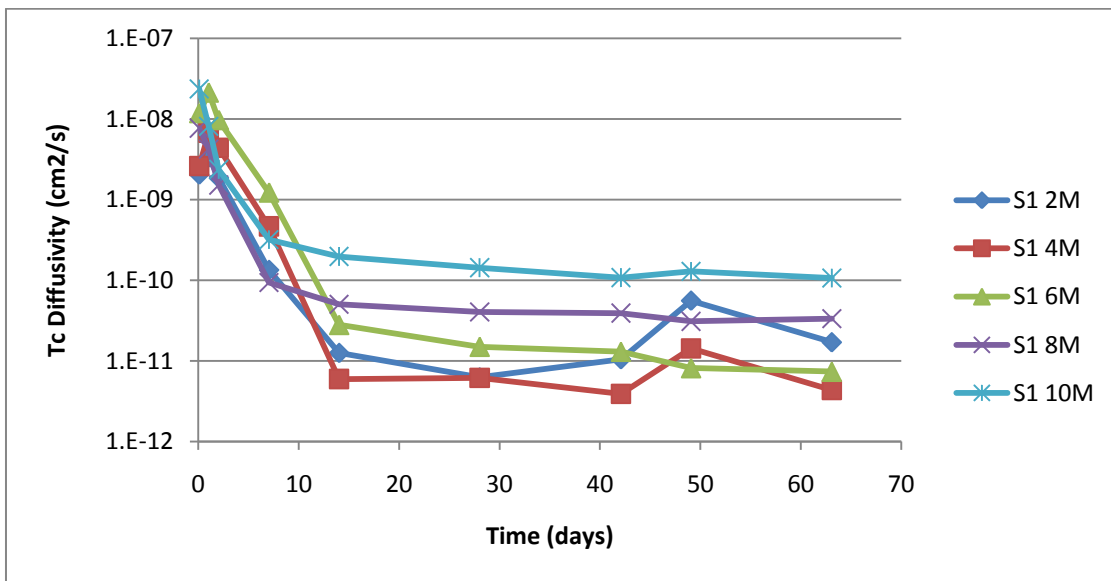**Figure 6.6**. LI of Technetium in Cast Stone Prepared with Simulants S1 to S4

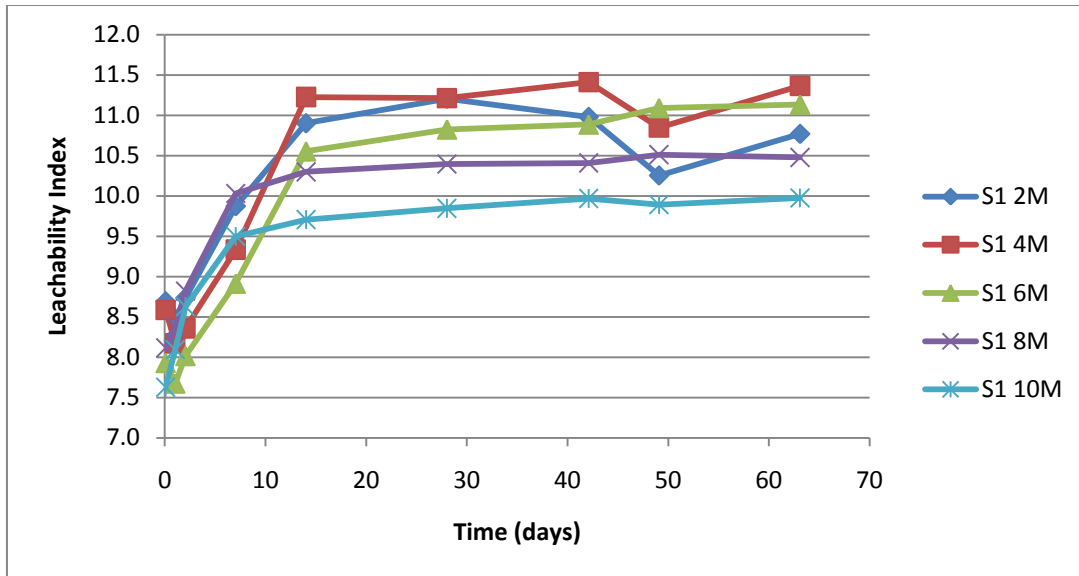**Figure 6.7**. Technetium Diffusivity of Simulant S1 over 2- to 10-M Concentration

Figure 6.8. Leaching Index of Simulant S1 over 2- to 10-M Concentration

6.4   Effect of pH on Leachability—EPA Draft Method 1313

EPA Draft Method 1313, *Leaching Test (Liquid-Solid Partitioning as a Function of Extract pH) of Constituents in Solid Materials Using a Parallel Batch Extraction Test* (EPA 2009a) evaluates the leachability of the waste form and the range of the solution pH.

6.4.1   EPA Draft Method 1313 Methodology

The EPA Draft Method 1313 is a static test where a set of parallel extraction experiments is conducted in dilute acid or base with DIW at a fixed pH (pH range from 4 to 12) and a liquid-to-solid ratio (10 mL/g) (EPA 2009a). Because the measured pH of the leachate solutions for Cast Stone powdered samples (before adding acid) were high (pH ~12 to 13) and similar to previous Phase 1 Cast Stone results, a pre-titration developed for Phase 1 Cast Stone was used to adjust the pHs by adding HNO_3 to lower the pH and achieve the targeted pH values after 24 hours of equilibration. Analytical grade HNO_3 (Optima) was used to prepare a solution of 2 N HNO_3 for these experiments. Based upon the pre-titration results, test samples were prepared by mixing 10 g of <0.3-mm sized material with a predetermined amount of 2 N HNO_3 and bringing the samples to volume with DIW. All samples were placed on a platform shaker and allowed to mix at room temperature (23 ±2°C) for 24 hours. After the 24-hour contact time was complete, the slurry samples were centrifuged and filtered with a syringe filter (0.45-μm size polypropylene membrane). The filtrate was used to measure the solution pH, electrical conductivity, and redox potential and was then submitted for additional chemical analyses of the filtrates. An example of the container used in EPA Draft Methods 1313 and 1316 (EPA 2009a, 2009c) tests is shown in Figure 6.9.
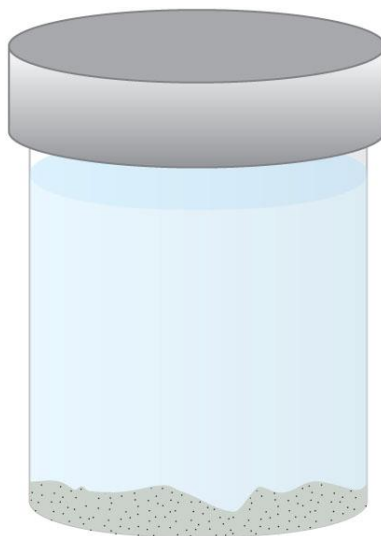
Figure 6.9. Schematic of Static Container Used to Conduct the EPA 1313 and 1316 Test Draft Methods

The measured moisture content and Brunauer-Emmett-Teller (BET) surface area of powdered Cast Stone samples used for EPA Draft Methods 1313 and 1316 (EPA 2009a, 2009c) are shown in Table 6.5. The moisture content showed a very narrow range between 16 and 19 (weight %), and there was no significant difference observed in Cast Stone samples prepared with the different simulant compositions and concentrations. The measured BET specific surface area was also similar (between 14.0 and 18.6 m^2/g) for the <0.3-mm Cast Stone waste forms that were prepared with different secondary waste simulants. The powdered samples also showed slightly lower surface areas compared to that measured on a chunk of Cast Stone from each waste form, which has a surface area from 21 –25 m^2/g (see Figures 6.28 and 6.29 in Section 6.7). Even though the powdered samples (<0.3 mm) have a smaller PSD compared to the chunk samples, the slightly higher surface area measured in the chunk of monolith sample suggests that more internal pores are present in the larger samples, including the chunk or cylindrical monolith.

Table 6.5. Moisture Content and Surface Area of Powdered Cast Stone for EPA Draft Method 1313 and 1316 Tests[a]

Cast Stone	Specific Surface Area (m^2/g) of Powder Sample by N_2-BET	Average Geometric Surface Area of Monolith (cm^2)	Moisture Content (weight fraction)
S1-2 M	17.1±0.04	186.4	0.16
S1-4 M	15.0±0.04	187.1	0.14
S1-6 M	18.2±0.05	191.1	0.16
S1-8 M	18.3±0.05	192.5	0.18
S1-10 M	18.6±0.04	187.8	0.19
S2-2 M	14.0±0.04	185.0	0.16
S3-2 M	16.6±0.05	184.7	0.18
S4-2 M	17.6±0.06	183.4	0.18

(a) EPA 2009a, 2009c, respectively.

6.4.2   Effect of pH on Leachability Results

Because a secondary waste simulant recipe used to prepare Cast Stone waste forms in Phase 2 are similar to the recipe used in Phase 1, the pre-titration step used for EPA Draft Method 1313 (EPA 2009a)

was not performed for the Phase 2 Cast Stone testing. The pre-titration curve developed for Cast Stone in Phase 1 was used to estimate the amount of acid needed to maintain the equilibrating solution at the various target pH values, which ranged between 4 and 12 in EPA Draft Method 1313. Because high-alkaline solutions (pH >12) are found after equilibrating a subsample of all Cast Stone samples with DIW for 24 hours, only acid (2N HNO_3) is needed to reach the desired pH target values. Therefore, crushed Cast Stone Phase 2 test samples were prepared by mixing 10 g of <0.3-mm sized material with 100 mL DIW to create the desired 10 mL/g of solid test ratio. The Phase 2 samples were allowed to react for 24 hours, and the resulting solutions were measured for pH, EC, Eh, alkalinity, and technetium concentrations (Table 6.6).

The alkalinity (as mg/L $CaCO_3$) of the leachate solutions decreased with decreasing pH for the Cast Stone Phase 2 samples prepared with the different simulants. However, the alkalinity values increased as the concentration of simulant S1 increased from 2 M to 10 M sodium. Irrespective of the pH range, the Cast Stone prepared with the higher concentration of simulant S1 showed higher alkalinity values because of a higher mass of caustic present in simulant S1 as its concentration increased from 2 to 10 M sodium. Cast Stone samples prepared with simulant S2 at a 2-M basis showed higher alkalinity than that of simulant S1 at a 2-M basis because of the higher CO_3^{2-} concentration in simulant S2. The lower alkalinity found in simulant S4 at a 2-M basis than simulant S2 at a 2-M basis is attributed to lower CO_3^{2-} concentration and the presence of NH_4^+ ion in simulant S4 (see Table 2.1 for chemical composition of simulants). The measured EC values represent the concentration of dissolved ions (or salts) in solution, so the higher EC values observed at low pH conditions of Cast Stone prepared with the different simulants are indicative of more dissolved ions present in solution at a low pH condition; that is, the acid treatment is dissolving some of the Cast Stone solid. The measured EC values also increased as the concentration of simulant S1 increased from 2 to 10 M sodium. Higher EC values were found in Cast Stone that was prepared with simulant S1 at a 10-M basis because the Cast Stone pore water likely contained a higher ionic strength, and there were more easily dissolvable precipitates or salts in the solid phase that redissolved from the acid attack. The measured Eh values for the EPA Draft Method 1313 (EPA 2009a) leachates for each Cast Stone prepared with the different simulants showed slightly increasing Eh values as the pH decreased in most of the samples. However, the degree of decreasing Eh as increasing pH was minor, and all the measured Eh values showed positive values, indicative of relatively oxidizing conditions. Based on the Eh values and an examination of the Eh-pH diagrams for ^{99}Tc from Phase 1, the dominant ^{99}Tc species observed at high pH is the pertechnetate ion, $Tc(VII)O_4^-$. Decreasing Eh values were found as the concentration of simulant S1 increased from 2 M to 10 M. Lower Eh values were also observed in the Cast Stone prepared with simulant S2, S3, and S4, perhaps because of the different simulant compositions. However, measuring the Eh of the Cast Stone eluents, which are not well poised (contain low concentrations of species with known redox active couples) in the open air is difficult. In addition, the data quality is very questionable because atmospheric oxygen can diffuse into the unpoised samples and cause the Eh values to continuously change.

Table 6.6. The Values of pH, EC, Eh, Alkalinity, and Tc of Cast Stone Waste Forms Measured from EPA Draft Method 1313

Cast Stone with Different Simulants	pH	EC (mS/cm)	Eh (mV)	Alkalinity (mg/L CaCO$_3$)	Tc* (µg of Tc/ g of solid)	Percent Tc Leached
Simulant 1, 2 M	12.3	5.98	241	1150	ND (<0.008)	< 49%
	12.9	5.93	241	1131	ND (<0.008)	< 49%
	10.6	19.1	264	78.2	ND (<0.008)	< 49%
	9.56	32.2	236	59.0	ND (<0.008)	< 49%
	10.1	25.0	229	63.9	ND (<0.008)	< 49%
	7.81	44.1	227	94.1	ND (<0.008)	< 49%
	7.30	43.2	226	22.1	ND (<0.008)	< 49%
	5.34	62.3	223	54.7	ND (<0.008)	< 49%
	3.41	73.6	260	NM	ND (<0.008)	< 49%
	4.14	69.1	240	NM	ND (<0.008)	< 49%
Simulant 1, 4 M	12.4	7.80	213	1402	0.0135	42%
	12.3	7.47	218	1357	0.0131	41%
	9.00	33.6	215	54.3	0.0177	55%
	8.88	34.4	218	59.9	0.0168	52%
	7.55	44.1	220	146	0.0116	36%
	7.57	43.9	219	160	0.0104	32%
	5.23	32.8	212	38.3	0.0078	24%
	4.94	33.0	217	17.5	0.00836	26%
	4.01	36.4	230	NM	ND (<0.008)	< 25%
	3.75	67.9	240	NM	ND (<0.008)	< 25%
Simulant 1, 6 M	12.4	9.58	171	1561	0.0191	41%
	12.3	5.07	169	1534	0.0168	36%
	8.91	34.9	164	53.2	0.0236	51%
	8.78	35.2	166	53.2	0.0219	47%
	7.16	45.6	163	245	0.0169	36%
	7.51	23.7	162	141	0.017	36%
	4.48	64.1	164	NM	0.0116	25%
	4.96	63.4	163	35.8	0.0114	24%
	3.83	36.9	161	NM	0.0102	22%
	3.98	69.2	162	NM	0.012	26%
Simulant 1, 8 M	12.4	11.4	172	1591	0.032	51%
	12.3	7.85	173	1572	0.0308	49%
	8.68	37.6	166	49.0	0.038	61%
	8.93	19.6	166	43.7	0.0346	55%
	7.14	25.2	170	283	0.0318	51%
	7.23	47.6	168	251	0.0248	40%
	5.55	66.4	168	77.1	0.0182	29%
	5.53	64.6	167	20.3	0.0166	27%
	4.04	72.7	169	NM	0.0139	22%
	4.35	72.5	168	NM	0.0174	28%

Table 6.6 (contd)

Cast Stone with Different Simulants	pH	EC (mS/cm)	Eh (mV)	Alkalinity (mg/L CaCO$_3$)	Tc* (µg of Tc/ g of solid)	Percent Tc Leached
Simulant 1, 10 M	12.4	12.4	134	1738	0.0309	42%
	12.3	6.87	118	1700	0.0267	36%
	8.64	20.1	127	60.1	0.0354	48%
	8.76	37.9	138	60.9	0.0356	48%
	7.26	25.2	146	251	0.0295	40%
	7.53	47.9	144	177	0.0271	36%
	4.92	65.5	144	10.9	0.0198	27%
	5.19	66.0	148	69.6	0.0226	30%
	3.62	38.7	176	NM	0.0203	27%
	3.78	72.3	181	NM	0.0193	26%
Simulant 2, 2 M	12.3	5.79	171	1213	ND (<0.008)	< 49%
	12.2	5.62	174	1142	ND (<0.008)	< 49%
	9.09	21.0	184	54.9	0.00845	52%
	9.10	32.8	186	49.4	ND (<0.008)	< 49%
	7.53	23.1	178	215	ND (<0.008)	< 49%
	7.24	43.5	178	251	ND (<0.008)	< 49%
	5.12	32.8	172	25.6	ND (<0.008)	< 49%
	5.32	61.6	175	10.2	ND (<0.008)	< 49%
	3.70	36.0	171	NM	ND (<0.008)	< 49%
	4.26	66.9	187	NM	ND (<0.008)	< 49%
Simulant 3, 2 M	12.1	4.53	179	863	ND (<0.008)	< 50%
	12.1	2.46	176	852	ND (<0.008)	< 50%
	7.74	32.3	174	111	0.00807	50%
	8.28	33.9	175	46.0	ND (<0.008)	< 50%
	6.52	23.4	193	560	ND (<0.008)	< 50%
	6.76	43.7	195	383	ND (<0.008)	< 50%
	5.83	32.6	192	185	ND (<0.008)	< 50%
	5.72	62.0	192	27.0	ND (<0.008)	< 50%
	5.19	69.7	177	25.6	ND (<0.008)	< 50%
	5.17	69.2	163	63.5	ND (<0.008)	< 50%
Simulant 4, 2 M	12.2	6.19	148	988	3.53	43%
	12.3	6.03	143	954	2.78	34%
	9.14	34.9	162	47.9	3.44	42%
	9.17	35.2	162	49.4	3.62	44%
	7.74	44.4	161	194	1.83	22%
	7.35	45.6	161	319	2.86	35%
	5.94	64.0	154	63.5	1.58	19%
	5.88	60.9	154	20.9	1.7	21%
	4.25	69.7	176	NM	1.42	17%
	4.56	70.2	158	8.29	1.4	17%

NM= Not measured - indicates sample pH was too low to measure alkalinity.

ND= Not detected by ICP-MS because of low technetium concentration below detection limit (0.8 µG/L *or* 0.008 µg/g).

Tc* = The percentage of total leached technetium is shown in the next column.

The measured concentration of technetium in the EPA Draft Method 1313 (EPA 2009a) leachates and the percentage of total technetium that leaches from the Cast Stone samples made with different simulants are shown as a function of pH in Table 6.6 and Figure 6.10. Technetium concentrations in the leachates were below the EQL for the Cast Stone prepared with simulants S1 (2 M), S2, and S3. Most of the EPA Draft Method 1313 leachates collected for these simulant conditions were below the detection limit—0.8 µg of Tc/L or 0.008 µg of Tc/g of solid. Even though the Cast Stone with simulant S4 at a 2-M basis had the same sodium concentration as simulants S1, S2, and S3 at 2 M, the Cast Stone with simulant S4 at a 2-M basis showed the highest leachable technetium concentration. The highest leached technetium concentration found in simulant S4 is attributed to a higher initial technetium concentration, 8.2 µg/g, compared to other initial technetium concentrations (0.016 to 0.074 µg/g) in simulants S1 (2M-10M), S2, and S3. An approximately two orders of magnitude higher technetium initial concentration in simulant S4 resulted in a much higher leachable technetium concentration from the Cast Stone prepared with simulant S4 than the other simulants. The percentage of the leachable amount of technetium ranged from 17 to 44 wt% in simulant S4, with the leached fraction of technetium decreasing as the pH decreased. Lower percent technetium leached as pH conditions decreased were also observed in simulant S1 with high sodium concentrations, 4 to 10 M. Decreased technetium leaching at lower pH conditions is attributed to the possibility of enhanced technetium sorption onto the Cast Stone solids at low pH conditions. Gradually increasing leachable technetium concentrations were observed as the pH increased in most of the samples for pH values between 3.5 up to less than 10.0 (Figure 6.10). At pH values higher than 10.0, the leachable technetium concentration dropped or became constant, which is similar to the results found in Phase 1 EPA Draft Method 1313 (EPA 2009a) results for Cast Stone and Geopolymer testing results (see Pierce et al. 2010a). The trend of decreasing or constant technetium leaching has been attributed to carbonation processes that result in calcite precipitates forming onto and perhaps inside the pore spaces of the Cast Stone at a high pH above 10.0. Because higher EC values were found in the EPA Draft Method 1313 leachates at the lower pH conditions, indicating an increase of dissolved solids at low pH conditions, reduced technetium concentrations at low pH resulted from additional retarding processes, such as sorption, so the technetium concentration also was lower than at the more neutral pH conditions in the Cast Stone. In addition, the leachable technetium concentration increased as the concentration of simulant S1 increased from 2 M to 10 M sodium, even though the same initial technetium concentration was used in simulant S1 with the different sodium molar concentrations (Figure 6.10). An increase in the leachable technetium concentration in the EPA Draft Method 1313 leachates as the simulant molarity was increased suggests the higher salt content of the simulant sodium is competing with the technetium, which was kept constant, for adsorption or co-precipitation sites within the Cast Stone.
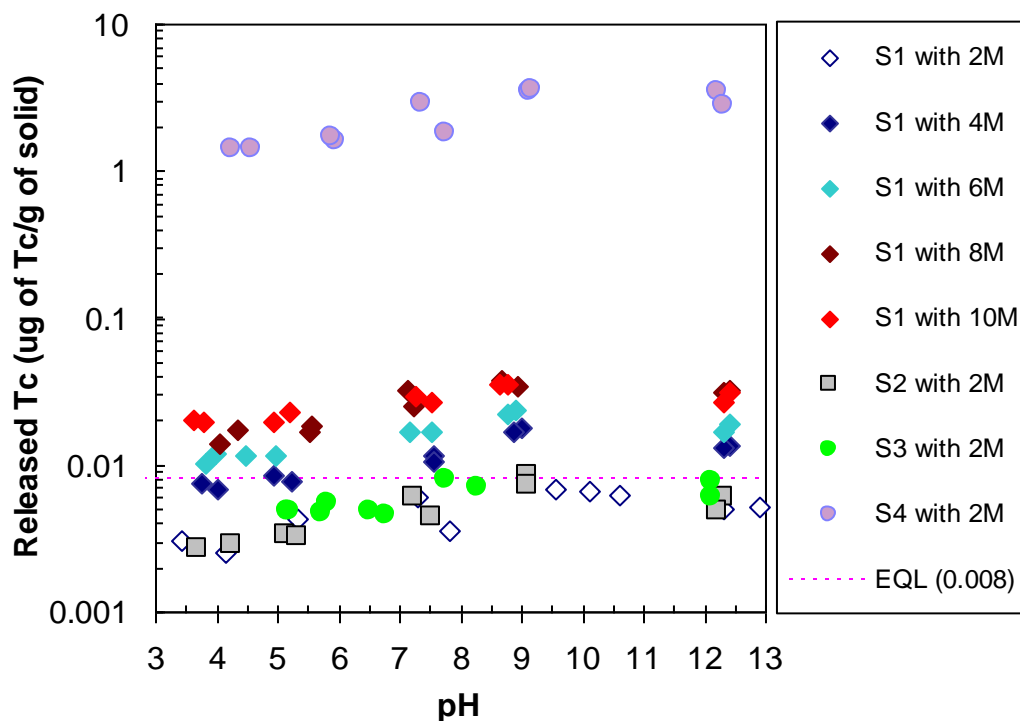
Figure 6.10. Leaching Tc Data (µg of Tc/g of solid) for Cast Stone with Different Simulants from EPA Draft Method 1313

The measured concentrations of major cations are shown in Appendix A. The concentration of the major cations in solution increased with deceasing pH, which is consistent with the EC measurements. Although some RCRA metals (chromium, mercury, and arsenic) are detected in EPA Draft Method 1313 (EPA 2009a) leachates, the concentrations are quite low. In addition, detectable concentrations of lead, copper, and cadmium were not found in any of EPA Draft Method 1313 leachates. Dominant cations in solution were sodium, calcium, and potassium, while NO_3^- (added for pH equilibration for the low pH samples) and alkalinity representing the sum of inorganic carbon (carbonate and bicarbonate) and hydroxyl are the dominant anions measured in the solution samples. Phosphate was not detected in most of the EPA Draft Method 1313.

6.5 Effect of Liquid-to-Solid Ratio - EPA Draft Method 1316

6.5.1 EPA Draft Method 1316 Methodology

Similar to 1313, EPA Draft Method 1316, *Leaching Test (Liquid-Solid Partitioning as a Function of Liquid-to-Solid Ratio) of Constituents in Solid Materials Using a Parallel Batch Extraction Test* is also a static test method that uses DIW as the leachant instead of a dilute acid or base at a variety of liquid-to-solid ratios (EPA 2009b). The purpose of this test method is to evaluate the effect of differing liquid-to-solid ratios on the release of contaminants. These experiments were conducted by adding DIW to the test vessel containing a predetermined amount of powdered cured Cast Stone material (<0.3 mm). These experiments were conducted at three different liquid-to-solid ratios (10, 5, and 2 mL/g). After preparation, all the samples were placed on a platform shaker and allowed to mix for 24 hours. After the

24-hour contact time was complete, the slurry samples were centrifuged and filtered using a syringe filter (0.45-μm size polypropylene membrane). The filtrate was then used to measure the solution pH, electrical conductivity, and redox potential and was submitted for additional chemical analyses.

6.5.2   Effect of Liquid-to-Solids Ratio Results

The EPA Draft Method 1316 (EPA 2009c) leachate results for pH, EC, Eh, alkalinity, and technetium concentrations for powdered Cast Stone prepared with different simulants are shown in Table 6.7. In EPA Draft Method 1316, the liquid-to-solid ratio is varied (10, 5, and 2 mL/g) to evaluate how these changes impact the leaching characteristics of the constituents of interest. Because of the highly alkaline solution resulting from equilibrating DIW with the Cast Stone samples, the majority of the measured pHs in the leachates (prepared without adding any acid or base) were between pH 12 and 13, irrespective of the changes in the liquid-to-solid ratio. Increasing EC and alkalinity values were observed in leachate solutions as the liquid-to-solid ratio decreased. The observed decrease in EC and alkalinity with an increase in the liquid-to-solid ratio is probably the result of a dilution effect at higher liquid-to-solid ratio conditions. This indicates that over the 24-hour time period allotted, most of the solutes do not reach a solubility limit (a constant concentration value irrespective of the liquid-to-solids ratio). The measured Eh values for many of the EPA Draft Method 1316 leachates decreased with the decreasing liquid-to-solids ratio from a ratio of 10 to 5, but then in general remained nearly constant for the drop in the ratio from 5 to 2. One explanation is that the pore solution becomes more anoxic between the liquid-to-solids ratio of 10 down to 5—perhaps reflective of the release of more of the reductants in the BFS. The fact that Eh does not continue to drop as the liquid-to-solids ratio drops from 5 to 2 may reflect that the reductant that is released reaches a solubility limit and remains in the leachates at a constant concentration. However, the authors of this report estimate that the Eh measurements performed open to air may not be meaningful measurements as described above.

The released technetium concentration and the percent leached from each Cast Stone EPA Draft Method 1316 (EPA 2009c) leachate is shown in the last two columns of Table 6.7. The technetium concentration in the leachates as a function of the liquid-to-solids ratio is shown in Figure 6.11. The leached technetium concentration was approximately constant in the leachates as the liquid-to-solids ratio increased, indicating solubility was not limiting release of the technetium. The fractions of technetium leached were in the range of 27% to 52%. These large percentages are expected given the fine particle size used in these tests.

The measured concentrations of major cations from EPA Draft Method 1316 (EPA 2009c) are also provided in Appendix A. Major cations in EPA Draft Method 1316 leachates showed higher concentrations at low liquid-to-solids ratios than at high liquid-to-solids ratios. Concentrations of RCRA metals were below the analytical detection limits (As < 1.0 E+04, Cd < 3.5 E+03, Cr < 9.5 E+02, Pb < 5.4 E+03, Ag <1.9 E+3 µg/L). In Cast Stone, the dominant anions are NO_3^- and alkalinity (CO_3^{2-} and hydroxyl) as found in the leachates from EPA Draft Method 1313.

Table 6.7. The Values of pH, EC, Eh, Alkalinity, and Tc of Cast Stone Waste Forms Measured from EPA Draft Method 1316

Simulant	LS Ratio (mL/g)	pH	EC (mS/cm)	Eh (mV)	Alkalinity (mg/L CaCO$_3$)	Tc* (μg of Tc/ g of solid)	Percent Tc Leached
S1, 2 M	10	12.3	5.98	241	1150	ND (<0.008)	< 49%
	10	12.9	5.93	241	1131	ND (<0.008)	< 49%
	5	12.5	9.36	178	1723	0.00436	27%
	5	12.5	9.43	157	1738	0.00445	27%
	2	12.6	16.3	157	3054	0.00445	27%
	2	12.5	16.6	157	3118	0.00479	30%
S1, 4 M	10	12.4	7.80	213	1402	0.0135	42%
	10	12.3	7.47	218	1357	0.0131	41%
	5	12.4	12.3	168	2160	0.0136	42%
	5	12.4	12.4	152	2145	0.0145	45%
	2	12.5	22.3	157	3502	0.0148	46%
	2	12.6	22.4	158	3536	0.0146	45%
S1, 6 M	10	12.4	9.58	171	1561	0.0191	41%
	10	12.3	5.07	169	1534	0.0168	36%
	5	12.5	15.1	154	2356	0.0203	44%
	5	12.5	15.3	156	2386	0.0194	42%
	2	12.6	28.1	167	3842	0.0203	44%
	2	12.6	27.5	157	3834	0.0209	45%
S1, 8 M	10	12.4	11.4	172	1591	0.032	51%
	10	12.3	7.85	173	1572	0.0308	49%
	5	12.4	18.7	156	2424	0.0311	50%
	5	12.5	18.7	156	2379	0.0292	47%
	2	12.5	35.5	158	3857	0.0315	50%
	2	12.5	38.3	157	4060	0.0324	52%
S1, 10 M	10	12.4	12.4	134	1738	0.0309	42%
	10	12.3	6.87	118	1700	0.0267	36%
	5	12.4	20.6	157	2605	0.0281	38%
	5	12.4	20.4	160	2647	0.0272	37%
	2	12.5	38.7	156	4264	0.0278	37%
	2	12.6	38.6	156	4249	0.0273	37%
S2, 2 M	10	12.3	5.79	171	1213	ND (<0.008)	< 49%
	10	12.2	5.62	174	1142	ND (<0.008)	< 49%
	5	12.4	9.40	165	1889	0.0059	36%
	5	12.4	9.40	153	1787	0.00597	37%
	2	12.6	16.7	159	3197	0.00617	38%
	2	12.6	16.6	165	3186	0.00671	42%
S3, 2 M	10	12.1	4.53	179	863	ND (<0.008)	< 49%
	10	12.1	2.46	176	852	ND (<0.008)	< 49%
	5	12.2	7.10	155	1074	0.00626	39%
	5	12.2	7.18	156	1082	0.00685	43%
	2	12.3	10.1	156	1572	0.00792	49%
	2	12.2	11.9	160	1610	0.0078	48%

Table 6.7. (contd)

Simulant	LS ratio (mL/g)	pH	EC (mS/cm)	Eh (mV)	Alkalinity (mg/L CaCO$_3$)	Tc* (µg of Tc/ g of solid)	Percent Tc Leached
S4, 2 M	10	12.2	6.19	148	988	3.53	43%
	10	12.3	6.03	143	954	2.78	34%
	5	12.2	9.52	165	1274	3.25	40%
	5	12.2	9.51	160	1221	2.99	37%
	2	12.4	17.9	155	1904	3.47	42%
	2	12.4	17.8	154	1998	3.46	42%
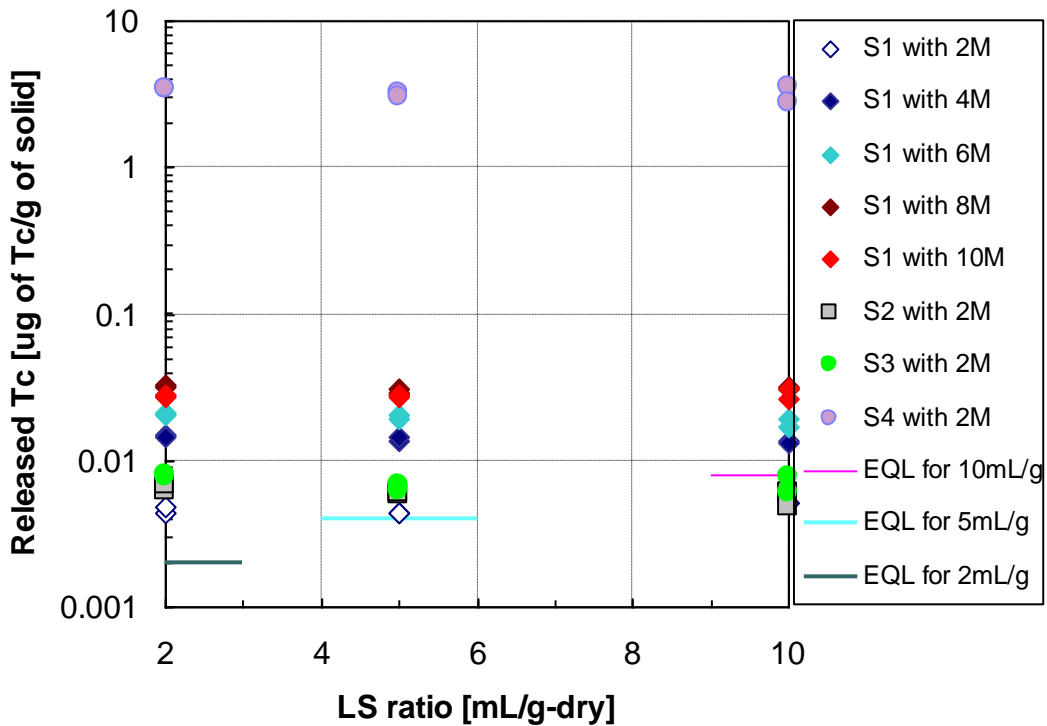
Figure 6.11. Leaching Tc Data (µg of Tc/g of solid) for Cast Stone with Different Simulants from EPA Draft Method 1316

6.6 Phase Assemblage and Microstructure of Monoliths

This section describes the characterization of the mineralogy of the Cast Stone waste forms.

6.6.1 Solid Phase Characterization Methods

Monoliths were characterized using well-established tools. These methods are briefly described in the remainder of this section.

6.6.1.1   X-Ray Diffraction

The phase compositions of type II Portland cement, Class F fly ash, and grade 100 BFS were analyzed with XRD to determine phases responsible for hydration of Cast Stone. To observe the shift of the amorphous band (originally present in fly ash and slag; not in unhydrated Portland cement) in the XRD pattern, three cementitious materials—8% cement, 45% fly ash, and 47% slag (weight basis) —were blended. A representative powder sample of this mixture was analyzed with XRD.

To investigate the phases responsible for the hydration and stiffening of Cast Stone, the hydration of the Cast Stone slurries was stopped using methanol (Chung 2004). Specimens were taken at 5 minutes (after mixing), 30 minutes, and 2 hours. Immediately after collection, specimens were placed in a 20-mL glass vial and filled approximately one-third with paste, and then methanol was added to stop hydration; it was then shaken to dilute the water. The cement paste was allowed to settle, the methanol-water liquid was carefully removed by pipette, and fresh methanol was added and a sample was shaken. This sample was stored for a few hours, and the liquid layer was again removed by pipette. Fresh methanol was added a third time, and the sample was stored until analysis began. Before XRD analysis, the methanol was removed by pipetting.

For the phase composition of hydrated Cast Stone, chunks of Cast Stone specimens were ground with a mortar and pestle. A small amount of acetone was added to prevent heat rise during the grinding process. Dry powdered specimens were packed into the container, and the sample container was then placed in the Bruker D8 to advance to the XRD that uses Cu Kα radiation. The photographic image of the XRD is shown in Figure 6.12. A scanned 2-theta angle was from 5º (2θ) to 70º with a step size of 0.015˚ and a dwell time of 1 second. The working voltage was 40 kV, and the electric current was 40 mA. The electronic scans were processed using Diffrac Plus XRD commander software and analyzed with Evaluation (EVA—a comprehensive and extremely versatile graphics program for easy, fast, and convenient 2- and 3-dimensional data evaluation and presentation), which incorporated the database published by the Joint Committee on Powder Diffraction Standards International Center for Diffraction Data.[1]

---

[1]Newtown Square, Pennsylvania.

Figure 6.12. Photographic Image of X-ray Diffraction Apparatus

6.6.1.2   Microscopy and Elemental Analysis

SEM was used to investigate the microstructure of the cured Cast Stone. Broken pieces of Cast Stone specimens with a size of approximately 8 to 9 mm were placed in a 105°C oven for 2 days to remove the moisture. The oven-dried specimen was then mounted with double-sided carbon tape attached to an aluminum stub. After being mounted, the side of the specimen was coated using silver paint to ensure a good transmission of electrons. The sample was sputter coated with palladium in a vacuum condition to improve the conductivity of the samples and the quality of the SEM images. The JEOL 5900 SEM, shown in Figure 6.13, was used to investigate the microstructural features of these samples. Using a 4-pi data acquisition system, secondary electron images were mostly recorded. When necessary, some back-scattered electron images were also recorded. Energy dispersive X-ray spectroscopy (EDS) was used to investigate the chemical compositions of specific regions (i.e., individual grains). A Metek EDS System was used to collect EDS spectra for qualitative elemental analysis. Again, EDS data were obtained from the 4-pi data acquisition system.

Figure 6.13. Photographic Image of Scanning Electron Microscope

6.6.2   Cast Stone Mineral Phase Characteristics

XRD patterns of hydrated Cast Stone specimens made with various simulants (S1 through S4) are presented in Figure 6.14. From the XRD pattern, the three most notable phases—calcite, quartz, and ettringite—were present in significant amounts in all the specimens. However, both calcite and quartz originated from the starting dry blend materials; thus, ettringite can be considered as the main crystalline phase in Cast Stone that is generated by the hydration process.

Other crystalline phases observed in the XRD patterns were AFm phases. Hemi-carbonate-based AFm ($AFm_{0.5C}$) and mono-carbonate AFm (AFm_c) were observed in the hydrated Cast Stone waste forms made with all secondary waste simulants. The XRD peak intensity of AFm_c was very small, but the XRD peak intensity of the $AFm_{0.5C}$ was quite noticeable in the Cast Stone solids made with simulants S1, S2, and S3. The Cast Stone made with simulant S4 exhibited a significantly decreased XRD intensity peak for $AFm_{0.5C}$ and showed a more prominent nitrate-based AFm (AFm_N) XRD peak instead. The main XRD peak positions for AFm phases can shift, depending on which anion is incorporated within the AFm structure. Anions get into the AFm structure as compounds form during the cement hydration process, depending on the pore solution composition (Matschei et al. 2007). Although it is reported that nitrate-based AFm exists (Renaudin et al. 2000), it has not been recognized or reported in the cement-based solids (Matschei et al. 2007, Taylor 1997). A possible reason for not observing a nitrate-based AFm phase is that normal cement and its pore solution are low in NO_3^{2-}. These secondary waste simulants provide a very different solution composition than the waters generally used to hydrate cement and can certainly change the reaction kinetics and types of minerals formed during the hydration of the Cast Stone. It appears a large amount of the anions present in the secondary waste simulants is consumed by the formation of both ettringite (for sulfate) and AFm phases (carbonate and nitrate). Vaterite, a polymorph of calcium carbonate, was also observed. This phase seems to be produced because of the presence of the high concentrations of CO_3^{2-} in the simulant solution.
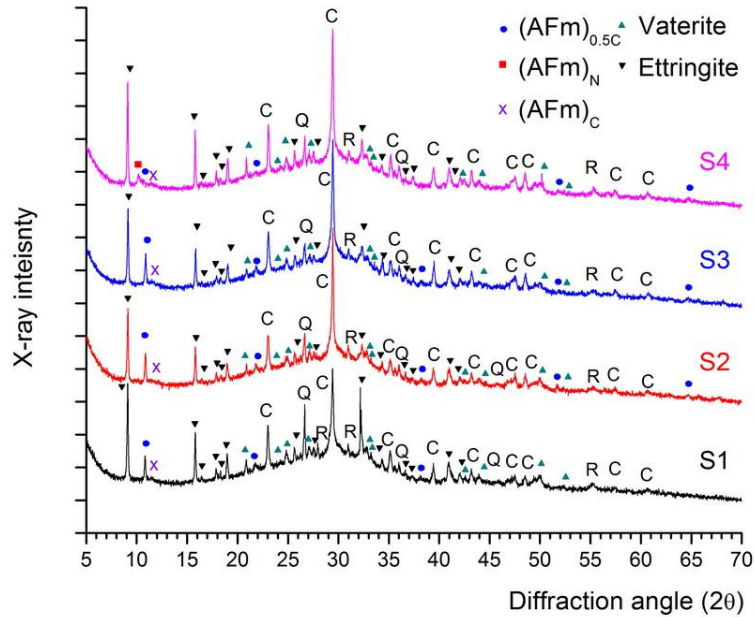
Figure 6.14. XRD Patterns of Hydrated Cast Stone with Various Simulant Solutions. Note that the concentration of simulant solution prepared is 2 M Na. Also note that the alphabet letter C indicates calcite, Q indicates quartz, and R indicates Rustumite, respectively.

It is difficult to investigate the amount of amorphous C-S-H (or C-A-S-H) formed during the Cast Stone hydration process using XRD, which identifies only crystalline solids. Two indirect ways to characterize the C-S-H are to observe the calcium hydroxide (portlandite) CH peak and the development of the amorphous band from cement paste. However, the former is impossible with Cast Stone because Cast Stone consumes all the CH through pozzolanic reactions. Therefore, the latter method has been used for our analysis, although it is still difficult to monitor the development of the amorphous XRD hump because of the presence of similar amorphous bands in raw materials (fly ash and slag). Therefore, the latter approach was slightly modified: if the phase structure is affected by any kind of reaction (either by hydration or pozzolanic reaction), the shift of the amorphous band can be observed from the XRD pattern. For this purpose, a dry mixture of raw materials with 8% cement, 45% fly ash, and 47% slag was prepared, and the center of the dry mixture's amorphous band was analyzed by XRD. The XRD patterns of the raw material mixture are presented in Figure 6.15. The center of the amorphous band was around 31°, which is close to that of the amorphous band for slag.
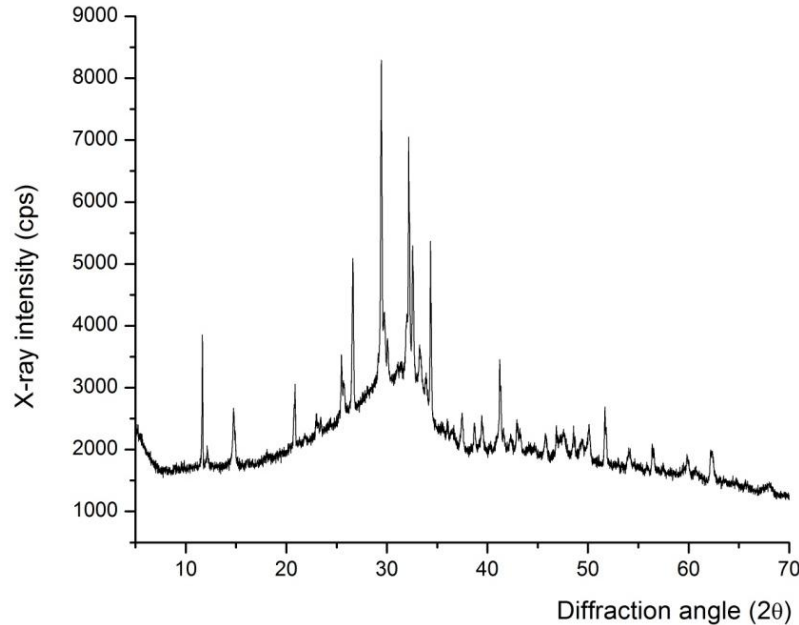
Figure 6.15. Dry Mixture (cement 8%, fly ash 45%, and slag 47%)

Hydrated Cast Stone XRD patterns shown in Figure 6.14 have the center of the amorphous hump at about 29.5°. The center of the hydrated Cast Stone hump has slightly shifted towards a lower angle, which is close to the center hump of the fly ash. Because the center of the band of the hydrated Cast Stone has shifted towards the center of the fly ash's amorphous band, the authors suggest that some amount of slag has reacted during the hydration process, but most of the fly ash has likely not reacted. Because the amorphous band of the hydrated Cast Stone was not broadened in comparison to the dry mixture shown in Figure 6.15, this result may also indicate that no significant reaction has occurred with Cast Stone.

XRD patterns of simulant solutions in various concentration levels of S1 simulant are presented in Figure 6.16. Calcite, quartz, and ettringite were the main crystalline phases, and $AFm_{0.5C}$ and AFm_C were also observed. The center of the amorphous hump was located at around 29.5°, which is the same as shown in Figure 6.14 with various simulants; thus, it can be considered that approximately the same amount of hydration has occurred.

The ettringite and $AFm_{0.5C}$ peaks decrease as the concentration of the simulant solution increases. With the 8-M simulant solution, there is a small hint of these peaks (the peak is also broadened a bit), suggesting that these phases are not stable in the high-concentration simulant solution. Both the ettringite and the $AFm_{0.5C}$ peaks completely disappeared at 10 M of simulant solution. From the 8-M simulant solution, two unknown hydration phases (most likely calcium [sodium] aluminosilicate hydrates) started to develop, indicating the changes in reaction kinetics with highly concentrated simulant solutions.

Researchers observed the quartz peak varies, but this does not correspond to the changes in the concentration of simulant solution. This change can be just associated with differences in specimen sampling. Quartz is not likely to show any changes associated with changes in solution concentration because quartz is very stable and does not easily dissolve in a high-pH solution unless significant changes (such as pressure or temperature rise) are involved (Taylor 1997).
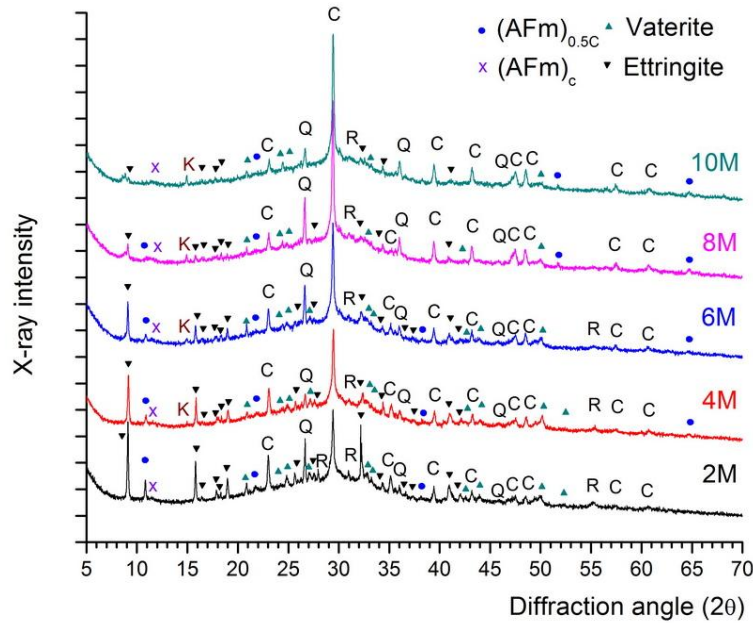
Figure 6.16. XRD Patterns of Hydrated Cast Stone Made with Various Concentrations of Simulant S1. Note the S1 simulant solutions varied from 2 M to 10 M. Also note the alphabet letter C indicates calcite, Q indicates quartz, and R indicates Rustumite, respectively.

A characteristic microstructural image generated using SEM, representing the typical Cast Stone specimen is presented in Figure 6.17. The image was obtained from the simulant S1-6 M specimen. As observed in Figure 6.17, a large amount of round spherical particles was present throughout the specimen. These spherical particles are characteristic of unreacted fly ash, which was confirmed by EDS analysis. There were many spherical open spaces generated during the processing of the sample for SEM characterization that were caused by the removal of fly ash particles that previously occupied the voids but were removed, indicating the binding between fly ash and the cementitious matrix of Cast Stone is not strong. The presence of so many unreacted fly ash particles in the Cast Stone suggests that less fly ash has reacted, so increased amounts of cement could be used in optimizing the dry blend. Adding cement will produce a larger amount of CH that is required for the pozzolanic reactions that incorporate fly ash into the final solid.
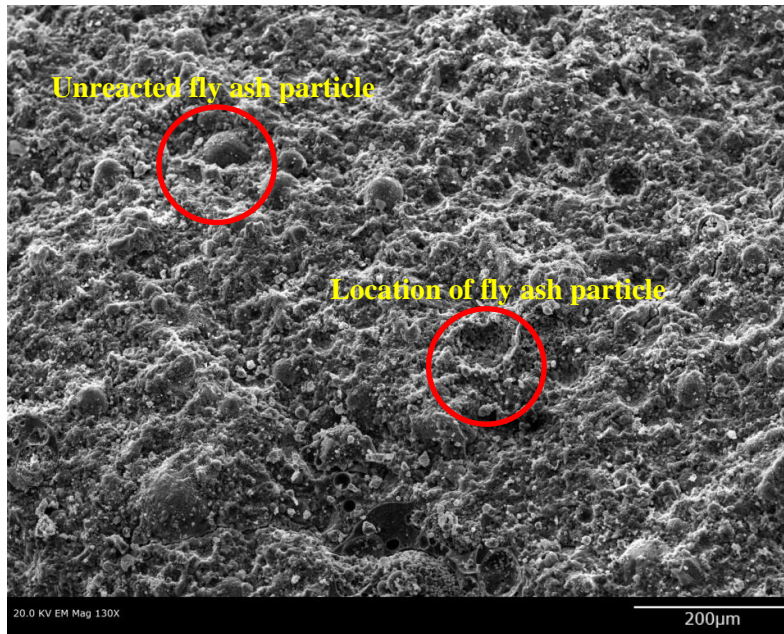
Figure 6.17. Secondary Electron Image of Specimen with Simulant S1-6 M Solution. The magnification was set at 130×. All the Cast Stone hydrated solids made with the different simulants also showed similar surface characteristics. Note the presence of unreacted fly ash particles in the red circle, which was confirmed with EDS analysis.

Typical secondary electron images of Cast Stone specimens using the various simulant 2-M solutions are presented in Figure 6.18 through Figure 6.22. The most characteristic features of these images are needle-like ettringite and hexagonal AFms. The chemical compositions were verified with EDS analysis. Ettringite and AFms were quite easy to observe in the open area where these crystals grow without any restrictions. Ettringite was observed to form on the surface of AFm crystals and on fly ash particles, and they can be easily recognized by their round shape in the background of the images. The results correlate the earlier observations based on the XRD patterns (Figure 6.14) that ettringite and AFms are the main crystalline hydration phases in Cast Stone.

Figure 6.18. Secondary Electron Image of Specimen with Simulant S1-2 M Solution. The magnification was set at 1500×. Note the hexagonal AFm and the needle-like ettringite in the red circle were verified by EDS analysis.
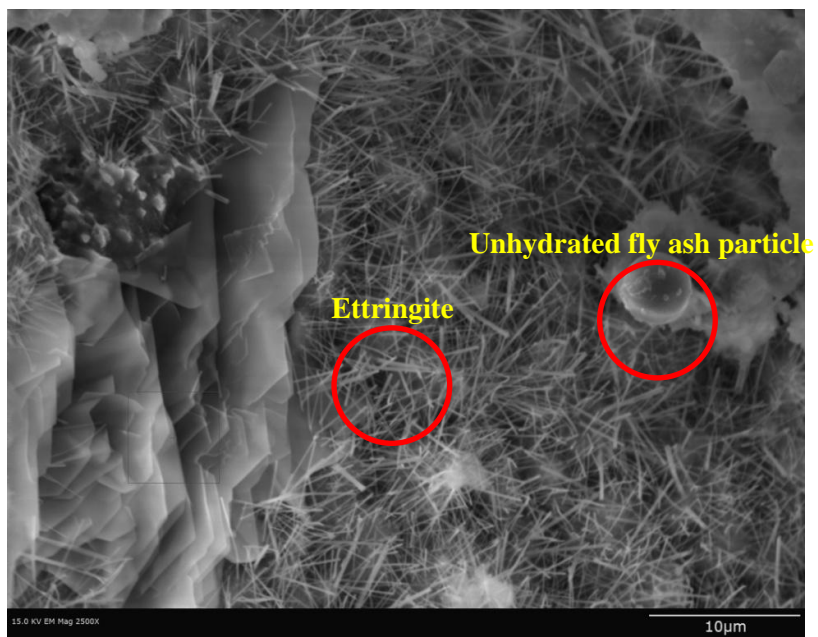

Figure 6.19. Secondary Electron Image of Specimen with Simulant S2-2-M Solution. The magnification was set at 2500 ×. Note the hexagonal AFm and the needle-like ettringite in the red circle were verified by EDS analysis.
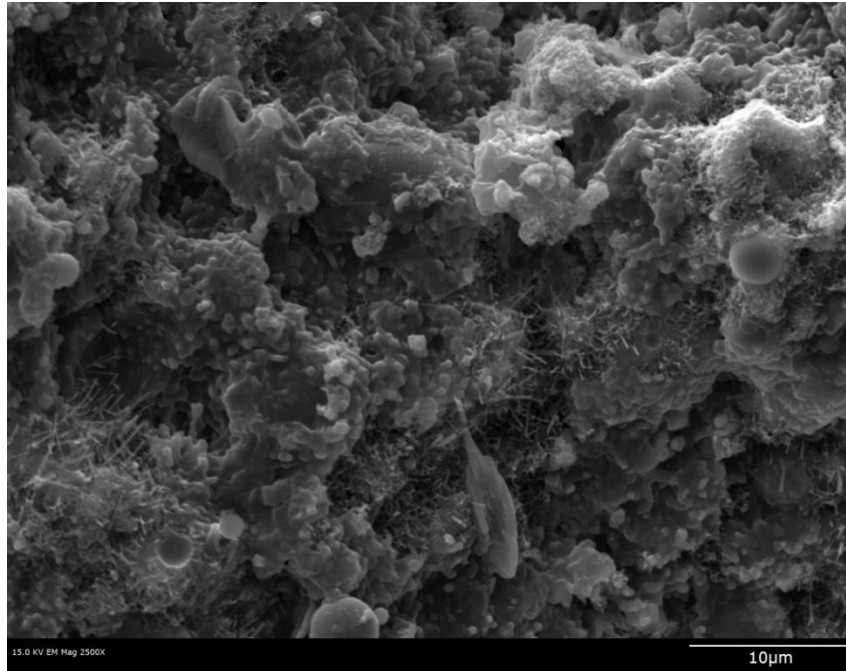
Figure 6.20. Secondary Electron Image of Specimen with Simulant S3-2-M Solution. The magnification was set at 2500×.
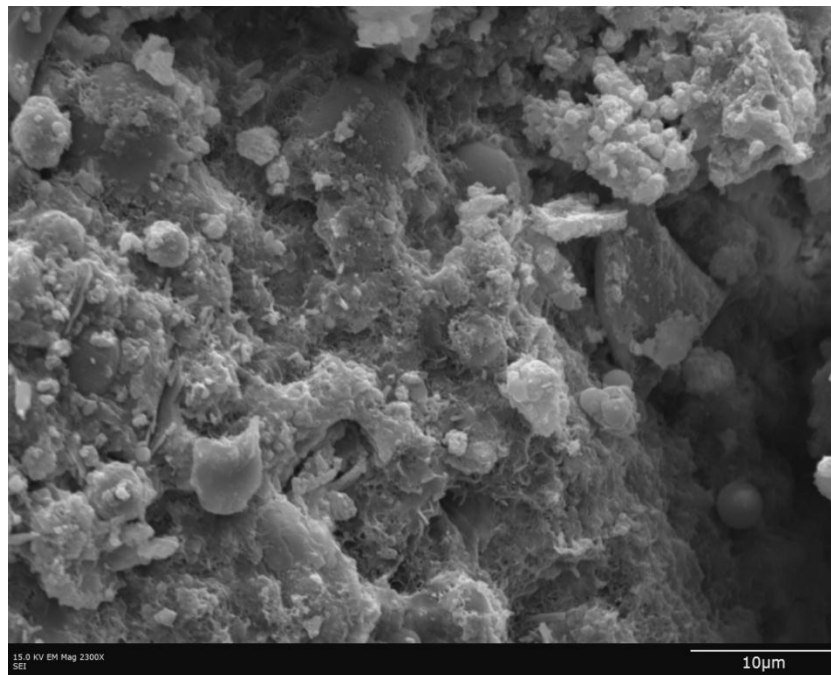

Figure 6.21. Secondary Electron Image of Specimen with Simulant S4-2-M Solution. The magnification was set at 2300×.
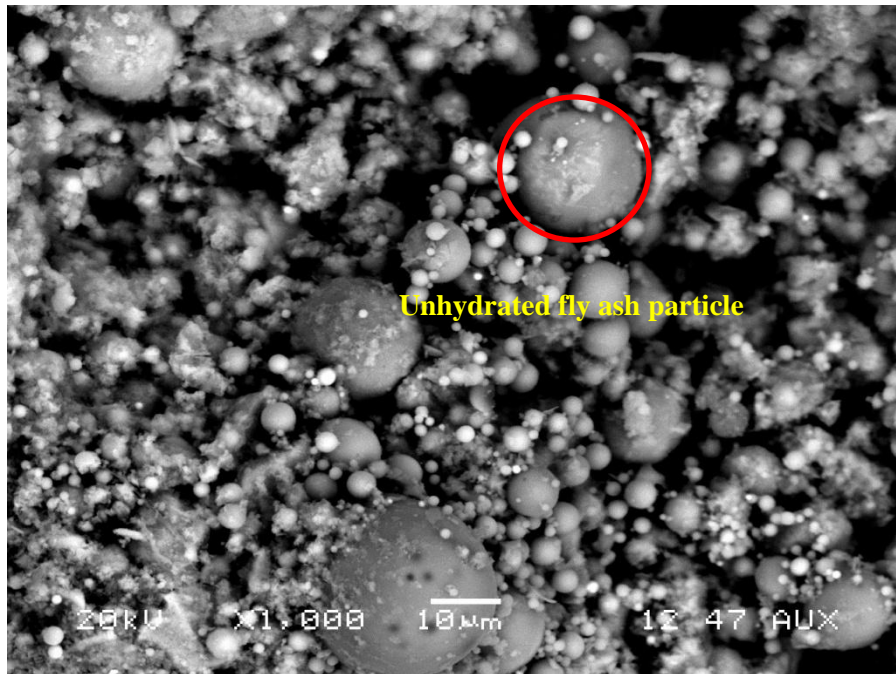
Figure 6.22. Back-Scattered Electron Image of Specimen with Simulant S4-2-M Solution. The magnification was set at 1000×.

Typical secondary electron images of Cast Stone specimens made with various concentrations of simulant S1 (from 4 M to 10 M) are presented in Figure 6.23 through Figure 6.26. The images show that the amount of ettringite and AFm decreases as the simulant sodium concentration increases. In addition, there was a phase in Figure 6.23 that is very likely to be calcium aluminosilicate hydrate (C-A-S-H). The EDS was used to verify this phase, but it was difficult to confirm because of the information from the background elements. The Cast Stone hydration products from simulant S1-8 M exhibit a platy-layered structure. The amount of platy structure increases in the hydrated Cast Stone made with the simulant S1-10 M solution. These observations agree with the XRD patterns (Figure 6.16), which suggest the distribution of phases changed as the concentration of simulant solution increased. This platy material can also be related to the aluminosilicate, but further investigation is required to identify the specific phases.
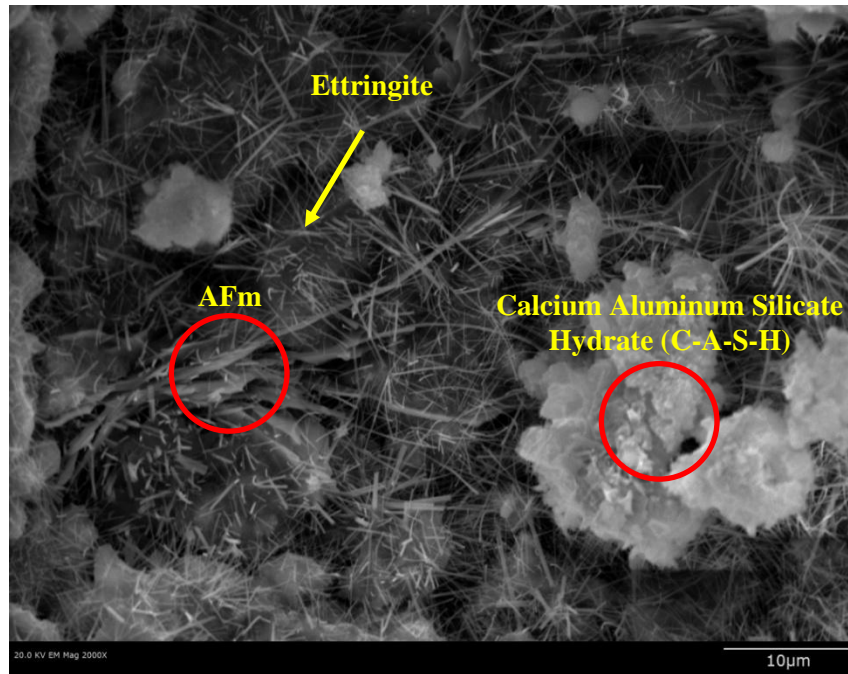
Figure 6.23. Secondary Electron Image of Specimen with Simulant S1-4 M Solution. The magnification was set at 2000×.

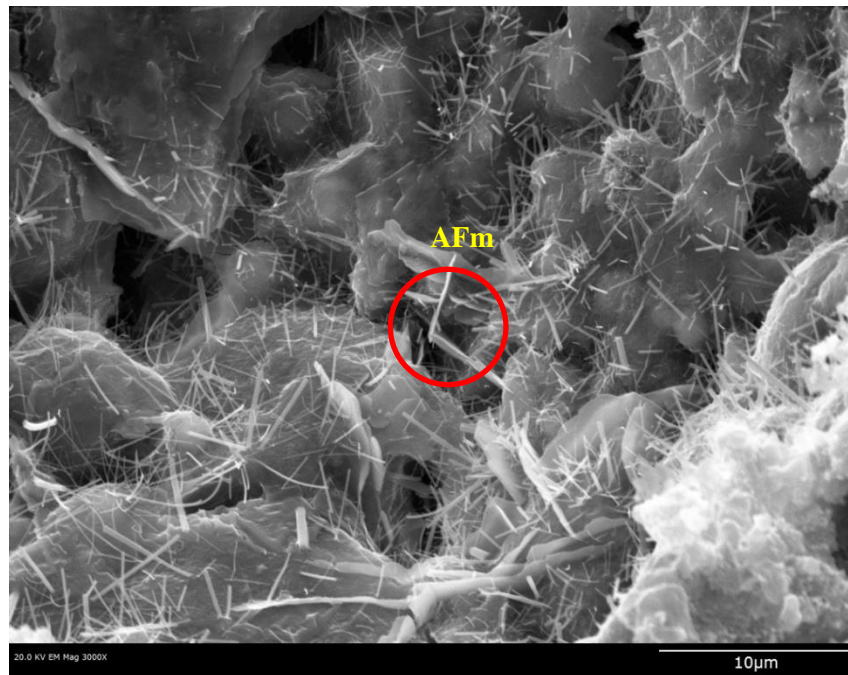**Figure 6.24**. Secondary Electron Image of Specimen with Simulant S1-6 M Solution. The magnification was set at 3000×.

Figure 6.25. Secondary Electron Image of Specimen with Simulant S1-8 M Solution. The magnification was set at 3000×.

Figure 6.26. Secondary Electron Image of Specimen with Simulant S1-10 M Solution. The magnification was set at 3300×.

6.7 Pore Structure

6.7.1 Surface Area and Porosimetry Methods

The surface area of small chunks or crushed powders of cured Cast Stone sample was determined using the Micrometrics Surface Area Analyzer[1], shown in Figure 6.27. The approach is based on the multi-point BET adsorption equation using nitrogen. A detailed description of the procedure to determine surface area is presented in the manufacturer's operating manual (Micromeritics 2006). Briefly, an air-dried sediment sample, which will provide at least 10 m^2 of total surface area, is placed in a surface area flask and out gassed for a minimum of 3 hours at 150°C and at 3 μm Hg. The out-gassing temperature was chosen to minimize altering the surface structure as described in Davis and Leckie (1978). During this time, physically adsorbed water and volatile organics are removed. To determine dryness, the vacuum pumps are isolated, and if a vacuum change of less than 2 μm Hg in 5 minutes occurs, the sample is considered clean and dry. After out-gassing, the adsorption of nitrogen then determines the surface area on the surface.

The equipment uses an imbalance of atomic forces on the surface of a clean evacuated solid to attract gas molecules. The gas molecules collide with the surface of the sediment and either bounce off or adsorb onto the surface. When the molecules leave the bulk gas to adsorb onto the sediment surface, the number of molecules in the gas decreases and thus the gas pressure decreases. By knowing the temperature, the volume of the container, and the change in pressure, the number of molecules adsorbed can be determined. From the number of adsorbed molecules, the surface area can be calculated. The specific surface area of the hydrated (cured) Cast Stone for each simulant was determined on crushed < 0.3-mm-sized particles.

To determine the pore-size distribution, the method described by Barrett, Joyner, and Halenda (BJH method) is used. As the nitrogen is added or removed from the pores with equal step changes in relative pressures, the pressure change represents the core volumes of the pores in that step. Assuming that the pore is a right circular cylinder, the volume of the pore can then be calculated. Using a thickness relationship, the radius of the pores can then be calculated.

---

[1] Model 2020 Micrometrics Instrument Corp., Norcross, Georgia.

Figure 6.27. Photographic Image of Nitrogen Gas Adsorption Instrument

6.7.2 Pore Structure Results

The specific surface area of the Cast Stone specimens made with the various simulants is presented in Figure 6.28. The surface area of the Cast Stone varied based on which simulant was used. The largest surface area was observed for the Cast Stone made with the S4-2-M solution, whereas the smallest surface area was observed for the Cast Stone made with the S1-2-M solution.
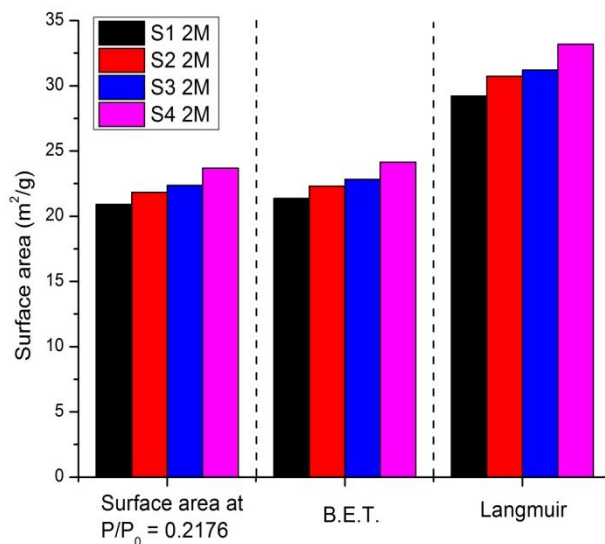

Figure 6.28. Specific Surface Area of Cast Stone Specimens Using Various 2-M Simulant Solutions

The specific surface area of the Cast Stone specimens with an S1 simulant solution at various concentration levels is presented in Figure 6.29. The surface area generally increased as the concentration

of solution increased. The largest surface area was observed with the S4-10-M solution, whereas the smallest surface area was observed with the S1-2 M solution. Although one exception exists (simulant S1-8 M solution), it can be concluded that the surface area of the Cast Stone was affected by the changes in simulant concentration. The variations of S1 4 M, 6 M, 8 M, and 10 M with BET surface area were ± 0.0615 m^2/g, 0.0771 m^2/g, 0.0703 m^2/g, and 0.0638 m^2/g, respectively. The differences in surface areas between each specimen were more than 0.617 m^2/g (between S1 4 M and 8 M) as shown in Figure 6.29, so the difference is statistically meaningful.

The surface area results on chunks of Cast Stone made with varying waste simulants appear to be controlled by the amount of open spaces that nitrogen gas can penetrate into. If it is considered that the surface area measurements are indicative of total porosity and that total porosity can be correlated with compressive strength, the Cast Stone specimen with the higher surface area must show the lowest compressive strength. However, it was observed the surface area did not show a good correlation with compressive strength (Section 6.1.2). With various simulant types, the largest surface area was recorded with the simulant S4 solution (Figure 6.28), whereas the smallest compressive strength was observed with simulant S3 (Figure 6.1). With various concentration levels of simulant S1 solution, the largest surface area was observed with the highest concentration of simulant solution—simulant S1 10 M. However, note that the compressive strength loss with S1-6 M, S1-8 M, and 10 M simulant solutions are associated with the addition of extra water needed to make the paste workable. In addition, the small variation in compressive strength that is not statistically meaningful also makes it difficult to correlate specific surface areas to the compressive strength.
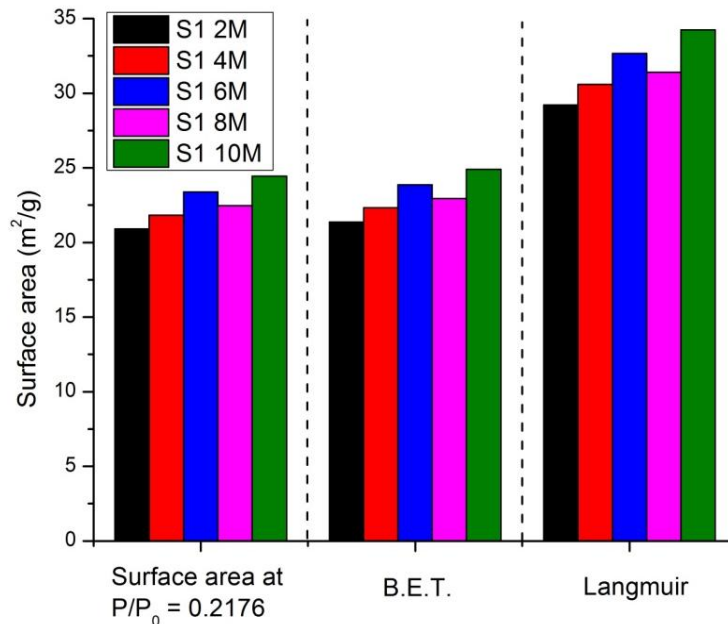
Figure 6.29. Specific Surface Area of Cast Stone Specimens with Simulant S1 Solutions at Various
Concentration Levels

In most of the materials, the surface area indicates the porosity of the material. However, with cement paste, this concept cannot be applied because C-S-H is a highly amorphous material with many nanometer-sized gel pores (approximately less than 3 nm) (Mehta and Monteiro 2006). Juenger and Jennings (2001) reported that cement with a higher degree of hydration shows a higher surface area. This

means that a higher degree of hydration indicates more production of C-S-H, so concrete becomes stronger although the surface area increases. The pore size type responsible for the durability and strength loss is the capillary pore and entrapped air void, which ranges from around 10 nm to 1 μm in size for capillary pore and above 50 μm and higher for air void, respectively.

The pore-size distribution (BJH method) of a Cast Stone specimen from the simulant S1-2 M solution was measured. The pore-size distribution calculated using the BJH method is presented in Figure 6.30. Most pores in this specimen are about 3 nm in size, which falls into a category called gel pore. However, some of the pores are larger than 3 nm. A very small fraction of pore sizes was larger than 10 nm. Thus, almost no capillary pores were detected from measuring nitrogen gas adsorption, so the authors of this report conclude that the surface area of the Cast Stone cannot be used as a criterion to determine the strength and durability of the Cast Stone, which are related to the leachability of the material.

Note that the hydration product in Cast Stone may not be as porous as C-S-H in normal concrete. Therefore, observation also rules out the concept of using the specific surface area or the pore-size distribution to interpret the degree of hydration in Cast Stone. Calorimetry data are also required to accurately interpret the data from nitrogen gas adsorption. To evaluate the total porosity responsible for microstructural development, it is crucial to have the data from mercury intrusion porosimetry, which is known to characterize the macrosized pores.
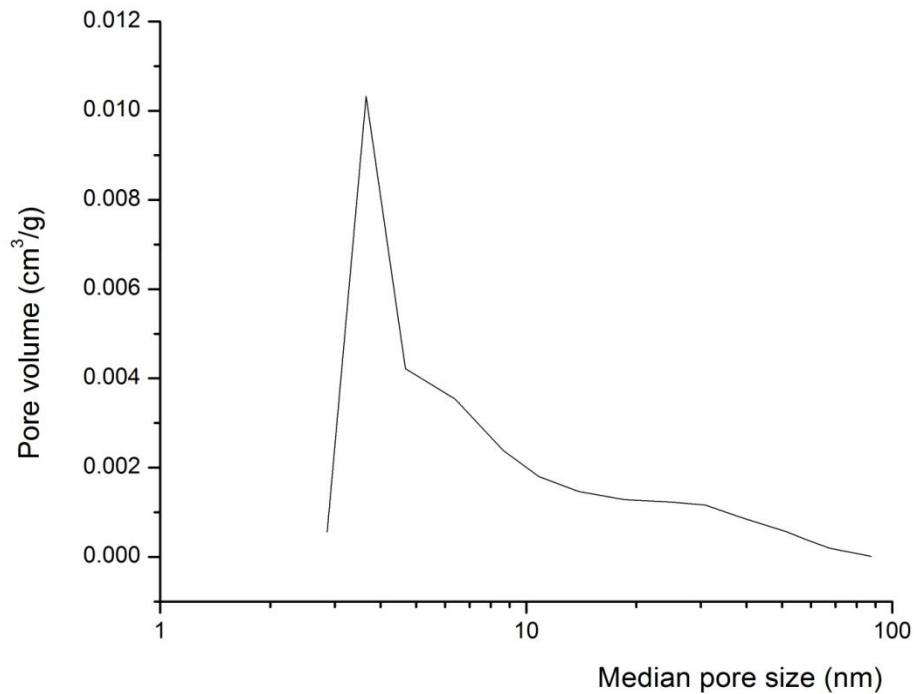

Figure 6.30. Pore-size Distribution (BJH) of a Cast Stone Specimen (Simulant S1-2 M solution)

7.0   Rheology and Curing Studies

This section describes additional studies on the rheology of waste form dry blend/aqueous waste stream slurries relevant to mixing and pouring. It also provides information on the Cast Stone curing process.

7.1   Rheology Studies

The rheology of a waste form slurry is important to its workability as the dry blend and aqueous waste stream are mixed and poured into the container for curing and disposal. Rheological properties—including viscosity, static or undisturbed yield stress, and dynamic yield stress—can impact the mixing, pumpability, segregation of sand and aggregate, and release of entrained air bubbles in the waste form slurry as it is prepared and cures. For concrete materials, there are engineering specifications to address the workability. For example, slumping tests can provide qualitative guidelines as to specific requirements to be used in construction. Although such specifications are implicitly related to "actual" rheological properties, such as viscosity and yield stress, they can only provide relative information and thus cannot provide quantitative rheological properties. Furthermore, even such qualitative specifications do not exist for waste form mixtures like Cast Stone, which significantly poses a challenge to understanding the workability issue.

Based on the particle-size analysis (see details in Section 4.2), the Cast Stone would possess an appreciable percentage of colloid-sized particles (particles less than ~ 10 μm diameter). This strongly implies that physicochemical parameters important for colloidal forces (such as pH, ionic strength, surface charges, and PSDs) can influence rheological properties of the Cast Stone (Russel et al. 1989). Appendix B describes a simple scaling and interaction model that provides characteristics of particle flocculation as the early stage of hydration as a function of particle size, particle density, and shear rate. More importantly, the hydration reaction of cement produces significant changes in ionic strength, pH, and surface charges (Jönsson et al. 2004). Although it is not as significant as cement, BFS (in some cases fly ash, too) hydration processes can also cause some changes in the chemical and physical properties of the final hardened product.

Because hydration has been known to dictate pore characteristics (e.g., pore structure and pore-size distribution) of the final reaction product, it will influence the leachability of the trace contaminants in waste form. Therefore, the hydration, rheological properties, and leachability of the waste form cannot be separately considered. Time evolution of rheological properties, which can also be analyzed by both ultrasonic wave reflection and complex impedance spectroscopy, not only allows researchers to evaluate the flow behavior of fresh paste at the time of placement but also provides a useful signature of hydration. Thus, researchers have performed both ultrasonic wave reflection and complex impedance spectroscopy to provide supplementary information on the evolution of the Cast Stone as it hydrates and hardens into its final form.

To characterize the rheological properties of the Cast Stone, rheological measurements based on the vane-in-cup geometry were used in a shear-rate range of 0 to 1000 sec^{-1} (upward (0 to 1000 sec^{-1}) and downward (1000 to 0 sec^{-1}) runs) and a temperature of 25ºC by using Anton Paar MCR 301. In the vane-in-cup geometry, a six-blade vane as an inner tool was immersed in an outer cylinder (i.e., cup) after placing a sample in the cup up to a designated fill line (typically 40 to 50 mL to confirm sufficient

immersion of vane tool). A flow resistance due to rotation of the vane inside the cup was collected digitally as a torque in a shear-rate range of 0 to 1000 sec^{-1}. The torque was converted into stress and thus raw data were stresses as a function of shear-rate in the range of 0 to 1000 sec^{-1}.

All data were collected, processed, and presented using the RHEOPLUS/32 V3.21 21003751-33024 software. The flow curve measurements based on vane-in-cup geometry are performed to avoid a potential slip issue associated with high solids content of the Cast Stone slurry (Barnes 1995). The shear-rate measurement increases/decreases were kept linear with upward/downward ramp times of 5 minutes each, and the maximum shear rate was maintained for 1 minute before the downward ramp started. The Cast Stone slurry used in the instrument ranged from about 40–50 mL. The measurements were performed as a function of time (typically up to 2.5 hours after mixing) to investigate different stages before the initial setting over different conditions (e.g., different constituents and simulants).

Unlike a conventional measurement based on the bob-in-cup geometry (i.e., cylindrical inner tool with an outer cylinder that gives rise to the annulus of one cylinder inside another), two important rheological data can be obtained from the vane-in-cup geometry at the same time: 1) static or undisturbed yield stress at a very low shear rate, similar to a conventional yield strength measurement; and 2) dynamic yield stress after static microstructures are taken apart (Barnes and Carnali 1990). Thus, the measurement based on the vane-in-cup geometry facilitates more complete rheological characterization of the Cast Stone slurry. An undisturbed yield stress was obtained as a maximum stress value at a very low shear rate from upward runs because the undisturbed microstructure of slurry would be mostly sustained in the upward run. The dynamic yield stress was calculated using the Bingham Plastic rheological model (i.e., $\tau = \tau_y + \eta_p \dot{\gamma}$), where τ and $\dot{\gamma}$ denote shear stress and shear rate, respectively. Here τ_y and η_p denote a Bingham Plastic yield stress and consistency or plastic viscosity, respectively.

To analyze the dynamic yield stress, the rheological data at very low shear rates (typically less than 50 to 100 sec^{-1}) were not included in the analysis to avoid overweighting the Bingham plastic curve fit calculations. In addition, the authors of this report did not include rheological data at intermediate and high shear rates (typically, above 400 to 500 sec^{-1}) because data in that range made it difficult to perform a reasonable analysis. Note the dynamic yield stress was obtained from the downward runs because of practical difficulties to obtain a fitting equation (associated with abnormalities of stress response) in the upward run. While dynamic yield stresses from the downward runs are more consistent, the numerical values are expected to be less than those from upward runs. Figure 7.1 shows the rheogram of the Cast Stone slurry prepared using DIW at 0.5 hr after mixing as an illustration of typical rheological behavior observed in the subsequent analyses of the Cast Stone slurries prepared with secondary waste simulants.
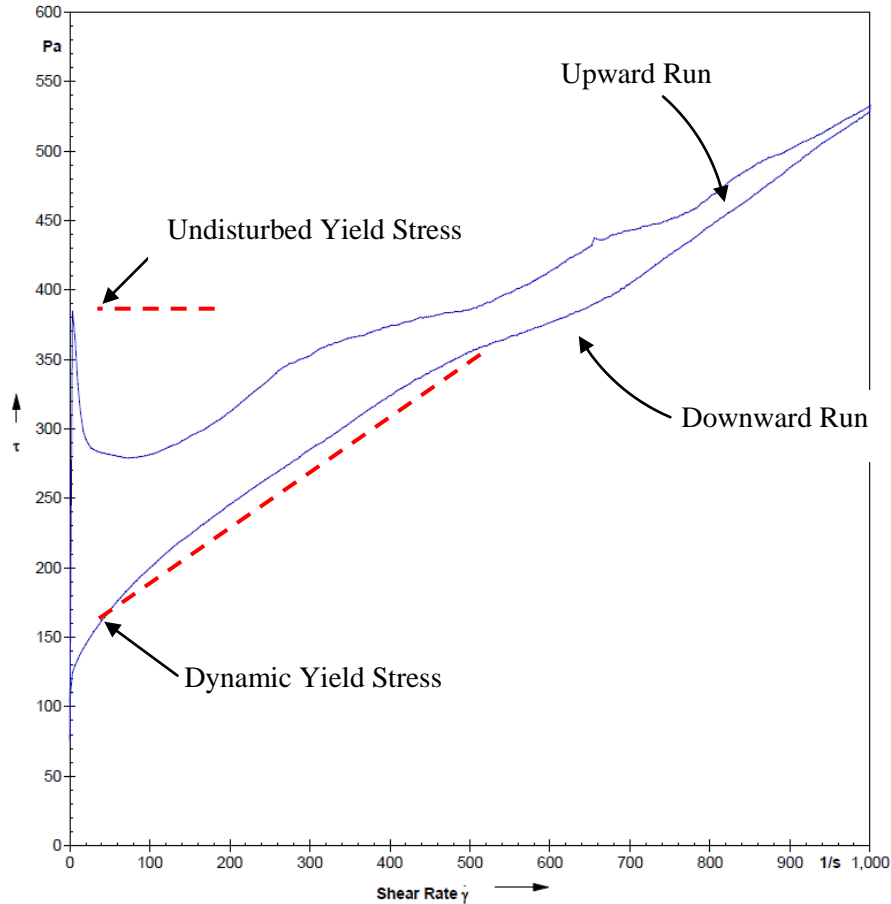
Figure 7.1. An Example of Stress Response as a Function of Shear Rate with the Vane-in-Cup Geometry for the Cast Stone Slurry (Cast Stone slurry with DIW at 0.5 hr after mixing)

Rheological measurements based on the vane-in-cup geometry would only provide a relative value, compared to the bob-in-cup geometry. However, a comparison between the bob-in-cup and vane-in-cup geometries with tap water and viscosity standard silicone oil (48 cP) revealed that the viscosities of silicone oil from both geometries are very close to each other (48.7 cP and 49.3 cP from bob-in-cup and vane-in-cup geometries respectively), whereas both geometries give rise to appreciable differences. Because most of the Cast Stone samples in this study are expected to have a yield stress and be more viscous than silicone oil, rheological measurements using the vane-in-cup geometry provide the most realistic stress responses for the Cast Stone slurry.

7.2   Rheology

As stated above, physicochemical parameters affecting colloidal forces (such as pH, ionic strength, surface charges, and PSDs) can influence the dynamics of particles in the Cast Stone and thus impact the rheological properties of the Cast Stone. Further, the hydration of cement is expected to drive large changes in ionic strength and pH of pore solution as well as the surface charge of the particles in the hardened solid. Therefore, the influences of these changes can be evaluated in the properties and interactions between Cast Stone particles that are necessary to understand the rheological response of Cast

Stone. A rheological model discussed in Appendix B that provides valuable physical insights into the successful preparation of the Cast Stone waste forms.

In this section, rheological measurements on a limited number of Cast Stone samples are used to perform the analysis. Rheological measurements with the vane-in-cup geometry were used to evaluate the initial stages of hydration and showed a strong dependence on simulant total ionic strength and the types of constituents in the simulant composition.

7.2.1   Rheological Measurements and Analysis

Rheological measurements and analyses were done for seven representative samples: (#1) cement/fly ash/slag in DIW, (#2) cement in DIW, (#3) fly ash in DIW, (#4) slag in DIW, (#5) simulant-1 (2 M sodium), (#6) simulant-1 (4 M sodium), and (#7) simulant-1 (8 M sodium). The first four samples were intended to understand the behavior of the three different components in the Cast Stone dry blend, compared to their mixture. The last three samples (in comparison to the sample #1) were tested to investigate the effect of ionic strength as well as to obtain basic rheological characteristics. The mass ratio of cement/fly ash/slag in Cast Stone mixture was 8/45/47. The total solids content in the slurries was set to about 71 wt% for all samples to eliminate the effect of solids content as an additional variable. Rheological measurements were performed as a function of time (up to 2.5 hours) to observe the time-evolving rheological properties of the samples. As described in Section 7.1, undisturbed and dynamic yield stresses were obtained from the upward and downward runs, respectively. The undisturbed yield stress can be considered as a maximum stress to be imposed to initiate a flow of slurry from a stationary state. Therefore, the microstructure of the slurry would be disturbed, at least partially, after this stress. In contrast, the dynamic yield stress can be interpreted as a stress that must be imposed continuously to sustain a flow of slurry. Both undisturbed yield stress and dynamic yield stress become significantly different when the microstructure (e.g., network or floc) spans an entire volume of sample. Otherwise, both values are expected to be comparable.

Figure 7.2 shows the variation of the undisturbed yield stresses for seven representative samples up to 2.5 hours. As shown in Figure 7.2, the tested samples show significant variations of undisturbed yield stresses (note the log scale on the Y-axis). Samples #1, #4, #5, and #6 show similar undisturbed yield stresses after 1.5 hours, but their initial rheological behaviors are different. The undisturbed yield stress of the Cast Stone made with simulant-1 does not change significantly for the Cast Stone made with 2-M and 4-M Na, but the same Cast Stone slurry made with DIW (sample #1) shows a very significant undisturbed yield stress at the beginning (2096 Pa). Considering a similar behavior of sample #4 (i.e., slag in DIW), this large undisturbed yield stress for the Cast Stone mix in DIW at the beginning clearly originates from the slag; a change in undisturbed yield stress (from 4487 Pa to 2096 Pa) reflects a change in wt% of slag in the total solids (from 100% to 47%). In addition, the reader can deduce that the observed significant undisturbed yield stress at the beginning in the Cast Stone made with DIW would be a signature of "false setting" based on the fact that the yield stress decays in a short time (within first 30 minutes to 1 hour). More importantly, Figure 7.2 shows that a reasonable amount of ions exist in the Cast Stone slurry made with simulant-1 such that the undisturbed yield stress is much lower than the stress generated from the slurry prepared with only slag. Sample #2 (only cement in DIW) shows a consistent increase in undisturbed yield stress with time, which is a clear indication of the ongoing hydration reaction. Cast Stone slurries #5 and #6, which contain 2 and 4-M sodium simulant-S1 (i.e., lots of ions), appear to suppress the hydration reaction to a certain degree over the first 2.5 hours, although the

fact that these Cast Stone formulations only contain a small amount of cement in the solids (~ 8 wt% of total solids) is an additional factor causing the undisturbed yield stress to not increase over the time interval monitored.

Interestingly, when the ion content in the slurries is more than 4 M sodium (i.e., 8-M sodium condition), hydration is readily promoted as indicated by a continuous increase in undisturbed yield stress in Figure 7.2. The rate of increase in undisturbed yield stress for sample #7 appears to be comparable to or slightly less than that of sample #2, but the value of undisturbed yield stress is significantly higher than that of sample #2. This implies a high concentration of ions existing in this slurry promotes a faster initial hydration, giving a high undisturbed yield stress (688 Pa). This behavior is completely different from that of Cast Stone slurries made with 2-M and 4-M sodium simulant S1. Therefore, there may be a threshold ion concentration above which the ions are capable of actively promoting hydration. Unlike other samples, sample #3 (fly ash in DIW) does not show any tendency to harden via hydration reactions because its undisturbed yield stress is noticeably low for the duration of the monitoring. The low undisturbed yield stress of sample #3 is closely related to both its broad PSD (i.e., higher percentage of larger particles shown in Figure 4.4) and no chemical reactivity.

Figure 7.2. Undisturbed Yield Stresses for the Seven Representative Samples as a Function of Time. Note the measurement of simulant-S1 (8 M) at 2.5 hours cannot be performed because of significant rigidity.

Figure 7.3 exhibits the variation of dynamic yield stresses for the same seven representative slurry samples up to 2.5 hours. All dynamic yield stresses are smaller than the corresponding undisturbed yield stresses, except that the dynamic yield stress of sample #3, which contains fly ash only, is close to its undisturbed yield stress. As indicated in Figure 7.2, it would be difficult to detect a slow development of

microstructure from the undisturbed yield stress because the undisturbed yield stress is also affected by the false setting caused by the BFS. The difficulty in probing such a slow development of microstructure from using the undisturbed yield stress data alone can be clearly illustrated by the results of the two stress measurements on sample #4. Comparing undisturbed yield and dynamic yield stresses of sample #4 (the slag only slurry), it can be deduced that the dynamic yield stress curve versus time (Figure 7.3) is not influenced by the false-setting phenomenon seen in the undisturbed yield stress curve (Figure 7.2).
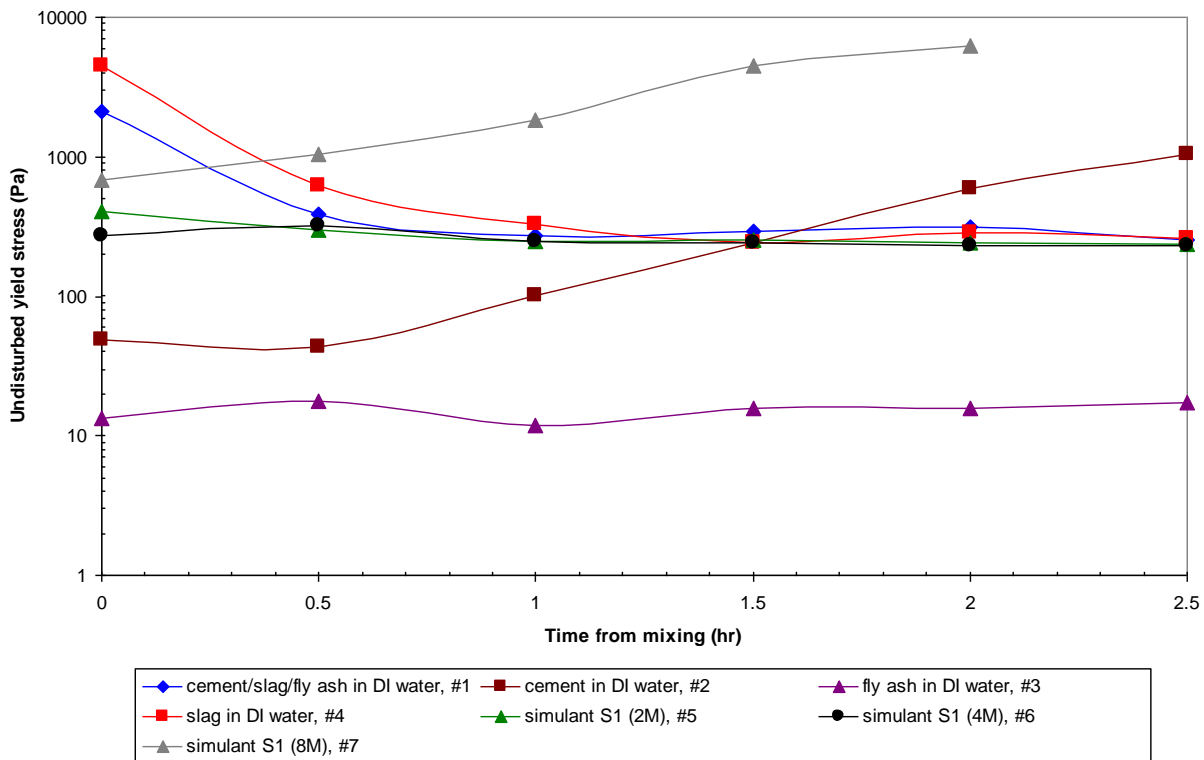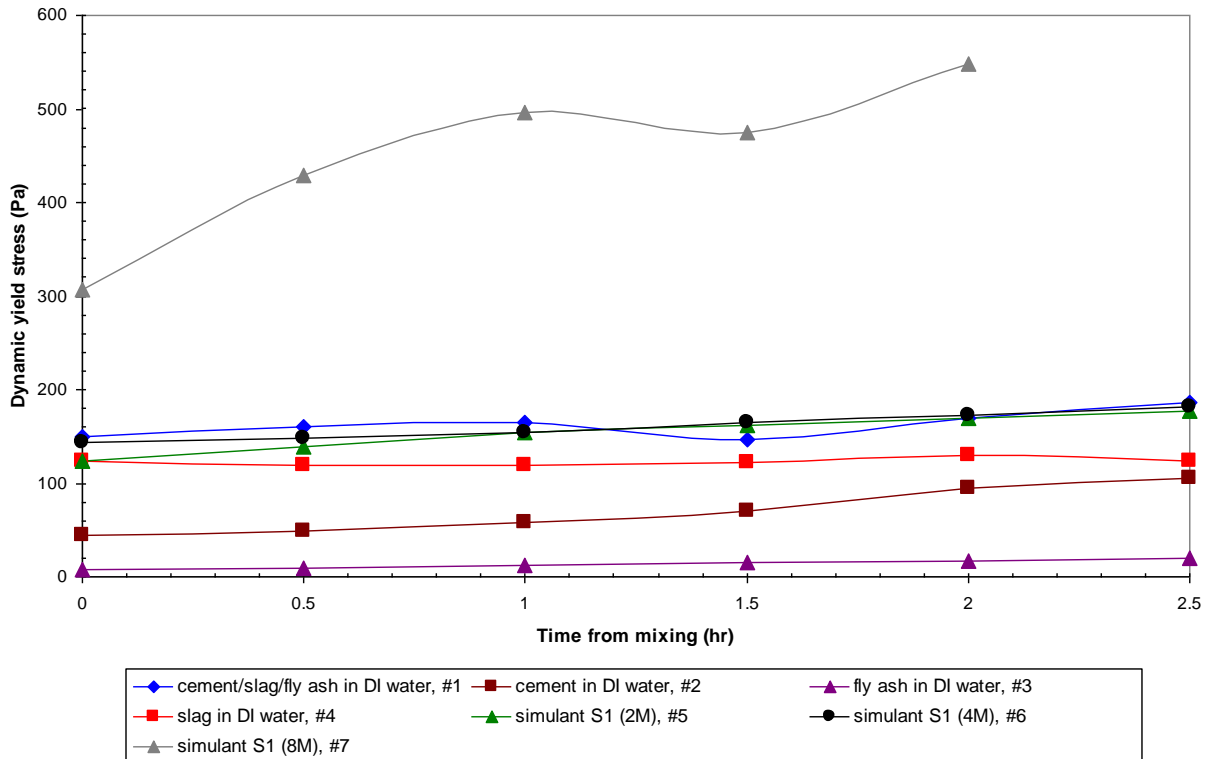

Figure 7.3. Dynamic Yield Stresses for the Seven Representative Samples as a Function of Time. Note the measurement of simulant-S1 (8 M) at 2.5 hours cannot be performed because of significant rigidity.

The Cast Stone slurry samples #5 and #6 show a slow monotonic increase in dynamic yield stress that suggests a slow development of microstructure. In contrast to samples #5 and #6, sample #7 (simulant-1 [8 M]) undergoes a faster development of microstructure because there are enough ions in the slurry, based on the significant dynamic yield stress at all times, compared to other slurries. Interestingly, the dynamic yield stress of sample #1 drops at a 1-hour measurement, although an overall trend from the start through 2.5 hours is an increase in dynamic yield stress (a clear indication of ongoing hydration). The drop in dynamic yield stress at 1.5 hours may be related to the appreciable C-S-H layer formation on the C_3S particle during hydration, which would reduce the flocculation of the particles. While there is a relatively high but decreasing undisturbed yield stress for sample #4 over the entire monitoring period, the absolute value and change in dynamic yield stress of sample #4 is not appreciable, which strongly suggests that slag is not significantly involved in any reaction driving a noticeable stiffening; the microstructure of the slag particles is not changing, and the slag slurry does not possess an appreciable resistance to flowing after an external stress is applied. That is, the slag particles do not coagulate into a cohesive mass after a stress is present to keep the particles separated.

7.3   Stiffening and Setting of Cast Stone

This section describes the investigation of the stiffening and setting process of Cast Stone slurries. Three methods—including ultrasonic wave reflection, XRD, and complex impedance spectroscopy—have been used to characterize the Cast Stone slurries.

7.3.1   Ultrasonic Wave Reflection

Ultrasonic wave reflection (UWR) is used to monitor the early hydration and stiffening of cement pastes.

7.3.1.1   Ultrasonic Wave Reflection Background

The Vicat test (ASTM C-191) and the Proctor test (ASTM C-403) have been widely used to determine the setting time of cement paste. The Vicat test uses mixtures with dry consistency and gives almost no information on the gradual changes in paste stiffening due to the hydration. For this reason, the Proctor test (C-403) has been mainly used by Struble and colleagues for monitoring the stiffening and setting of cement paste (Chung 2004; Struble et al. 2001; Chung et al. 2009, 2010a). They also applied the dynamic shear rheology technique to correlate the hydration and rheological behavior of cement-based materials (Chung 2004; Struble et al. 2001; Zhang 2001; Lei 1995; Chen 2007).

In most cases, the Proctor test and dynamic rheology are sufficient to monitor the stiffening and setting of cement pastes. However, some of the cement pastes that showed premature stiffening (AFm and syngenite formation) could not be tested with dynamic rheology because they had already passed the stress limit of the instrument (Chung 2004). The ASTM Proctor test (ASTM C-403) was able to measure stiffening until the final set, but this technique measures data at discrete time periods, and it is likely to miss any hydration events in between each measurement that are necessary to understand the stiffening associated with a specific hydration reaction.

The UWR technique has been successfully applied for monitoring early hydration and stiffening of cement paste to resolve these problems (Chung 2010). UWR measures reflected ultrasonic wave energy at the interface between a buffer material and cement paste or concrete. When cement paste shows fluid consistency, the amount of reflected wave energy is relatively large, especially for incident shear waves. As the cement paste hydrates, and its acoustic impedance increases to be closer to that of buffer material, more ultrasonic wave energy passes through the concrete and less reflects back to the transducer; hence, the reflection coefficient is decreased, allowing microstructural changes due to hydration to be detected. The experimental setup is shown in Figure 7.4.
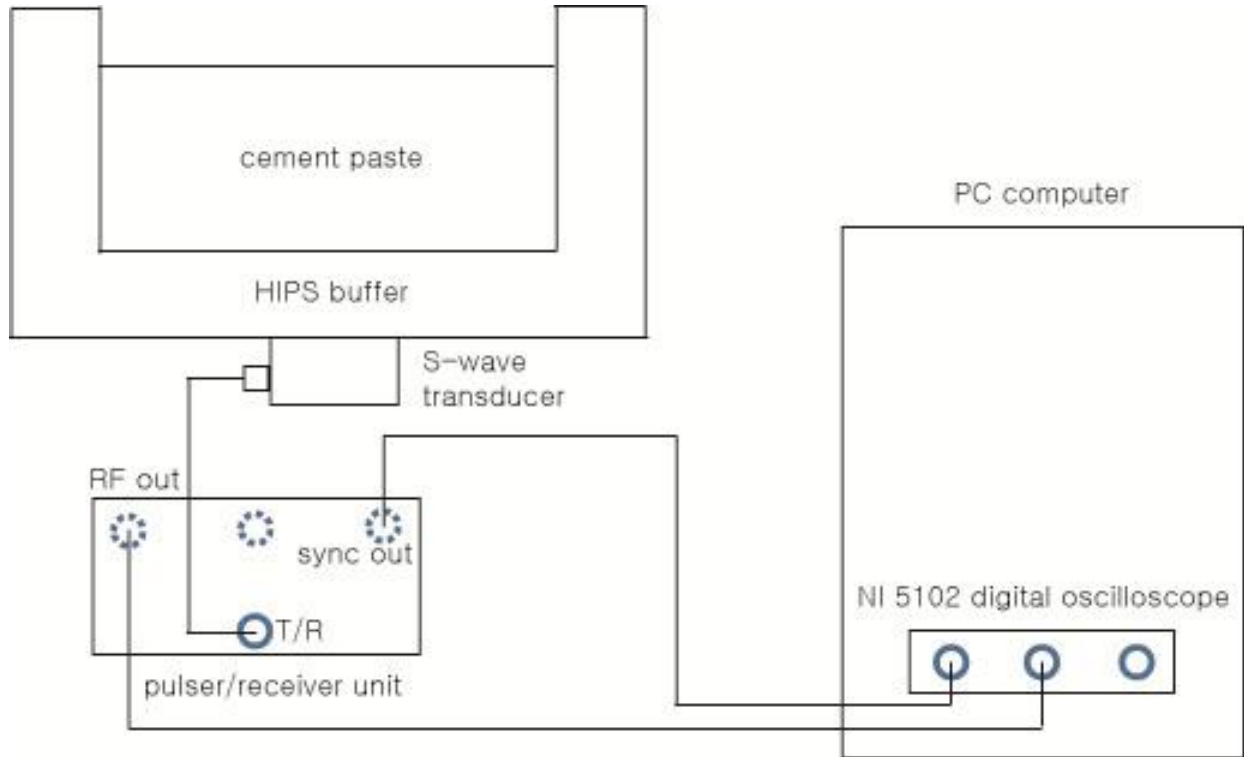
Figure 7.4. Dual Pulser Receiver Ultrasonic Wave Reflection Measurement Setup

7.3.1.2 Ultrasonic Wave Reflection Basic Concept

The concept of the UWR technique is described here. If the material properties of the buffer are known or are constant, the properties of the cementitious materials can be computed by applying the normal incidence reflection formula as shown in Equation (7.1):

$$|r| = \frac{A_r}{A_i} = \frac{Z_P - Z_B}{Z_P + Z_B}$$ (7.1)

where
r = normal incidence reflection coefficient
A_r = amplitude of the reflected wave
A_i = amplitude of the incident wave
Z_B and Z_P = S-wave acoustic impedances of the buffer and cementitious paste, respectively.

The reflection coefficient (r) obtained by Equation (7.1) is an absolute value. When the acoustic impedance of cement paste becomes higher than that of buffer, an inversion occurs.

According to Equation (7.1), the reflection coefficient is mainly determined by the relative difference in the acoustic impedance of paste (Z_P) and buffer (Z_B). If Z_B is much higher than Z_P, the relative change in ($Z_P - Z_B$) is negligible, although Zp increases as a result of hydration. If Z_B is close to Z_P, the relative change in ($Z_P - Z_B$) becomes larger as Zp increases as a result of hydration. Therefore, it is necessary to use a low acoustic impedance buffer (close to that of Z_P) to maximize the sensitivity of the measurement in the early stage hydration period, as shown in Figure 7.5. According to Figure 7.5, UWR measurements using high impact polystyrene (HIPS) as the buffer material (low acoustic impedance of 2.27×10^6

7.8

kg/[s·m^2]) maximized the sensitivity of the measurement. HIPS is also chemically resistant to acid and base, does not absorb water, and is stable at the pH values of cement paste (Chung 2010).
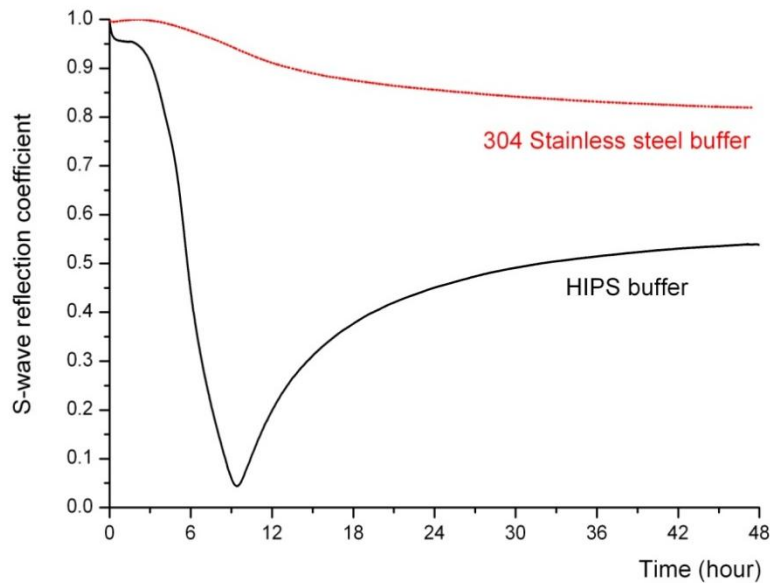
Figure 7.5. The effect of Buffer Type (stainless steel and HIPS polymer) on Ultrasonic Wave Reflection Measurements on Hydrating Cement Paste (Chung 2010a)

7.3.1.3   Ultrasonic Wave Reflection Sample Preparation

The cement used in this study was a commercial Portland cement[1] meeting the Type II requirements in ASTM C-150. The cement properties are presented in Table 4.1. Cast Stone pastes with water to solid ratios (w/s) were prepared by mixing 347.04 g cementitious mixtures (27.76 g cement, 156.17 g fly ash, and 163.11 g BFS) with 35 ml of simulant solution and 100 ml of DIW (making 26 volume % concentration). Cast Stone slurries were mixed using a commercial Magic Bullet blender for about 3-5 minutes. The overall mixing time varied depending on the consistency of the mixture that affects the removal of all solid particles from the wall of the mixing container. The hand-mixing time usually takes from 2-4 minutes. After hand-mixing was completed, the blade cover was tightly closed and attached to the base that applies shear forces. The mixture was then blender-mixed for 1 minute and used for the experiments. Note that the separate mixing procedure was applied for the measurement (including rheological measurement and UWR) because shear history (especially by irregular hand mixing) affects the early stiffening significantly.

As soon as the cement paste was mixed, approximately 150 mL was placed in the container designed for ultrasonic wave reflection and impedance spectroscopy measurements. UWR data were obtained by using 1-MHz and 2.25-MHz normal-incidence, S-wave transducers that were attached to the bottom of the container using phenol salicylate couplant on the transducer face. The transducers were further supported with adhesive tape to provide firm contact with the buffer. The thickness of the HIPS buffer at the bottom of the container was 6.25 mm. Each transducer was connected to a pulser/receiver unit (Panametrics 5077). A digital oscilloscope (NI 5102) was used to digitize the data with a sampling rate of

---

[1]Lafarge Corp.

10 MHz for each transducer. In the experiment, an ultrasonic pulse was sent from the transducer through the buffer to the interface with the sample.

7.3.1.4   Ultrasonic Wave Reflection Signal Processing

To obtain meaningful UWR data for analysis, a series of signal processing techniques have been applied. The reflected wave pulse of interest in the time domain signal was windowed for a duration of 5 μs and zero-padded for 10 μs on each side. One hundred of these processed pulses were averaged, and the resulting time domain signal was mapped to the frequency domain using the fast Fourier transform algorithm.

To isolate the reflection coefficient of the interface, effects of the natural wave propagation losses within the buffer and the coupling of the transducer to the buffer material should be eliminated through empirical compensation, called the compensating algorithm, which was originally developed by Öztürk et al. (1999) and further modified by Suburmaniam et al. (2005) and Chung (2010). The Fourier transform of the first reflected pulse F_1 is given by Equation (7.2):

$$F_1(f) = S_T\, d_1\, r\, d_2$$

(7.2)

where S_T is the transducer function, which describes the characteristics of the transducer and how it is coupled to the buffer surface, r is the absolute value of the normal incidence reflection coefficient (r) at the buffer-cement paste interface, and d_1 and d_2 represent signal energy losses resulting from wave dissipation, wave scattering, and beam spreading within the buffer material along the transmitted and reflected wave paths, respectively. Because the reflection coefficient at the buffer-air interface is nearly unity[1], the Fourier transform of the first pulse reflected at air is shown in Equation (7.3):

$$F_{1,\ air}(f) = S_T\, d_1\, d_2$$

(7.3)

Dividing the reflection obtained from the Cast Stone by that obtained from air, the normalized reflection coefficient r as a function of frequency can be obtained as shown in Equation (7.4):

$$\frac{F_1(f)}{F_{1,\ air}(f)} = \frac{S_T\, d_1\, r\, d_2}{S_T\, d_1\, d_2} = r$$

(7.4)

To correlate the specific hydration reaction with the stiffening response of Cast Stone slurries measured by UWR, XRD was used for phase investigation for hydrated Cast Stone slurries at 5 min, 30 min, and 2 hours, respectively. To better understand the UWR results, the following will help interpret the results: 1) flat or slightly sloping parts of the curves represent little stiffening over time, which can be also interpreted as a workable time period; 2) conversely, steeply sloping parts of the curve reflect rapid stiffening over time, and the paste is not workable any more; and 3) the "inversion" simply reflects the fact that the mix has become stiffer than the buffer.

---

[1] With HIPS buffer in air, r is equal to 1.0000 for S-waves and 0.9996 for P-waves.

7.3.1.5   Ultrasonic Wave Reflection Results

The S-wave reflection response from cement only paste, Cast Stone made with DIW, and Cast Stone made with S1-2 M and the S1-4 M solutions are presented in Figure 7.6. The S-wave reflection coefficient for cement paste is near unity right after mixing, and there is a slight decrease in the reflection coefficient during the next 140 minutes or so. Although this cement paste does not show a plateau during this period, this slight decrease is associated with the dormant period commonly observed using calorimetry. The slight decrease in the reflection coefficient during the dormant period suggests that cement particles are developing a more strongly flocculated microstructure, even during the induction period, a finding that confirms observations using oscillatory shear rheology (Struble et al. 2000).

At about 140 min of reaction, the reflection coefficient for cement paste only begins to decrease rapidly. The decrease is attributed to the development of solid microstructures caused by hydration. The time when the rapid decrease in the S-wave reflection coefficient begins is considered as the onset of stiffening. This S-wave measurement of the onset of stiffening occurs earlier than the initial set measured by penetration resistance measurements (Chung 2010). The reflection coefficient continues to decrease until the inversion point when the acoustic impedance of cement paste exceeds that of the buffer, which is seen in Figure 7.6 at about 330 minutes. After the inversion, because the paste impedance continues to increase, the reflection coefficient increases with time.

The S-wave reflection response of Cast Stone (8% cement, 45% fly ash, and 47% slag) mixed with DIW is presented in Figure 7.6 (black line). This slurry was prepared and measured to provide a reference slurry to compare with Cast Stone made with various secondary simulants. The magnitude of the drop in the S-wave reflection coefficient for the Cast Stone mix is smaller compared to that of cement paste only, but the dormant period is extended from about 140 to 260 minutes. That is the dormant period that the Cast Stone mix lasts, which is 120 minutes longer than that of cement paste. Thus, the onset of rapid hydration is delayed. After the onset of stiffening at 260 minutes, the Cast Stone with DIW starts to show rapid microstructural development. The interesting finding is that S-wave inversion of the Cast Stone slurry occurred at around the reflection coefficient 0.3. Theoretically, the inversion should occur at a reflection coefficient of 0, but a higher inversion point has been attributed to viscous energy loss (Subramaniam 2007), which originates from the polymer buffer and the hydrating cementitious material. Viscous energy loss is often observed for the cement pastes when a HIPS buffer is used for UWR measurement, but inversion at a reflection coefficient higher than 0.3 is quite unusual because most of the cement paste studied showed the S-wave inversion to be lower than or closer to a value equal to 0.1 (Chung 2010).

The Cast Stone slurry made with S1-2 M solution showed inversion at an even higher reflection coefficient. It is not certain why the Cast Stone slurry shows an inversion point at this higher reflection coefficient, but it is recognized these materials are more lossy (attenuation in ultrasonic wave energy) in their characteristics compared to normal cement paste (considering the same energy loss occurs in the HIPS buffer). The stiffening characteristics of Cast Stone made with highly saline waste simulants are quite different from that of cement paste. In addition, the dormant period extended to 360 minutes. The extension of the dormant period correlates very well with a decrease in yield stress from rheological measurements presented in the previous section.

The Cast Stone slurry made with S1-4 M solution showed a more rapid early drop in the reflection coefficient than the other slurries for the first 30 minutes. This indicates fast stiffening of the mixture.

This rapid drop in the reflection coefficient was found to be associated with the premature stiffening of cement paste caused by secondary gypsum formation (Chung 2010). However, note there is no significant change in other rheological measurements (presented in previous sections) on this Cast Stone made with the S1-4 M solution. After the initial rapid drop in the reflection coefficient, the slope for S1-4-M Cast Stone slurry becomes slower, indicating the dormant period is occurring. The onset of stiffening in the S1-4-M Cast Stone slurry occurred at about 400 minutes based on the resumed rapid rate of decrease in the S-wave reflection coefficient. The UWR results suggest that the presence of secondary waste solution S1 up to 4-M sodium concentration delays the hydration of Cast Stone.
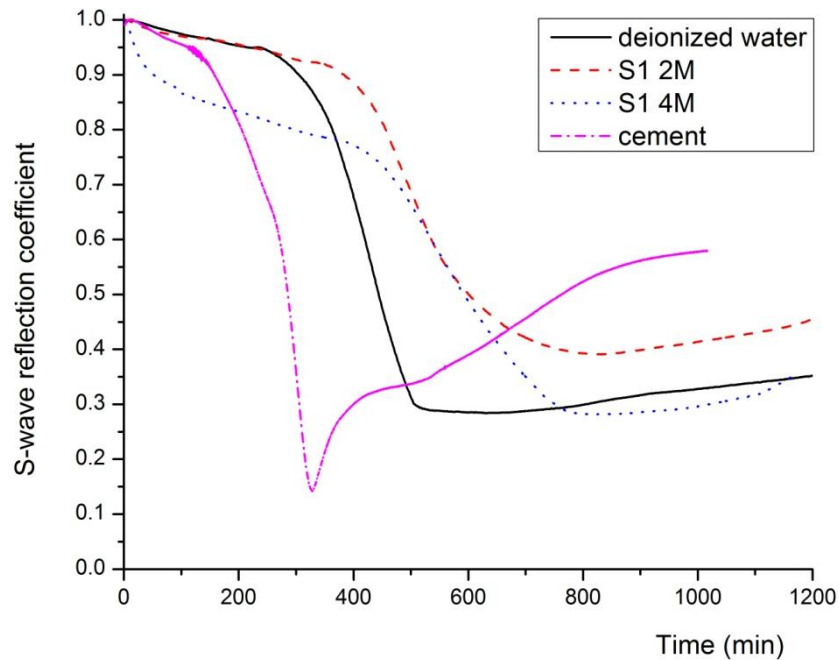
Figure 7.6. S-Wave Reflection Coefficient of Cement Paste, Cast Stone with DIW, S1-2-M Solution, and S1-4-M Solution, Respectively

The UWR response of S1-6-M, S1-8-M, and S1-10-M specimens are presented in Figure 7.7. The UWR response of the Cast Stone slurries at these concentration levels showed significantly different UWR responses compared to Cast Stone slurries made with waste solutions with lower concentrations (Figure 7.6). There is no dormant period observed in the more concentrated waste slurries shown in Figure 7.7. The inversion occurred at a value about 0.1, which is close to that of normal cement paste. The S-wave reflection coefficient drops fairly rapidly right away for three Cast Stone slurries made with the more concentrated S1 wastes. The S1-8-M and S1-10-M-based Cast Stone slurries showed even faster stiffening than S1-6-M slurry. In fact, the stiffening trends for the S1-8-M and 10-M-based slurries are very similar. For these Cast Stone slurries with the two highest waste concentrations, it seems the hydration kinetics has been significantly changed in comparison to Cast Stone slurries made with S1 simulants with lower concentrations and Cast Stone made with DIW. The inversion of S1-10-M-based slurry occurred at about 250 minutes, at least an hour faster than the inversion of cement paste, which occurred at 330 minutes (see purple dashed line in Figure 7.6). The higher concentration waste solutions seem to promote faster stiffening. This is based on the faster drop in the reflection coefficient for the Cast Stone S1 slurries with concentration levels above 8 M. However, effectively solidifying the higher concentrated S1 waste simulant in Cast Stone required the use of the dispersing agents, such as a superplasticizer, because of their rapid early stiffening characteristics.
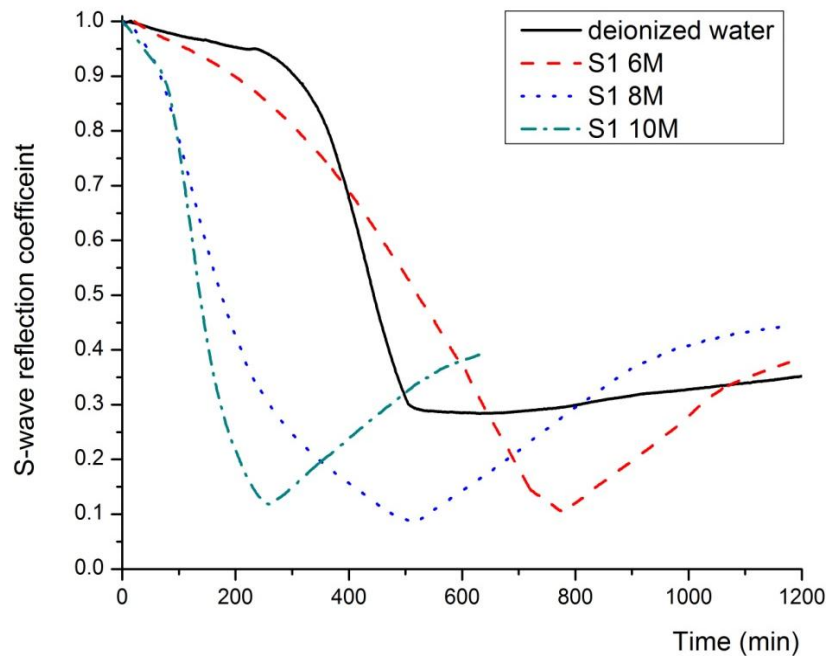
Figure 7.7. S-Wave Reflection Coefficient of Cast Stone with DIW, S1-6-M Solution, S1-8-M Solution, and S1-10-M Solution, Respectively

UWR responses of Cast Stone slurries made with the four simulants at a 2-M sodium concentration are presented in Figure 7.8. The UWR measurements for the S1, S2, and S3 based slurries show quite similar responses. The duration of the dormant period for both S1- and S2-based 2-M sodium specimens was the same, whereas the duration of the dormant period for S3-2-M slurry is a bit extended. However, considering the slope of the decreasing reflection coefficient during the dormant period, these materials do develop similar early stiffening characteristics. Because the S1-2-M sodium composition is a median concentration for anions and S2 and S3 represent the high and lower range values for carbonate and nitrate concentrations, the UWR response of S1-2 M being located in between those of S2- and S3-2 M is a reasonable result. The variation in anion compositions within the 2-M sodium based simulants did not cause significant changes in rheological properties, such as early stiffening of the Cast Stone.

However, the S4-2-M-based cast Stone slurry showed a quite different UWR response. This simulant showed inversion of the reflection coefficient curve at values of about 0.4, which is similar to both S1 and S3, but the inversion occurred about 200 minutes earlier than S1. The initial slope is higher for S4-2 M compared to the other S1-, S2-, and S3-based simulant slurries. The onset of stiffening for the S4-based Cast Stone slurry occurred at about 220 minutes, which is earlier than the onset of stiffening in the slurries containing S1, S2, and S3 simulants. This indicates the stiffening characteristic of S4-2-M simulant is quite different from the other three simulants.
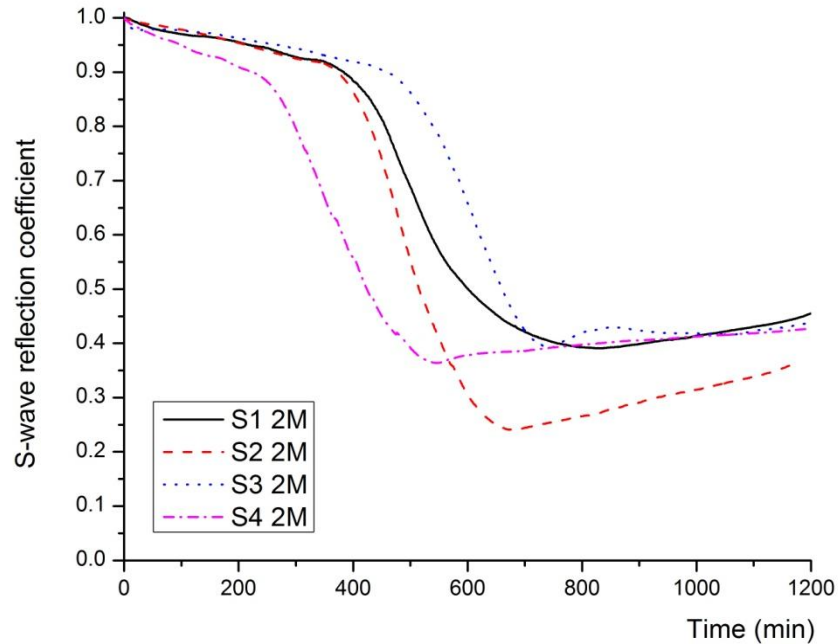
Figure 7.8. S-Wave Reflection Coefficient of Cast Stone with S1-2-M Solution, S2-2-M Solution, S3-2-M Solution, and S4-2-M Solution, Respectively

7.3.2   X-ray Diffraction

Figure 7.9 through Figure 7.11 present the XRD patterns of hydrated Cast Stone slurries made with DIW, S1-2-M, S1-4-M, S1-6-M, S1-8-M, and S1-10-M specimens at 5 min, 30 min, and 2 hours, respectively. According to the XRD patterns on these slurries, the gypsum peak (at a 2θ angle of 11.59°) dominates other peaks. The calcium sulfate hemihydrate (bassanite) peak (at a 2θ angle of 14.72°) that was found in the original Cast Stone dry blend disappeared, the anhydrite peak (at a 2θ angle of 25.44°) intensity decreased, and the gypsum peak increased as a result of the early reactions. This is a clear indication of recrystallization of gypsum. It occurs because the calcium sulfate polymorphs have the same final solubility when they are dissolved in water, but their rate of dissolution, based on the release of SO_4^{2-} ions, is much faster (approximately three times) for calcium sulfate hemihydrate than for gypsum (Aitcin 1998). Therefore, if sulfate ions are not consumed rapidly by hydration of C_3A to form ettringite and monosulfoaluminate, then the ions reach their maximum allowable concentration level and start to precipitate by consuming calcium and water to form secondary gypsum. Stiffening is often mentioned as a false set and is associated with interlocking of particles caused by the needle-like gypsum crystals in addition to the reduction in water content. Unlike a flash set, the rigidity can be overcome and plasticity can be regained by further mixing without adding water (Mindess et al. 2003). The subsequent strength development is not affected.

Secondary gypsum formation occurred in the Cast Stone slurries made with DIW, S1-2 M, and S1-4 M. These time series XRD measurements on the slurries clearly show the gypsum peak keeps increasing in the early stage of hydration. That is, the early hydration of the Cast Stone is dominated by gypsum formation. However, from the rheological measurements shown in Section 7.2.1, the S1-2 M and S1-4 M did not show as much yield stress as the Cast Stone specimen made with DIW. It is not certain

7.14

why the secondary gypsum formation did not affect the rheological measurement on Cast Stone slurries made with S1-2 M and 4 M whereas it did for Cast Stone made with DIW and the pure slag slurries. It is also not clear why the secondary gypsum formation was not at all captured by the UWR except for the Cast Stone slurries made with S1 4 M. The UWR with the HIPS buffer is supposed to effectively capture premature stiffening associated with secondary gypsum formation with cement paste (Chung 2010). A likely explanation here is that although calcium sulfate precipitates, in some cases, it may not form interlocking crystals or bridges between grains of other solid particles; hence, its presence or absence may have no systematic relationship to the stiffening profiles. A small amount of ettringite (at a 9.09° 2-theta angle) was observed in the slurries, but the ettringite formation does not seem to affect the stiffening of the Cast Stone slurries.
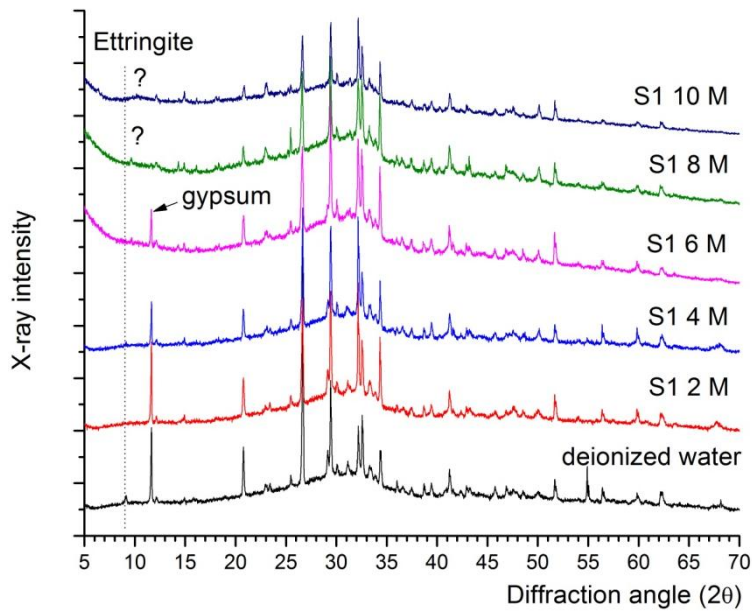
Figure 7.9. XRD Patterns of Cast Stone with Various S1 Simulant Concentrations after 5 Minutes of Hydration
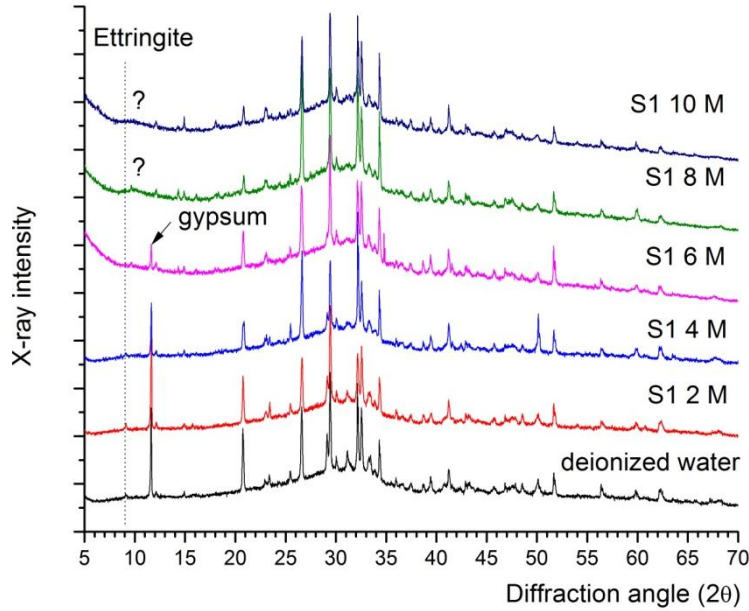
Figure 7.10. XRD Patterns of Cast Stone with Various S1 Simulant Concentrations after 30 Minutes of Hydration
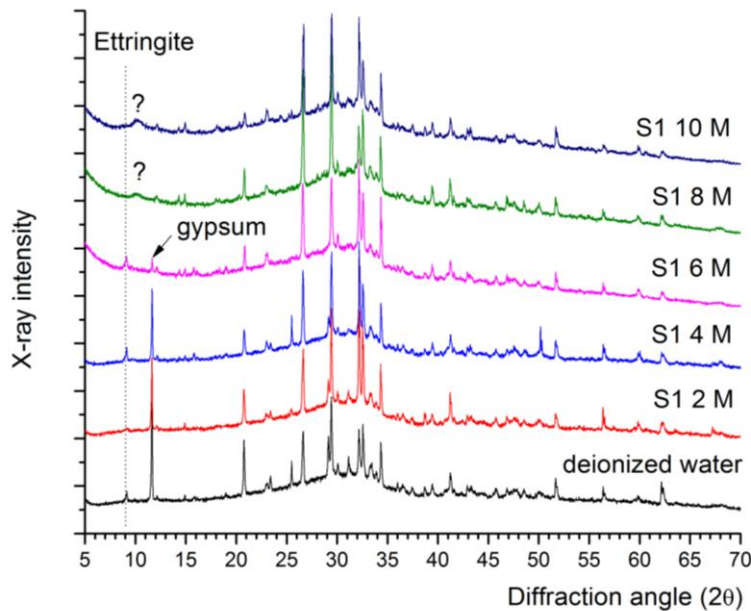
Figure 7.11. XRD Patterns of Cast Stone with Various S1 Simulant Concentrations after 2 Hours of Hydration

As shown in the XRD patterns in Figure 7.9 through Figure 7.11, the S1-6-M-based Cast Stone slurry indicates that some gypsum peak is present, but the gypsum peak intensity is much lower compared to DIW, S1-2-M, and S1-4-M-based Cast Stone slurries. In addition, it is less likely that the gypsum peak is associated with secondary gypsum formation because the gypsum peak from a raw mixture (Figure 6.15) is higher than the gypsum peak observed from the S1-6-M specimen. The decrease in the gypsum peak

indicates that some of the gypsum originally present in Cast Stone dry blend was consumed during the hydration reaction. Considering the UWR response of the S1-6-M specimen, it is very likely that 6 M is a transition concentration level that changes the hydration kinetics of Cast Stone waste forms made with the S1 simulant.

The S1-8-M and 10-M-based Cast Stone slurry XRD patterns at various hydration times did not show any evidence of a gypsum peak. The results from the two highest concentration slurries indicate that two different kinds of hydration reactions exist during the early hydration period of Cast Stone made with the S1 waste simulant. The formation of gypsum is dominant in Cast Stone slurries made with the lower concentration of S1 (up to and including 4 M sodium), whereas another as yet not defined hydration reaction is dominant in Cast Stone slurries made with S1 simulant with concentrations at or above 8 M sodium. The XRD peak for slurries made with S1 concentrations at or above 8 M sodium at around a 2θ angle of $10°$ is most likely calcium (aluminate) silicate hydrate. Further investigation is required to verify this result.

Because there is no gypsum peak observed from Cast Stone specimens hydrated more than 28 days (Figure 6.14 and Figure 6.16), the gypsum observed in low-concentration S1 slurries characterized at the early time is very likely consumed during the hydration of C_3A to produce ettringite, as described in Equation (3.4). The high intensity ettringite peak in Figure 6.16 from Cast Stone made with the lower concentration solutions seems to be mainly associated with the higher gypsum formation in the early ages and the consumption of gypsum to form ettringite at the later stages. However, the low ettringite peak from Cast Stone waste forms (Figure 6.16) made with the higher concentration S1 simulant is most likely associated with the consumption of gypsum from an unknown hydration reaction so that the ettringite formation is suppressed in later stages.

Figure 7.12 through Figure 7.14 present the XRD patterns of hydrated Cast Stone slurries made with S1-2-M, S2-2-M, S3-2-M, and S4-2-M simulants at 5 min, 30 min, and 2 hours of reaction, respectively. Similar to S1-based Cast Stone slurries with the lower sodium concentration levels, the gypsum peak in the other three slurries made with the S2, S3, and S4 dominates other peaks. This is an indication of recrystallization of gypsum. However, the gypsum peak intensity of the S4-2-M specimen is higher than for other three simulant slurries, especially at 2 hours of hydration. This indicates that stiffening caused by secondary gypsum formation is higher in the Cast Stone made with S4-2 M compared to the Cast Stone made with the other simulants. A small amount of ettringite (at a 2θ angle of $9.09°$) was observed with all specimens, but it does not seem to affect the early stiffening of any of the secondary waste containing Cast Stone.
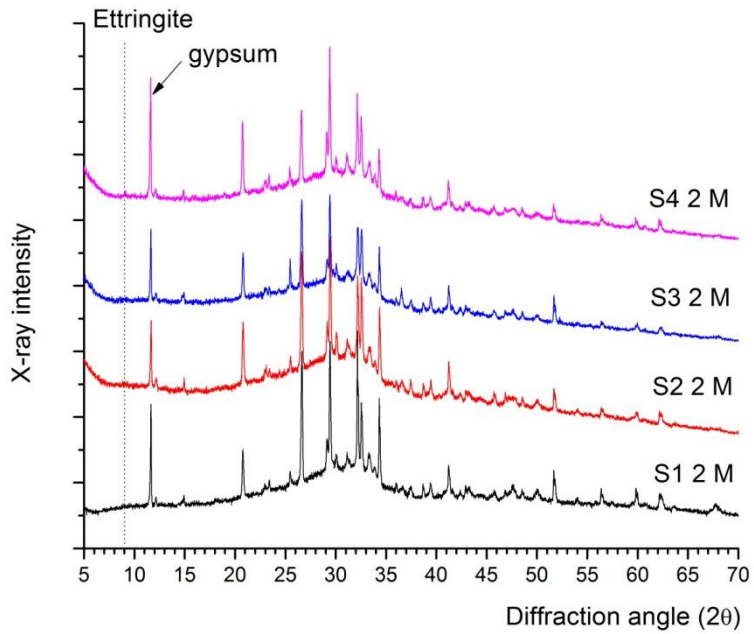
Figure 7.12. XRD Patterns of Cast Stone with Various Simulant Solutions after 5 Minutes of Hydration. Note each simulant solution was diluted with DIW to make a 30% concentration.
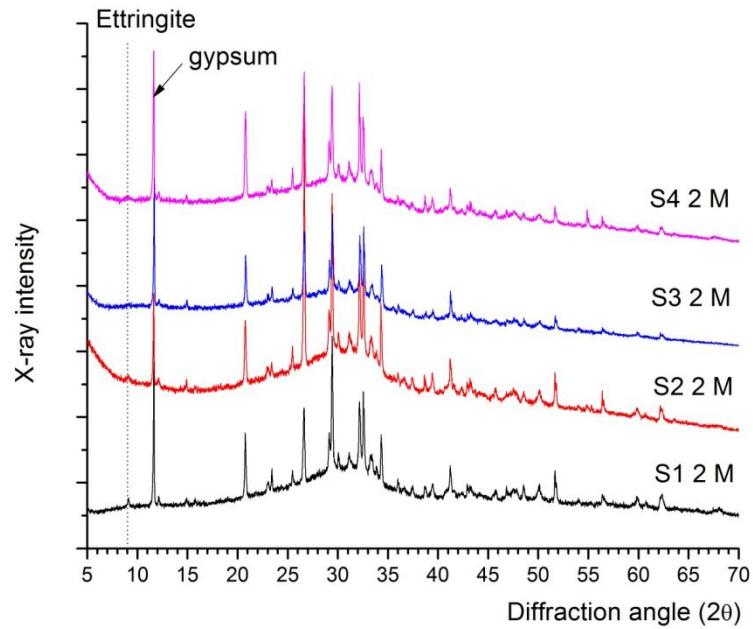
Figure 7.13. XRD Patterns of Cast Stone with Various Simulant Solutions after 30 Minutes of Hydration. Note each simulant solution was diluted with DIW to make 30% concentration.
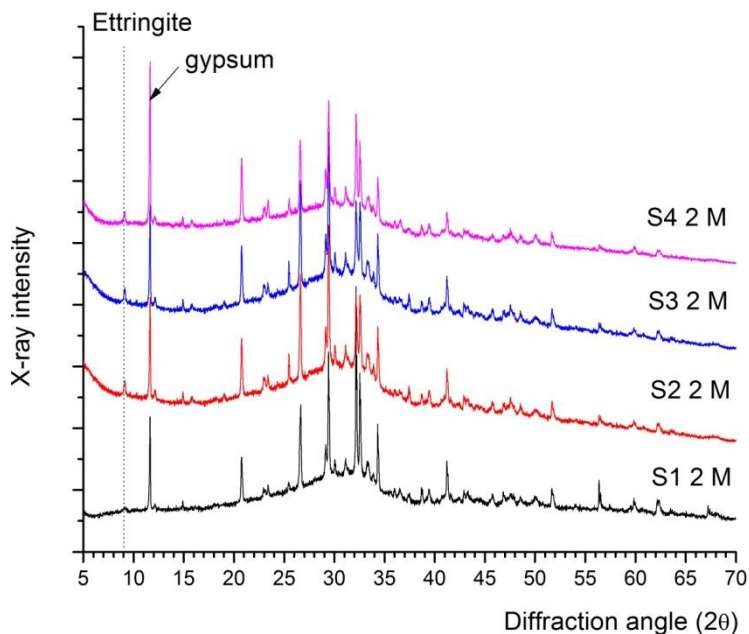
Figure 7.14. XRD Patterns of Cast Stone with Various Simulant Solutions after 2 Hours of Hydration. Note that each simulant solution was diluted with DIW to make a 30% concentration.

7.3.3   Complex Impedance Spectroscopy

Impedance spectroscopy (IS) has been used for understanding various features of hydration of cementitious materials since the early 1980s. Professor T. O. Mason's group at Northwestern University has pioneered using this tool for studying the evolution of microstructures in cement-based materials (Chrisensen et al. 1992). In combination with pore fluid conductivity modeling and measurement, the IS data can be used for predicting ion diffusivities of cement pastes (Christensen et al. 1994), which will be valuable in the case of nuclear waste disposal; e.g., Olson and coworkers (Olson et al. 1997) have applied the IS to study the immobilization of the high-alkaline solution simulating low-level radioactive waste in blended cement. This nondestructive electrical characterization tool can provide insights about the solution and interfacial processes and the phases formed as a function of time in the waste form. The authors of this report used the Solartron Cell Test® (shown in Figure 7.15) to study the hydration of selected Cast Stone mixtures.
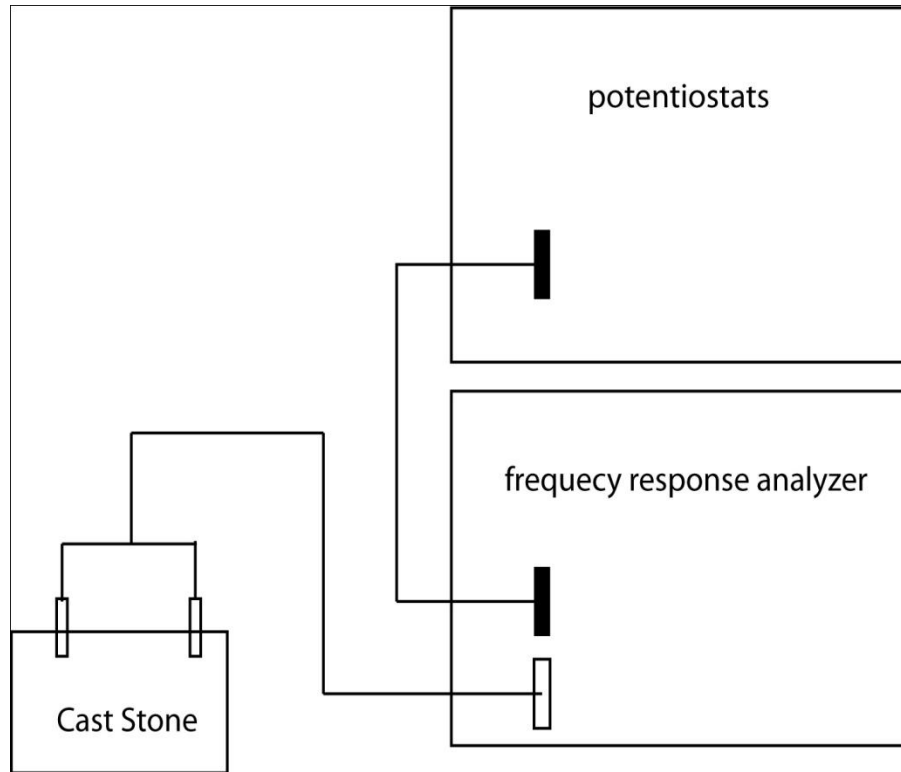
Figure 7.15. Experimental Setup for Impedance Spectroscopy Measurements

Preliminary IS data obtained on selected samples are shown in Figure 7.16 and Figure 7.17. Preliminary results indicate (Figure 7.16) that researchers need to cover a greater frequency range than that used to date (1 mHz to 13 MHz) in measurements to deconvolute the data. An optimum scan rate will also be needed to capture the dynamics of hydration in the Cast Stone samples. At this point, the data collected are inadequate. Figure 7.17 shows a slow increase in real impedance at the beginning of hydration, and then the rate of increase starts to accelerate at approximately 8 hours. Realistically, it is reasonable to expect that hydration leads to more connectivity and strength development and the real impedance plots can quantify the strength development. Whether this expectation can be fulfilled using impedance analysis will be investigated in the early stages of Phase 3 and implemented if appropriate.
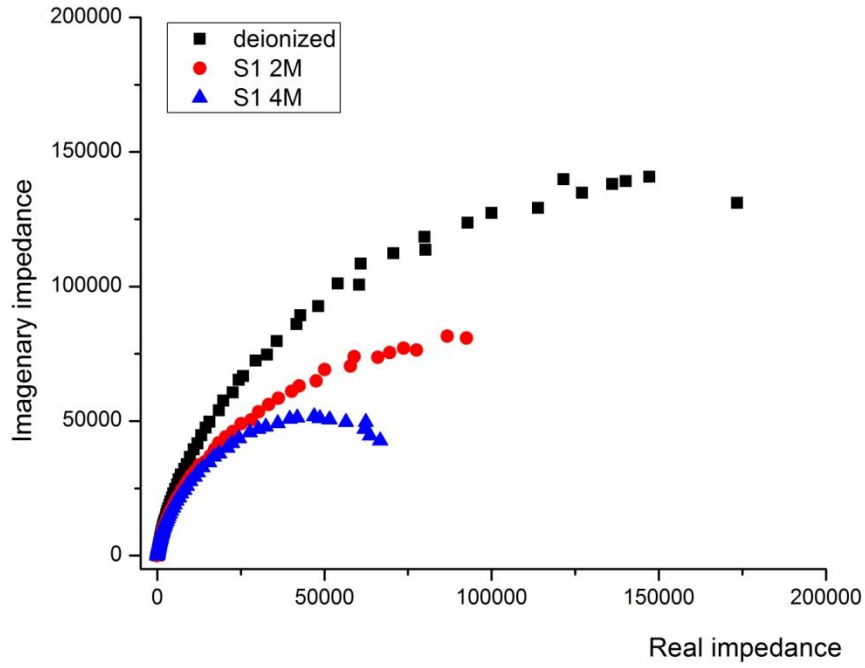
Figure 7.16. Real Versus Imaginary Impedance of the Samples after 24 Hours of Hydration
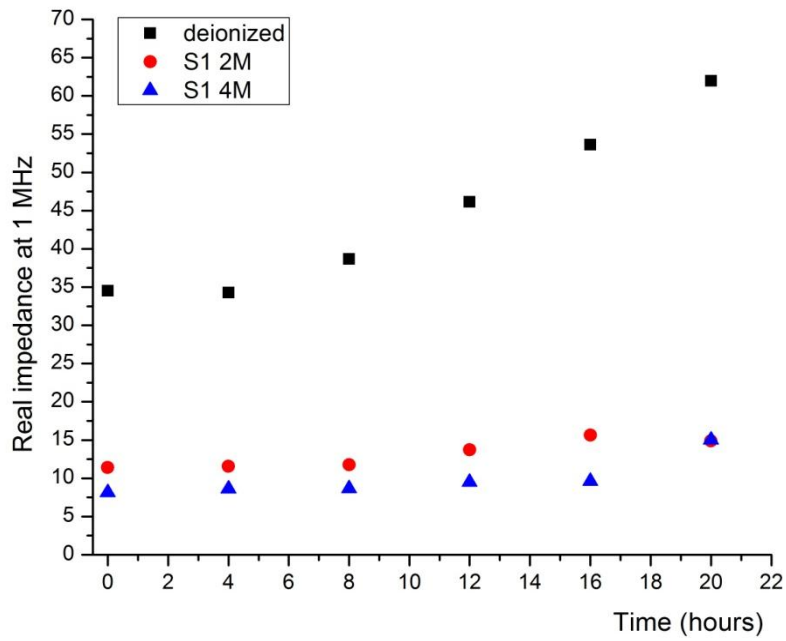
Figure 7.17. Real Impedance (at 1 MHz) Versus Time of Samples after 24 Hours of Hydration

8.0   Conclusions and Recommendations

Overall, key performance properties of the Cast Stone samples, including mechanical strength, technetium diffusivity, and LI met and exceeded target values, confirming that Cast Stone is a promising waste form candidate for solidifying WTP liquid secondary wastes. Leachable concentrations of technetium from Cast Stone samples prepared with different simulant recipes were affected by simulant pH, liquid-to-solid ratio, simulant type, simulant concentration (or waste loading), and the initial technetium concentration added to the simulants. Increasing technetium leaching was found as both the sodium concentration of simulant S1 and the pH increased. At leachate pH values higher than 10.0, the increasing technetium leaching was probably stopped by a carbonation reaction that formed calcite precipitates that could block the technetium mass transfer through the solid waste form's pore spaces. The technetium diffusivity and LI were affected by the concentration of the waste simulants (or waste loading) used in making the Cast Stone monoliths. Increasing technetium diffusivity was also found in Cast Stone prepared in simulant S1 as the concentration was increased from 2 M to 10 M sodium. However, most of the calculated technetium LI values, based on 63 days of leachate collection, were higher than 9.0, which is a target based on performance assessment analyses, suggesting that Cast Stone is one of the good candidates for stabilizing WTP secondary liquid wastes. There was no observed impact on the diffusivities for the S2 and S3 simulants, which are variants on the baseline S1 simulant. Interestingly, the S4 simulant with a higher ionic strength and higher technetium concentration showed lower technetium diffusivities compared to the S1 simulants at 4M to 10M sodium. The cause is not known but warrants further investigation.

Phase assemblage and microstructural features for the simulant-bearing Cast Stone are consistent with the findings from cement and concrete technical literature. Detailed characterization of pore-size, pore-structure, and pore-distribution attributes for waste forms is needed to develop a correlation to the long-term waste form performance and the individual contaminant leachability. Preliminary rheological measurements, such as yield stress and ultrasonic S-wave reflectance as well as modeling, show promise for developing a good correlation between the starting Cast Stone recipe and curing dynamics and waste form performance. Based on our Phases I and II results on Cast Stone testing, the authors of this report make the following recommendations:

1. **Fly Ash Addition:** The most common use of fly ash is to reduce the heat of hydration. For this purpose, Class F fly ash was originally selected for Cast Stone. However, the authors of this report found the fly ash used in the Phase 2 studies may generate some heat of hydration in the early curing period. It should also be noted that although the fly ashes used in both Phases I and II were obtained from the same vendor and both were classified as Class F, according to XRD patterns of both fly ashes, the fly ash used in Phase 2 contained much more crystalline phases. That is, although both fly ashes were claimed to be the same, the observed crystalline phases were significantly different. This could have been associated with the processing conditions during the production of fly ash (cooling rates, etc.) but could have also been associated with the differences in the chemical compositions caused by the impurities in the fuel (coal). This not only indicates the complex chemistry of fly ash but also suggests the properties of fly ash are not well controlled, which is mainly because fly ash is not a manufactured material like cement, but rather a by-product material. Although the fly ash develops early strength, there are two other binders in the Cast Stone—the Portland cement and the pozzolanic BFS, which are capable of forming an adequately strong solid. Considering these findings, it is suggested the Cast Stone dry blend that will be used in the Phase 3 research plan be significantly

modified. Adding fly ash only increases the complexity of the hydration chemistry. It is recommended either to find an alternative low-calcium fly ash (CaO content lower than 5%) or to completely remove fly ash from the dry blend for further Cast Stone optimization testing.

2. **Slag Quality:** From the hydration studies and rheological measurements, it is certain the secondary gypsum formation originated from the BFS. As mentioned earlier, the slag is not supposed to contain such calcium sulfate phases. Because it is generally understood that an excessive content of sulfate deteriorates the physical stability of most cement-based materials, the use of such slag should be minimized for future Cast Stone optimization studies. The vendor may have added some ingredients into the slag during the grinding process to match the slag performance with its cement product for clients in the building industry. However, this kind of treatment is not recommended because it will adversely impact the rheological behavior of the Cast Stone. It is crucial to obtain the BFS directly from the steel manufacturer or at least to request a slag that does not contain any calcium sulfate phases.

3. **Addition of Superplasticizer:** The use of a dispersing agent, such as a superplasticizer, is a key question for producing Cast Stone. Results showed that the rheological behavior and stiffening of Cast Stone are significantly affected by the ionic concentration of the simulants. When the waste simulants contain concentrations above a certain threshold, the stiffening or paste setting occurs earlier than desired. A superplasticizer could address this early stiffening problem by making Cast Stone more fluent in the early stages of hydration and thus improving the workability of the fresh Cast Stone. It is known that superplasticizers, when used in appropriately small dosages, do not affect the durability and strength of concrete, making this approach appealing for the production of Cast Stone, particularly at higher waste loadings. However, it should be noted that some material characteristics of cementitious solids can be changed by of the use of superplasticizers, including the leachability of select contaminants stabilized in the Cast Stone. An evaluation of the trade-offs would require more study using monolith leaching tests.

4. **Thermal Effects:** The temperature profile generated during the curing of Cast Stone is a very important parameter that influences long-term performance. Because the actual production of Cast Stone will be into large monoliths, the temperature profile based on the small 50-mm-diameter $\times$ 100-mm-long cylindrical specimens studied to date is not particularly instructive. Heat generation and release in the full-size waste form needs to be addressed to prevent thermal cracking and an abnormal hydration reaction (e.g., delayed ettringite formation) that may significantly deteriorate the Cast Stone. Additional experimental studies (e.g., at a larger scale or at elevated temperatures) are recommended.

5. **Rheological Characterization:** The original purpose of the rheological measurements was to observe the earlier stages of Cast Stone hydration and stiffening. UWR applies to the range outside the capability of the rheometer and it further correlates to the setting of the Cast Stone. From current studies, rheological characterizations (mainly focused on undisturbed and dynamic yield stress measurements based on vane-in-cup geometry) were shown to provide good complementary, quantitative information on Cast Stone workability. More importantly, UWR measurements have been very useful to characterize the stiffening and setting of Cast Stone. Using both rheological measurement and UWR for Cast Stone was quite successful. Note the sensitivity of the UWR method is low, especially in the early stage of hydration. Rheological and UWR measurements complement each other in validating waste form processing performance. Therefore, recommend that these rheological characterization techniques continue to be performed at the same time on Cast Stone slurries to evaluate their workability and to probe the hydration reaction.

6. **Pore Size Distribution, Total Porosity, and Surface Area Measurements:** The classical surface area technique known as BET was not useful when measuring Cast Stone chunks or ground powders to predict strength and durability. The pore-size range for BET is nanometer-sized pores, which are more responsible for the production of calcium (alumino) silicate hydrate. The pores more responsible for strength development and durability are capillary pores, whose size is in the micrometer range. To characterize micrometer-sized pores, mercury intrusion porosimetry (MIP) is a superior approach. Thus, we recommend further pore size and distribution characterization (using MIP, X-ray tomography) and modeling together with BET surface area measurements. These techniques would more accurately measure the total porosity, the pore sizes, and their distribution so that more objective correlations between these fundamental parameters and long-term contaminant leaching can be performed.

7. **Correlation Between Initial (e.g., hydration) and Later Stages (e.g., leachability):** The leachability of the Cast Stone is the most important property of the waste form with respect to controlling the release of contaminants within the IDF disposal system. We know that the more the Cast Stone hydrates, the more the leachability is reduced. In preparing the Cast Stone, we can control and measure the initial stages of the Cast Stone hydration. We need a more systematic understanding of how hydration correlates with contaminant long-term leachability. This will aid in further optimizing the Cast Stone formulation with respect to dry materials blends and processing parameters.

8. **Accelerated/Advanced Leach Testing:** Understanding the long term performance of the Cast Stone is important for performance assessment analyses of the IDF. It is important to leach test the waste form selected for solidifying the secondary wastes over a range of temperatures and humidity with leachants that are relevant to the long-term disposal conditions. These types of tests will be the emphasis of the Phase 3 leaching studies.

9. **Waste Loading:** Our results show that the optimum waste loading lies around 6 M sodium concentration (target), corresponding to 1.42 M corrected sodium concentration. This is based on the workability range in addition to the general performance of Cast Stone. From a ^{99}Tc leachability perspective, the Cast Stone performance was very good over the entire range of simulant concentrations and compositions studied. For Cast Stone prepared with the 6-M, 8-M, and 10-M simulants, the ^{99}Tc diffusivity increased with increasing simulant concentration, ranging from 1.4×10^{-11} to 3.9×10^{-11} to 1.4×10^{-10} cm^2/s, respectively from 14 to 63 days leaching. The S4 Cast Stone had a diffusivity of 6.5×10^{-13} cm^2/s over the same leaching period. These compare favorably with a target diffusivity of less than 1×10^{-9} cm^2/s. From a processing perspective, the stiffening and setting studies showed that, before the 6-M region (from Figures 7.6 and 7.8), the lower sloping region is about 300 minutes (6 hours). Beyond 6 M (from Figure 7.7), workability becomes a practical issue, probably providing less than an hour working time. Ideally, at least an hour of workability is needed to facilitate production. Adding a superplasticizer may also help to attain the workability window without lowering the waste loading.

10. **Waste Loading:** With ^{99}Tc diffusivities below 2×10^{-10} cm^2/s at an adjusted sodium concentration in the waste of 2 M, there is the potential to increase the sodium concentration above the currently demonstrated range to 3 M to 5 M for secondary waste blended with the dry materials without additional water. Testing at these concentrations will need to address both the leaching performance and the stiffening and setting behavior of the Cast Stone. These studies may include steps such as adding SPs or set retarders to improve the workability and reducing the pH of the waste stream to slow the hydration reactions.

9.0   References

ANSI—American National Standards Institute. 2003. *"Measurement of the Leachability of Solidified Low Level Radioactive Waste by a Short-Term Test Procedure."* In: Institute, A. N. S. (Ed.). American Nuclear Society, La Grange Park, Illinois.

ASTM International. 1998. *Direct Moisture Content Measurement of Wood and Wood-Base Materials.* ASTM D4442 – 07, West Conshohocken, Pennsylvania.

ASTM International. 2008a. *"ASTM Standard Specification for Coal Fly Ash and Raw or Calcined Natural Pozzolan for Use in Concrete* (C 618)." In: *Annual Book of ASTM Standards*, Vol. 04. 01, West Conshohocken, Pennsylvania.

ASTM C-191. 2008. *ASTM Test Method for Time of Setting of Hydraulic Cement by Vicat Needle.* ASTM International, West Conshohocken, Pennsylvania.

ASTM C-403. 2008. *ASTM Test Method for Time of Setting of Concrete Mixtures by Penetration Resistance.* ASTM International, West Conshohocken, Pennsylvania.

ASTM C-150. *ASTM Standard Specification for Portland Cement.* ASTM International, West Conshohocken, Pennsylvania.

Badogiannis E, Kakali G, Dimopoulou G, Chaniotakis E, Tivoli's S. 2005. "Metakaolin as a main cement exploitation of poor Greek kaolins." *Cement Concrete and Composite* 27:197–203.

Barnes HA. 1995. "A Review of the Slip (Wall Depletion) of Polymer Solutions, Emulsions and Particles Suspensions in Viscometers: Its Cause, Character, and Cure." *J. Non-Newtonian Fluid Mech.* 56:221–251.

Barnes HA and JO Carnali. 1990. "The Vane-in-Cup as a Novel Rheometer Geometry for Shear Thinning and Thixotropic Materials." *J. Rheology* 34:841–866.

Bergström L. 1997. "Hamaker Constants of Inorganic Materials." *Adv. Coll. Int. Sci.* 70:125–169.

Brown CF, KN Geiszler, and TS Vickerman. 2005. "Extraction and Quantitative Analysis of Iodine in Solid and Solution Matrixes." *Anal. Chem.* 77:7062–7066.

Brown CF, KN Geiszler, and MJ Lindberg. 2007. "Analysis of [129]I in groundwater samples: Direct and quantitative results below the drinking water standard." *Applied Geochemistry* 22:648–655.

Chen C-T. 2007. "Interactions between Portland cements and carboxylated and naphthalene-based superplasticizers." Ph.D. Dissertation, University of Illinois at Urbana-Champaign.

Christensen BJ, TO Mason, and HM Jennings. 1992. "Influence of Silica Fume on the Early Hydration of Portland Cements using Impedance Spectroscopy." *J. Am. Ceram.* 75(4):939–945.

Christensen BJ, RT Coverdale, RA Olson, SJ Ford, EJ Garboczi, HM Jennings, and TO Mason. 1994. "Impedance Spectroscopy of Hydrating Cement-Based Materials: Measurement, Interpretation, and Application." *J. Am. Ceram.* 77(11):2789–2804.

Chung C-W. 2004. "Effect of premature stiffening and its relationship to flow behavior of cement paste." MS thesis, Urbana (IL), University of Illinois at Urbana-Champaign.

Chung C-W. 2010. "Ultrasonic wave reflection measurements on stiffening and setting of cement paste." Ph.D. Dissertation, University of Illinois at Urbana-Champaign.

Chun J and DL Koch. 2005. "Coagulation of Monodisperse Aerosol Particles." *Phys. Fluids* 17:027102.

Chung C-W, JS Popovics, and LJ Struble. 2009. "Early Age Stiffening of Cement Paste Using Ultrasonic Wave Reflection." In: *Transition from Liquid to Solid: Re-examining the Behavior of Concrete at Early Ages*, ACI, Farmington Hills MI, *SP-259-1*, pp. 7–16.

Chung C-W, JS Popovics, and LJ Struble. 2010. "Using Ultrasonic Wave Reflection to Measure Solution Properties." *Ultrasonics Sonochemistry* 17:266–272.

Chung C-W, M Mroczek, I-Y Park, and LJ Struble. 2010. "On the evaluation of setting time of cement paste based on ASTM C403 penetration resistance test." *Journal of Testing and Evaluation* 38(5):527–533.

Clark BA, DG Atteridge, M Avila, VR Baca, KM Bishop, GA Cooke, LL Lockrem, RJ Lee, and MR Silsbee. 2005. "Development of a Cast Stone Formulation for Hanford Tank Wastes." Presented at the RemTech 2005 Symposium, Banff, Alberta, October 19-21, 2005. CH2M Hill, Richland, Washington. Available at: RPP-RPT-27297-FP (Full Paper).

Clark BA, LL Lockrem, GA Cooke, M Avila, R Westberg, MR Silsbee, and RJ Lee. 2006. "Hanford Site Cement-Based Waste Stream Solidification Studies." Presented at the *Cementitious Materials for Waste Treatment, Disposal, Remediation and Decommissioning Workshop*, December 12-14, 2006, Savannah River National Laboratory, Aiken, SC, CH2M Hill, Richland, Washington. Available at: RPP-31811-VA.

Cooke GA and LL Lockrem. 2005. *ETF Waste Stream Stabilization Testing*. RPP-RPT-26851, Rev. 0, CH2MHill, Richland, Washington.

Cooke GA, KM Bishop, and LL Lockrem. 2003. *Containerized Cast Stone Facility, Task 1 – Process Testing and Development Final Test Report*. Fluor Federal Services (entered into RMIS as: LL Lockrem, RPP-RPT-26742, 07-13-2005, *Hanford Containerized Cast Stone Facility Task - 1 Process Testing And Development Final Test Report*. Text thru Appendix E, and Appendix F thru Appendix J, CH2M Hill, Richland, Washington.

Cooke GA, LL Lockrem, M Avila, and RA Westberg. 2006a. *Effluent Treatment Facility Waste Stream Monolith Testing, Phase II*. RPP-RPT-31077, CH2M Hill, Richland, Washington.

Cooke GA, LL Lockrem, MD Guthrie, KJ Lueck, and M Avila. 2006b. *Development and Testing of a Cement-Based Solid Waste Form Using Synthetic UP-1 Groundwater*. CH2M Hill, Richland, Washington. Available at: RPP-RPT-31740.

Cooke G, LL Lockrem, M Avila, R Westberg, MR Silsbee, B Clark, MD Guthrie, GL Koci, and KJ Lueck. 2006c. "Cement Solidification of Ammonium Sulfate Rich Basin 42 Waste Water from the Hanford Effluent Treatment Facility." Presented at the Cementitious Materials for Waste Treatment,

Disposal, Remediation and Decommissioning Workshop, December 12-14, 2006, RPP-31803-VA, Savannah River National Laboratory, Aiken, South Carolina, CH2M Hill, Richland, Washington.

Cooke G, LL Lockrem, M Avila, R Westberg, MR Silsbee, GL Koci, MD Guthrie, and KJ Lueck. 2006d. "Radionuclide & Heavy Metal Waste Stream Stabilization Testing at The Hanford Site" (Abstract). RPP-31816-A, for presentation at the WM'07 33rd Waste Management Conference, Tucson, Arizona, February 25-March 01, 2007, CH2M Hill, Richland, Washington.

Cooke GA, JB Duncan, LMD Guthrie, and LL Lockrem. 2009. "Assessment of Pertechnetate Getters, Reductants and Stabilization." Presented at the DOE Technical Exchange, Denver, Colorado, Washington River Protection Solutions, LLC, Richland, Washington. Available at: RPP-41231-VA.

Coreno J, A Martinez, A Bolarin, and F Sanchez. 2001. "Apatite Nucleation on Silica Surface: A ζ Potential Approach." *J. Biomed. Mater. Res.* 57:119–125.

Diamond S. 1986. "Particle Morphology in Fly Ash." *Cement and Concrete Research* 16:569–579.

Dixon K, J Harbour, and M Phifer. 2008. *Hydraulic and Physical Properties of Saltstone Grouts and Vault Concretes*. SRNL-STI-2008-00421, Savannah River National Laboratory, Aiken, South Carolina.

Duncan JB and SP Burke. 2008. *Results of IONSIV® IE-95 Studies for the Removal of Radioactive Cesium from KE Basin Spent Nuclear Fuel Pool During Decommissioning Activities*. CH2M Hill, Richland, Washington. Available at: RPP-RPT-37055, Rev. 0. 6.6.

Duncan JB, GA Cooke, LL Lockrem, and MD Guthrie. 2008. *Assessment of Technetium Leachability in Cement-Stabilized Basin 43 Groundwater Brine.* RPP-RPT-39195. CH2M Hill Hanford Group, Inc., Richland, Washington.

Duncan JB, GA Cooke, and LL Lockrem. 2009. *Assessment of Technetium Leachability in Cement-Stabilized Basin 43 Groundwater Brine*. Washington River Protection Solutions, LLC, Richland, Washington. Available at: RPP-RPT-39195, Rev. 1).

Dunster AM, Parsonage JR, Thomas MJK. 1993. "The pozzolanic reaction of metakaolin and its effects on portland cement hydration." *Journal of Material Science* 28:1345–50.

EPA—U.S. Environmental Protection Agency. 1984. "Determination of Inorganic Anions." EPA Method 300.0A in *Test Method for the Determination of Inorganic Anions in Water by Ion Chromotography.* EPA-600/4-84-0 17, U.S. Environmental Protection Agency, Washington, D.C.

EPA. 1992. *Toxicity Characteristic Leaching Procedure*. EPA Method 1311, Revision 0, U.S. Environmental Protection Agency, Washington, D.C.

EPA. 1996. "Microwave Assisted Acid Digestion of Siliceous and Organically Based Matrices." EPA Method 3052 in *Test Method for Evaluating Solid Waste, Physical/Chemical Methods.* SW-846, U.S. Environmental Protection Agency, Washington, D.C.

EPA. 2000a. "Inductively Coupled Plasma-Atomic Emission Spectrometry." EPA Method 6010B in *Test Methods for Evaluating Solid Waste, Physical/Chemical Methods*. SW-846, U.S. Environmental

Protection Agency, Washington, D.C. Accessed September 20, 2008, at
http://www.epa.gov/epaoswer/hazwaste/test/sw846.htm.

EPA. 2000b. "Inductively Coupled Plasma-Mass Spectrometry." EPA Method 6020, in *Test Methods for Evaluating Solid Waste, Physical/Chemical Methods*. SW-846, U.S. Environmental Protection Agency, Washington, D.C. Accessed September 20, 2008, at
http://www.epa.gov/epaoswer/hazwaste/test/sw846.htm.

EPA. 2009a. "Leaching Test (Liquid-Solid Partitioning as a Function of Extract pH) of Constituents in Solid Materials Using a Parallel Batch Extraction Test." EPA Draft Method 1313, U.S. Environmental Protection Agency, Washington, D.C.

EPA. 2009b. "Mass Transfer Rates of Constituents in Monolith or Compacted Granular Materials Using a Semi-Dynamic Tank Leaching Test." EPA Draft Method 1315, U.S. Environmental Protection Agency, Washington, D.C.

EPA. 2009c. "Leaching Test (Liquid-Solid Partitioning as a Function of Liquid to Solid Ratio) of Constituents in Solid Materials Using a Parallel Batch Extraction Test." EPA Draft Method 1316, U.S. Environmental Protection Agency, Washington, D.C.

Ferraris CF, Guthrie W, Aviles AI, Peltz M, Haupt R, and MacDonald BS. 2006. "Certification of SRM 114q: Part II (Particle size distribution)," NIST Special Publication 260-166.

Flatt RJ. 2004. "Dispersion Forces in Cement Suspensions." *Cement and Concrete Res.* 34:399–408.

Harbour JR and AS Aloy. 2007. *International Program: Summary Report on the Properties of Cementitious Waste Forms*. WSRC-STI-2007-0056, Savannah River National Laboratory, Aiken, South Carolina.

Harbour JR and TB Edwards. 2009. *Performance Properties of Saltstone Produced Using SWPF Simulants*. SRNL-STI-00810, Savannah River National Laboratory, Aiken, South Carolina.

Harbour JR and VJ Williams. 2008. *Measurement of Waste Loading in Saltstone*. WSRC-STI-2008-00336, Savannah River National Laboratory, Aiken, South Carolina.

Harbour, JR, TB Edwards, TH Lorier, CA Langton, RC Moore, JL Krumhansl, C Holt, F Salas, and CA Sanchez. 2004. *Stabilizing Grout Compatibility Study*, WSRC-TR-2004-00021, Rev. 0, Savannah River National Laboratory, Aiken, South Carolina.

Harbour JR, EK Hansen, TB Edwards, VJ Williams, RE Eibling, DR Best, and DM Missimer. 2006. *Characterization of Slag, Fly Ash and Portland Cement for Saltstone*. WSRC-TR-2006-00067, Savannah River National Laboratory, Aiken, South Carolina.

Harbour JR, VJ Williams, and TB Edwards. 2007. *Heat of Hydration of Saltstone Mixes – Measurement by Isothermal Calorimetry*. WSRC-STI-2007-00263, Savannah River National Laboratory, Aiken, South Carolina.

Harbour JR, TB Edwards, and VJ Williams. 2009. *Impact of Time/Temperature Curing Conditions and Aluminate Concentrations on Saltstone Properties*. SRNL-STI-2009-00184, Savannah River National Laboratory, Aiken, South Carolina.

Hewlett PC. 1998. *Lea's Chemistry of Cement and Concrete*. Fourth Edition, Reed, Educational and Professional Publishing Ltd.

Jönsson B, H Wennerström, A Nonat, and B Cabane. 2004. "Onset of Cohesion in Cement Paste." *Langmuir* 20:6702–6709.

Jönsson B, A Nonat, C Labbez, B Cabane, and H Wennerström. 2005. "Controlling the Cohesion of Cement Paste." *Langmuir* 21:9211–9221.

Juenger MCG and HM Jennings. 2001. "The use of nitrogen adsorption to assess the microstructure of cement paste." *Cement and Concrete Research* 31:883–892.

Lei WG. 1995. "Rheological Studies and Percolation Modeling of Microstructure Development of Fresh Cement Paste." Ph.D. Dissertation, University of Illinois at Urbana-Champaign.

Lewis JA, H Matsuyama, G Kirby, S Morissette, and JF Young. 2000. "Polyelectrolyte Effects on the Rheological Properties of Concentrated Cement Suspensions." *J. Am. Ceram. Soc.* 83:1905–1913.

Lockrem LL. 2005. *Hanford Containerized Cast Stone Facility Task 1 - Process Testing and Development, Final Report*. RPP-RPT-26742, Rev. 0, Fluor Hanford, Richland, Washington.

Lockrem LL, GA Cooke, GL Troyer, and JL Person. 2003. *Cast Stone Technology for Treatment and Disposal of K Basin Sludge Demonstration Test Report*. RPP-19163 Rev. 0, CH2M Hill, Richland, Washington.

Lockrem LL, GA Cooke, BA Clark, and R Westburg. 2008. *Cast Stone Technology for Treatment & Disposal of Iodine Rich Caustic Waste Demonstration Final Report*. CH2M Hill, Richland, Washington (RPP-RPT-26725), Rev. 0-A.

Mann FM, RJ Puigh, R Khaleel, S Finfrock, BP McGrail, DH Bacon, and RJ Serne. 2003. *Risk assessment supporting the decision on the initial selection of supplemental ILAW technologies*. RPP-17675, Rev. 0; CH2M HILL Hanford Group Inc., Richland, Washington.

Matschei T, B Lothenbach, and FP Glasser. 2007. "The AFm phase in Portland cement." *Cement and Concrete Research* 37:118–130.

Mattigod SV, RJ Serne, and GE Fryxell. 2003. *Selection and Testing of "Getters" for Adsorption of Iodine-129 and Technetium-99: A Review*. PNNL-14208, Pacific Northwest National Laboratory, Richland, Washington.

Mehta PK and PJM Monteiro. 2006. *Concrete microstructure, properties, and materials*. 3rd edition, McGraw Hill.

Mindess S, JF Young, and D Darwin. 2003. *Concrete*, second edition, Prentice Hall.

NRC—U.S. Nuclear Regulatory Commission. 1991. *Technical Position on Waste Form, Rev. 1*. Final Waste Classification and Waste Form Technical Position Papers, NRC, Washington, DC.

Olson RA, PD Tennis, D Bonen, HM Jennings, TO Mason, BJ Christensen, AR Brough, GK Sun, and JF Young. 1997. "Early Containment of High-Alkaline Solution Simulating Low-Level Radioactive Waste in Blended Cement." *Journal of Hazardous Materials* 52:223–236.

Orebaugh EG. 1992. *DWPF Saltstone Study: Effects of Thermal History on Leach Index and Physical Integrity- Part II- Final Report*. WSRC-RP-92-568, Savannah River Site, Aiken, South Carolina.

Öztürk T, J Rapoport, JS Popovics, and SP Shah. 1999. "Monitoring the Setting and Hardening of Cement-Based Materials with Ultrasound." *Concrete Science and Engineering* 1:83~91.

Pierce EM, RJ Serne, W Um, SV Mattigod, JP Icenhower, NP Qafoku, JH Westsik, Jr., and RD Scheele. 2010. *Review of Potential Candidate Stabilization Technologies for Liquid and Solid Secondary Waste Streams*. PNNL-19122, Pacific Northwest National Laboratory, Richland, Washington.

Pierce EM, U Um, KJ Cantrell, MM Valenta, JH Westsik, Jr., RJ Serne, and KE Parker. 2010a. *Secondary Waste Form Screening Test Results—Cast Stone and Alkali Alumino-Silicate Geopolymer*. Draft report, Pacific Northwest National Laboratory, Richland, Washington.

Probstein RF. 1994. *Physicochemical Hydrodynamics*. 2nd Ed., John Wiley & Sons Inc.

Renaudin G, J-P Rapin, B Humbert, and M Francois. 2000. "Thermal Behavior of the nitrated AFm phase $Ca_4Al_2(OH)_{12}(NO_3)_2 \cdot 4H_2O$ and structure determination of the intermediate hydrate $Ca_4Al_2(OH)_{12}(NO_3)_2 \cdot 2H_2O$." *Cement and Concrete Research* 30:307–314.

Russel WB, DA Saville, and WR Schowalter. 1989. *Colloidal Dispersions*. Cambridge Univ. Press.

Russell RL, MJ Schweiger, JH Westsik, PR Hrma, DE Smith, AB Gallegos, MR Telander, and SG Pitman. 2006. *Low Temperature Waste Immobilization Testing*. Pacific Northwest National Laboratory, Richland, Washington.

Salas A, S Delvasto, RM Guaatierrez, and D Lange. 2009. "Comparison of two processes for treating rice husk ash for use in high performance concrete." *Cement and Concrete Research* 39:773-778.

Struble LJ, T-Y Kim, and H Zhang. 2001. "Setting of Cement and Concrete." *Cement, Concrete, and Aggregates*. 23(2):88–93.

Subramaniam KV, JJ Lee, and BV Christensen. 2005. "Monitoring the Setting Behavior of Cementitious Materials Using One-Sided Ultrasonic Measurements." *Cement and Concrete Research* 35:850–857.

Suzuki K, T Nichikawa, K Kato, H Hayashi, and S Ito. 1981. "Approach by Zeta-Potential Measurement on the Surface Charges of Hydrating C_3S." *Cement and Concrete Res.* 11:759–764.

Taylor HFW. 1997. *Cement Chemistry*, Academic Press, Thomas Telford edition.

Thomas NL and DD Double. 1981. "Calcium and Silicon Concentrations in Solution During the Early hydration of Portland Cement and Tricalcium Silicate." *Cement and Concrete Res.* 11:675–687.

WAC. 2000b. "Land Disposal Restrictions." WAC 173-303-140. *Washington State Administrative Code,* Olympia, Washington.

Young JF and W Hansen. 1987. "Volume Relationships for C-S-H Formation Based on Hydration Stoichiometries." *Mat. Res. Soc. Symp. Proc.* 85:313–321.

Yu W and SUS Choi. 2003. "The Role of Interfacial Layers in the Enhanced Thermal Conductivity of Nanofluids: a Renovated Maxwell Model," *J. Nanoparticle Res.* **5**, 167-171.

Zhang, H. 2001. Using Dynamic Rheology to Explore the Microstructure and Stiffening of Cementitious Mixtures. Ph.D. Dissertation, University of Illinois at Urbana Champaign.

Appendix A

**Additional Test Results from EPA Methods
1315, 1313, and 1316**

Appendix A: Additional Test Results from EPA Methods 1315, 1313, and 1316

The Concentration of Major Cations Measured in Leachate from Method 1313

Simulant	pH	Na µg/L	Ca µg/L	K µg/L	Al µg/L	Si µg/L	Mg µg/L	S µg/L	Fe µg/L
Simulant 1, 2 M	12.3	5.00E+05	3.40E+04	6.51E+04	1.57E+04	ND	ND	4.38E+04	ND
	12.9	5.18E+05	3.26E+04	6.44E+04	1.58E+04	ND	ND	4.63E+04	ND
	10.6	5.86E+05	3.20E+06	7.28E+04	2.05E+02	ND	1.29E+04	2.14E+05	ND
	9.56	5.93E+05	6.15E+06	6.00E+04	ND	ND	1.52E+05	4.86E+05	ND
	10.1	5.97E+05	4.57E+06	6.71E+04	ND	ND	5.60E+04	3.04E+05	ND
	7.81	6.36E+05	9.53E+06	5.89E+04	ND	ND	3.98E+05	6.35E+05	ND
	7.30	5.96E+05	8.64E+06	5.84E+04	ND	ND	3.90E+05	5.92E+05	ND
	5.34	6.77E+05	1.39E+07	8.73E+04	3.49E+02	3.25E+04	9.90E+05	5.47E+05	1.62E+05
	3.41	7.01E+05	1.51E+07	1.26E+05	9.74E+05	9.51E+04	1.19E+06	7.44E+05	4.05E+05
	4.14	6.78E+05	1.41E+07	1.10E+05	5.46E+04	4.04E+04	1.11E+06	6.01E+05	3.45E+05
Simulant 1, 4 M	12.4	8.07E+05	2.54E+04	5.77E+04	2.24E+04	1.40E+04	ND	9.30E+04	ND
	12.3	8.13E+05	2.40E+04	5.88E+04	2.33E+04	1.57E+04	ND	9.23E+04	ND
	9.00	9.87E+05	6.31E+06	5.66E+04	ND	ND	1.58E+05	4.96E+05	ND
	8.88	9.62E+05	6.31E+06	5.61E+04	ND	ND	1.68E+05	4.96E+05	ND
	7.55	9.75E+05	8.51E+06	5.67E+04	ND	3.68E+03	3.71E+05	6.27E+05	ND
	7.57	9.92E+05	8.54E+06	6.01E+04	ND	ND	3.85E+05	6.28E+05	ND
	5.23	1.05E+06	1.27E+07	9.03E+04	2.02E+02	2.93E+04	9.02E+05	5.84E+05	1.76E+05
	4.94	1.05E+06	1.27E+07	8.98E+04	4.11E+03	3.66E+04	9.09E+05	6.05E+05	1.80E+05
	4.01	1.07E+06	1.41E+07	1.10E+05	9.50E+04	5.39E+04	1.08E+06	5.65E+05	3.08E+05
	3.75	1.07E+06	1.40E+07	1.09E+05	2.44E+05	7.74E+04	1.06E+06	6.17E+05	2.92E+05
Simulant 1, 6 M	12.4	1.12E+06	2.15E+04	6.03E+04	3.00E+04	1.54E+04	ND	1.59E+05	ND
	12.3	1.10E+06	1.90E+04	5.51E+04	3.01E+04	1.69E+04	ND	1.53E+05	ND
	8.91	1.38E+06	6.29E+06	6.04E+04	ND	ND	1.83E+05	5.33E+05	ND
	8.78	1.38E+06	6.26E+06	6.19E+04	ND	ND	2.05E+05	5.11E+05	ND
	7.16	1.39E+06	8.57E+06	6.20E+04	ND	ND	3.87E+05	6.36E+05	ND
	7.51	1.40E+06	8.55E+06	6.42E+04	ND	ND	3.98E+05	6.40E+05	ND
	4.48	1.41E+06	1.24E+07	9.15E+04	1.61E+04	4.43E+04	8.78E+05	6.38E+05	2.16E+05
	4.96	1.48E+06	1.27E+07	9.44E+04	1.09E+03	3.25E+04	9.13E+05	5.40E+05	2.03E+05
	3.83	1.48E+06	1.40E+07	1.16E+05	1.82E+05	5.83E+04	1.05E+06	6.83E+05	3.12E+05
	3.98	1.51E+06	1.40E+07	1.14E+05	1.37E+05	6.60E+04	1.08E+06	5.19E+05	3.16E+05
Simulant 1, 8 M	12.4	1.60E+06	2.59E+04	6.31E+04	3.37E+04	ND	ND	3.44E+05	ND
	12.3	1.53E+06	2.47E+04	5.91E+04	3.55E+04	ND	ND	3.42E+05	ND
	8.68	1.93E+06	6.45E+06	6.23E+04	ND	ND	1.83E+05	6.20E+05	ND
	8.93	1.90E+06	6.34E+06	6.52E+04	ND	ND	1.90E+05	6.25E+05	ND
	7.14	1.94E+06	8.73E+06	6.72E+04	ND	ND	4.03E+05	6.99E+05	ND
	7.23	1.96E+06	8.76E+06	6.80E+04	ND	ND	4.13E+05	6.85E+05	ND
	5.55	1.94E+06	1.26E+07	9.27E+04	ND	1.98E+04	8.90E+05	4.58E+05	1.63E+05
	5.53	2.05E+06	1.31E+07	9.06E+04	ND	1.60E+04	9.01E+05	4.99E+05	1.44E+05
	4.04	2.05E+06	1.41E+07	1.16E+05	7.24E+04	4.29E+04	1.10E+06	4.88E+05	3.01E+05

The Concentration of Major Cations Measured in Leachate from Method 1313

Simulant	pH	Na µg/L	Ca µg/L	K µg/L	Al µg/L	Si µg/L	Mg µg/L	S µg/L	Fe µg/L
	4.35	2.10E+06	1.44E+07	1.15E+05	4.23E+04	4.07E+04	1.13E+06	4.70E+05	2.97E+05
Simulant 1, 10 M	12.4	1.72E+06	2.34E+04	6.20E+04	4.45E+04	ND	ND	3.82E+05	ND
	12.3	1.72E+06	2.07E+04	6.34E+04	4.54E+04	ND	ND	3.70E+05	ND
	8.64	2.14E+06	6.33E+06	6.66E+04	ND	ND	1.74E+05	6.06E+05	ND
	8.76	2.12E+06	6.23E+06	6.81E+04	ND	ND	1.98E+05	6.08E+05	ND
	7.26	2.23E+06	8.87E+06	6.94E+04	ND	ND	3.96E+05	6.67E+05	ND
	7.53	2.17E+06	8.57E+06	6.75E+04	ND	ND	4.03E+05	6.20E+05	ND
	4.92	2.24E+06	1.26E+07	1.03E+05	3.16E+03	2.63E+04	9.11E+05	4.41E+05	1.73E+05
	5.19	2.30E+06	1.26E+07	9.42E+04	ND	2.08E+04	9.03E+05	4.45E+05	1.49E+05
	3.62	2.43E+06	1.39E+07	1.25E+05	4.97E+05	7.70E+04	1.04E+06	6.25E+05	2.96E+05
	3.78	2.32E+06	1.36E+07	1.21E+05	2.86E+05	6.86E+04	1.06E+06	4.94E+05	2.80E+05
Simulant 2	12.3	5.16E+05	3.43E+04	6.15E+04	1.52E+04	ND	ND	7.07E+04	ND
	12.2	5.16E+05	2.96E+04	6.11E+04	1.63E+04	ND	ND	8.09E+04	ND
	9.09	6.16E+05	6.58E+06	5.62E+04	ND	ND	1.76E+05	4.58E+05	ND
	9.10	6.16E+05	6.47E+06	5.72E+04	ND	ND	1.95E+05	4.65E+05	ND
	7.53	6.34E+05	8.96E+06	5.98E+04	ND	ND	4.01E+05	5.97E+05	ND
	7.24	6.26E+05	9.05E+06	5.86E+04	ND	ND	4.18E+05	6.13E+05	ND
	5.12	6.54E+05	1.29E+07	8.32E+04	ND	4.08E+04	9.23E+05	5.59E+05	2.11E+05
	5.32	6.50E+05	1.26E+07	7.86E+04	ND	2.71E+04	8.98E+05	5.22E+05	1.89E+05
	3.70	6.94E+05	1.43E+07	1.06E+05	2.64E+05	1.04E+05	1.09E+06	5.73E+05	3.18E+05
	4.26	6.94E+05	1.46E+07	1.05E+05	4.63E+04	5.34E+04	1.14E+06	4.62E+05	3.36E+05
Simulant 3	12.1	4.74E+05	6.32E+04	3.86E+04	7.33E+03	ND	ND	1.18E+05	ND
	12.1	4.77E+05	6.28E+04	3.46E+04	7.87E+03	ND	ND	1.08E+05	ND
	7.74	6.22E+05	6.58E+06	4.86E+04	ND	ND	2.60E+05	5.96E+05	ND
	8.28	6.16E+05	6.47E+06	5.01E+04	ND	ND	2.73E+05	5.95E+05	ND
	6.52	6.23E+05	8.90E+06	5.52E+04	ND	ND	4.42E+05	6.92E+05	ND
	6.76	6.42E+05	8.75E+06	5.71E+04	ND	ND	4.56E+05	6.90E+05	ND
	5.83	6.89E+05	1.31E+07	7.94E+04	ND	2.39E+04	9.06E+05	5.25E+05	1.40E+05
	5.72	6.83E+05	1.31E+07	7.83E+04	ND	1.95E+04	9.11E+05	5.30E+05	1.26E+05
	5.19	7.11E+05	1.43E+07	9.32E+04	1.16E+03	4.02E+04	1.10E+06	4.80E+05	2.88E+05
	5.17	7.16E+05	1.48E+07	9.36E+04	ND	3.60E+04	1.12E+06	4.68E+05	2.61E+05
Simulant 4	12.2	5.78E+05	1.36E+05	8.67E+04	8.86E+03	ND	ND	ND	ND
	12.3	5.82E+05	1.28E+05	8.46E+04	9.57E+03	ND	ND	ND	ND
	9.14	6.88E+05	7.29E+06	7.39E+04	ND	ND	2.06E+05	5.02E+05	ND
	9.17	6.11E+05	6.57E+06	6.58E+04	ND	ND	1.93E+05	5.21E+05	ND
	7.74	6.63E+05	9.32E+06	7.39E+04	ND	ND	4.38E+05	6.69E+05	ND
	7.35	6.77E+05	9.58E+06	7.46E+04	ND	ND	4.54E+05	7.11E+05	ND
	5.94	6.93E+05	1.34E+07	9.54E+04	ND	2.67E+04	9.48E+05	4.86E+05	1.83E+05
	5.88	6.82E+05	1.33E+07	9.32E+04	ND	2.08E+04	9.34E+05	4.64E+05	1.59E+05
	4.25	6.95E+05	1.47E+07	1.16E+05	7.57E+04	7.33E+04	1.12E+06	4.43E+05	3.05E+05
	4.56	7.19E+05	1.48E+07	1.17E+05	1.84E+04	5.34E+04	1.14E+06	4.40E+05	3.15E+05

The Concentration of Major Cations Measured in Leachate from Method 1316

Simulant	LS Ratio (mL/g)	Na µg/L	Ca µg/L	K µg/L	Al µg/L	Si µg/L	Mg µg/L	S µg/L	Fe µg/L
Simulant 1, 2 M	2	1.78E+06	1.54E+04	2.00E+05	3.96E+04	1.96E+04	ND	1.72E+05	ND
	2	1.86E+06	1.65E+04	2.12E+05	4.11E+04	2.05E+04	ND	1.76E+05	ND
Simulant 1, 4 M	2	2.92E+06	1.41E+04	1.94E+05	4.91E+04	2.58E+04	ND	3.11E+05	ND
	2	2.88E+06	1.36E+04	1.91E+05	4.84E+04	2.56E+04	ND	2.99E+05	ND
Simulant 1, 6 M	2	4.11E+06	1.27E+04	2.01E+05	5.82E+04	2.66E+04	ND	5.05E+05	ND
	2	4.05E+06	1.19E+04	2.01E+05	5.92E+04	2.69E+04	ND	5.22E+05	ND
Simulant 1, 8 M	2	5.98E+06	1.64E+04	2.34E+05	5.66E+04	2.75E+04	ND	1.16E+06	4.12E+03
	2	6.07E+06	1.77E+04	2.39E+05	5.74E+04	2.84E+04	ND	1.16E+06	4.18E+03
Simulant 1, 10 M	2	6.74E+06	ND	2.51E+05	7.45E+04	2.68E+04	ND	1.23E+06	3.69E+03
	2	6.69E+06	ND	2.52E+05	7.60E+04	2.71E+04	ND	1.25E+06	3.69E+03
Simulant 2	2	1.79E+06	1.56E+04	1.84E+05	3.89E+04	2.28E+04	ND	2.76E+05	ND
	2	1.72E+06	1.29E+04	1.80E+05	3.77E+04	2.21E+04	ND	2.63E+05	ND
Simulant 3	2	1.79E+06	3.91E+04	1.09E+05	1.34E+04	1.82E+04	ND	3.86E+05	ND
	2	1.79E+06	3.88E+04	1.07E+05	1.35E+04	1.84E+04	ND	3.76E+05	ND
Simulant 4	2	2.53E+06	8.28E+04	3.44E+05	1.72E+04	ND	ND	ND	ND
	2	2.60E+06	8.51E+04	3.55E+05	1.73E+04	ND	ND	ND	ND
Simulant 1, 2 M	5	9.77E+05	2.37E+04	1.16E+05	2.40E+04	ND	ND	8.26E+04	ND
	5	9.26E+05	2.22E+04	1.12E+05	2.48E+04	ND	ND	8.10E+04	ND
Simulant 1, 4 M	5	1.48E+06	1.68E+04	1.04E+05	3.20E+04	1.85E+04	ND	1.52E+05	ND
	5	1.48E+06	1.74E+04	1.04E+05	3.19E+04	1.87E+04	ND	1.54E+05	ND
Simulant 1, 6 M	5	2.01E+06	1.39E+04	1.03E+05	3.99E+04	2.04E+04	ND	2.55E+05	ND
	5	2.06E+06	1.41E+04	1.04E+05	4.10E+04	2.04E+04	ND	2.52E+05	ND
Simulant 1, 8 M	5	2.88E+06	2.12E+04	1.11E+05	4.27E+04	1.81E+04	ND	5.51E+05	ND
	5	2.87E+06	2.09E+04	1.11E+05	4.29E+04	1.82E+04	ND	5.60E+05	ND
Simulant 1, 10 M	5	3.10E+06	1.53E+04	1.16E+05	5.73E+04	1.75E+04	ND	6.08E+05	ND
	5	3.17E+06	1.57E+04	1.15E+05	5.71E+04	1.76E+04	ND	6.02E+05	ND
Simulant 2	5	9.43E+05	2.23E+04	1.04E+05	2.30E+04	1.48E+04	ND	1.25E+05	ND
	5	9.06E+05	2.08E+04	9.99E+04	2.31E+04	1.52E+04	ND	1.22E+05	ND
Simulant 3	5	8.86E+05	5.13E+04	5.79E+04	9.46E+03	ND	ND	1.88E+05	ND
	5	8.94E+05	5.11E+04	5.93E+04	9.46E+03	ND	ND	1.87E+05	ND
Simulant 4	5	1.14E+06	1.15E+05	1.61E+05	1.15E+04	ND	ND	ND	ND
	5	1.13E+06	1.14E+05	1.62E+05	1.15E+04	ND	ND	ND	ND

Calculated Diffusivity and Leachability Index from EPA Method 1315

Waste Form	Cumulative Leaching Time (days)	I Diffusivity (cm^2/s)	LI	Tc Diffusivity (cm^2/s)	LI	Na Diffusivity (cm^2/s)	LI
Simulant 1, 2M	0.08	<3.87E-07	>6.4	1.12E-09	9.0	5.23E-09	8.3
	0.08	<3.79E-07	>6.4	2.96E-09	8.5	9.79E-09	8.0
	1	1.42E-07	6.8	2.59E-09	8.6	7.13E-09	8.1
	1	2.85E-07	6.5	4.06E-09	8.4	8.04E-09	8.1
	2	6.52E-08	7.2	1.82E-09	8.7	4.19E-09	8.4
	2	9.93E-08	7.0	1.88E-09	8.7	4.76E-09	8.3
	7	4.52E-08	7.3	1.97E-10	9.7	1.58E-09	8.8
	7	5.26E-08	7.3	7.10E-11	10.1	1.75E-09	8.8
	14	<3.40E-06	>5.5	<1.27E-11	>10.9	7.75E-10	9.1
	14	<3.33E-06	>5.5	<1.24E-11	>10.9	7.65E-10	9.1
	28	<1.34E-08	>7.9	<6.30E-12	>11.2	3.17E-10	9.5
	28	1.62E-08	7.8	<6.17E-12	>11.2	3.64E-10	9.4
	42	<2.26E-08	>7.6	<1.06E-11	>11.0	2.29E-10	9.6
	42	<2.21E-08	>7.7	<1.04E-11	>11.0	2.59E-10	9.6
	49	<3.01E-08	>7.5	<5.63E-11	>10.2	1.98E-10	9.7
	49	<2.95E-08	>7.5	<5.52E-11	>10.3	2.25E-10	9.6
	63	<9.17E-09	>8.0	<1.72E-11	>10.8	1.44E-10	9.8
	63	<8.98E-09	>8.0	<1.68E-11	>10.8	1.45E-10	9.8
Simulant 1, 4M	0.08	1.04E-07	7.0	2.80E-09	8.6	1.07E-08	8.0
	0.08	<9.67E-08	>7.0	2.46E-09	8.6	9.12E-09	8.0
	1	1.58E-07	6.8	7.38E-09	8.1	1.42E-08	7.8
	1	1.62E-07	6.8	6.27E-09	8.2	1.57E-08	7.8
	2	7.24E-08	7.1	5.04E-09	8.3	1.01E-08	8.0
	2	6.43E-08	7.2	3.85E-09	8.4	9.99E-09	8.0
	7	2.85E-08	7.5	5.17E-10	9.3	3.07E-09	8.5
	7	2.56E-08	7.6	4.23E-10	9.4	2.92E-09	8.5
	14	<8.79E-07	>6.1	4.26E-12	11.4	1.42E-09	8.8
	14	<8.49E-07	>6.1	7.76E-12	11.1	1.37E-09	8.9
	28	7.52E-09	8.1	5.98E-12	11.2	6.04E-10	9.2
	28	5.94E-09	8.2	6.42E-12	11.2	5.96E-10	9.2
	42	<5.85E-09	>8.2	3.69E-12	11.4	4.10E-10	9.4
	42	<5.65E-09	>8.2	4.17E-12	11.4	4.06E-10	9.4
	49	<7.78E-09	>8.1	<1.47E-11	>10.8	3.70E-10	9.4
	49	<7.51E-09	>8.1	<1.42E-11	>10.8	3.51E-10	9.5
	63	<2.37E-09	>8.6	<4.47E-12	>11.3	2.33E-10	9.6
	63	<2.29E-09	>8.6	<4.32E-12	>11.4	2.26E-10	9.6
Simulant 1, 6M	0.08	2.42E-07	6.6	1.51E-08	7.8	2.36E-08	7.6
	0.08	1.18E-07	6.9	8.43E-09	8.1	1.54E-08	7.8
	1	2.39E-07	6.6	1.96E-08	7.7	3.28E-08	7.5
	1	2.96E-07	6.5	2.27E-08	7.6	3.76E-08	7.4
	2	1.14E-07	6.9	8.18E-09	8.1	2.29E-08	7.6
	2	2.04E-07	6.7	1.11E-08	8.0	2.86E-08	7.5
	7	3.73E-08	7.4	7.96E-10	9.1	6.74E-09	8.2
	7	5.86E-08	7.2	1.65E-09	8.8	1.08E-08	8.0
	14	<4.05E-07	>6.4	2.83E-11	10.5	2.64E-09	8.6
	14	<3.90E-07	>6.4	2.76E-11	10.6	3.18E-09	8.5

Calculated Diffusivity and Leachability Index from EPA Method 1315

Waste Form	Cumulative Leaching Time (days)	I Diffusivity (cm²/s)	LI	Tc Diffusivity (cm²/s)	LI	Na Diffusivity (cm²/s)	LI
	28	4.21E-09	8.4	1.54E-11	10.8	8.59E-10	9.1
	28	5.99E-09	8.2	1.46E-11	10.8	1.17E-09	8.9
	42	<2.70E-09	>8.6	1.14E-11	10.9	5.80E-10	9.2
	42	<2.60E-09	>8.6	1.46E-11	10.8	6.81E-10	9.2
	49	<3.59E-09	>8.4	8.77E-12	11.1	5.57E-10	9.3
	49	<3.45E-09	>8.5	7.51E-12	11.1	6.71E-10	9.2
	63	<1.09E-09	>9.0	8.11E-12	11.1	2.94E-10	9.5
	63	<1.05E-09	>9.0	6.59E-12	11.2	3.20E-10	9.5
Simulant 1, 8M	0.08	2.51E-07	6.6	6.04E-09	8.2	5.66E-08	7.2
	0.08	3.91E-07	6.4	9.33E-09	8.0	6.11E-08	7.2
	1	1.45E-07	6.8	3.88E-09	8.4	2.92E-08	7.5
	1	1.43E-07	6.8	4.55E-09	8.3	3.10E-08	7.5
	2	8.04E-08	7.1	1.55E-09	8.8	1.76E-08	7.8
	2	5.94E-08	7.2	1.48E-09	8.8	1.68E-08	7.8
	7	1.32E-08	7.9	1.03E-10	10.0	4.70E-09	8.3
	7	9.69E-09	8.0	8.41E-11	10.1	3.34E-09	8.5
	14	<2.15E-07	>6.7	4.53E-11	10.3	1.88E-09	8.7
	14	<2.08E-07	>6.7	5.55E-11	10.3	2.26E-09	8.6
	28	<8.50E-10	>9.1	3.81E-11	10.4	8.10E-10	9.1
	28	1.52E-09	8.8	4.26E-11	10.4	9.30E-10	9.0
	42	<1.43E-09	>8.8	3.98E-11	10.4	5.99E-10	9.2
	42	<1.38E-09	>8.9	3.84E-11	10.4	6.88E-10	9.2
	49	<1.90E-09	>8.7	3.41E-11	10.5	5.46E-10	9.3
	49	<1.84E-09	>8.7	2.76E-11	10.6	5.34E-10	9.3
	63	<5.80E-10	>9.2	3.38E-11	10.5	3.36E-10	9.5
	63	<5.62E-10	>9.3	3.30E-11	10.5	3.75E-10	9.4
Simulant 1, 10M	0.08	6.29E-07	6.2	2.02E-08	7.7	9.11E-08	7.0
	0.08	7.79E-07	6.1	2.70E-08	7.6	1.16E-07	6.9
	1	3.10E-07	6.5	7.52E-09	8.1	4.86E-08	7.3
	1	2.65E-07	6.6	8.66E-09	8.1	4.79E-08	7.3
	2	8.69E-08	7.1	2.53E-09	8.6	3.27E-08	7.5
	2	6.98E-08	7.2	2.20E-09	8.7	3.19E-08	7.5
	7	1.27E-08	7.9	2.86E-10	9.5	6.01E-09	8.2
	7	1.46E-08	7.8	3.50E-10	9.5	7.39E-09	8.1
	14	<1.69E-07	>6.8	1.94E-10	9.7	3.06E-09	8.5
	14	<1.64E-07	>6.8	2.00E-10	9.7	3.16E-09	8.5
	28	<6.68E-10	>9.2	1.35E-10	9.9	1.34E-09	8.9
	28	<6.51E-10	>9.2	1.51E-10	9.8	1.36E-09	8.9
	42	1.38E-09	8.9	1.26E-10	9.9	8.99E-10	9.0
	42	1.47E-09	8.8	8.94E-11	10.0	7.24E-10	9.1
	49	<1.49E-09	>8.8	1.28E-10	9.9	9.10E-10	9.0
	49	<1.46E-09	>8.8	1.30E-10	9.9	8.67E-10	9.1
	63	<4.56E-10	>9.3	9.86E-11	10.0	5.13E-10	9.3
	63	<4.44E-10	>9.4	1.14E-10	9.9	5.04E-10	9.3
Simulant 2	0.08	<3.92E-07	>6.4	1.05E-09	9.0	9.27E-09	8.0
	0.08	<3.90E-07	>6.4	1.19E-09	8.9	8.74E-09	8.1
	1	3.14E-08	7.5	1.90E-09	8.7	5.11E-09	8.3

Calculated Diffusivity and Leachability Index from EPA Method 1315

Waste Form	Cumulative Leaching Time (days)	I Diffusivity (cm^2/s)	LI	Tc Diffusivity (cm^2/s)	LI	Na Diffusivity (cm^2/s)	LI
	1	4.89E-08	7.3	2.05E-09	8.7	5.76E-09	8.2
	2	<4.77E-08	>7.3	1.33E-09	8.9	3.01E-09	8.5
	2	<4.73E-08	>7.3	1.39E-09	8.9	3.37E-09	8.5
	7	<5.46E-09	>8.3	4.68E-11	10.3	7.31E-10	9.1
	7	6.75E-09	8.2	8.23E-11	10.1	1.11E-09	9.0
	14	<3.44E-06	>5.5	<1.28E-11	>10.9	4.64E-10	9.3
	14	<3.42E-06	>5.5	<1.27E-11	>10.9	4.77E-10	9.3
	28	<1.36E-08	>7.9	<6.37E-12	>11.2	2.17E-10	9.7
	28	<1.35E-08	>7.9	<6.33E-12	>11.2	2.09E-10	9.7
	42	<2.29E-08	>7.6	<1.07E-11	>11.0	1.42E-10	9.8
	42	<2.28E-08	>7.6	<1.06E-11	>11.0	1.48E-10	9.8
	49	<3.05E-08	>7.5	<5.70E-11	>10.2	1.27E-10	9.9
	49	<3.03E-08	>7.5	<5.66E-11	>10.2	1.17E-10	9.9
	63	<9.30E-09	>8.0	<1.74E-11	>10.8	8.66E-11	10.1
	63	<9.23E-09	>8.0	<1.73E-11	>10.8	8.58E-11	10.1
	0.08	4.21E-07	6.4	8.32E-09	8.1	9.71E-09	8.0
	0.08	<3.81E-07	>6.4	5.26E-09	8.3	1.05E-08	8.0
	1	1.12E-07	7.0	8.23E-09	8.1	4.64E-09	8.3
	1	9.27E-08	7.0	6.18E-09	8.2	4.70E-09	8.3
	2	<4.72E-08	>7.3	3.40E-09	8.5	2.65E-09	8.6
	2	<4.63E-08	>7.3	2.29E-09	8.6	2.31E-09	8.6
	7	1.58E-08	7.8	5.36E-11	10.3	8.10E-10	9.1
	7	2.16E-08	7.7	4.23E-11	10.4	1.07E-09	9.0
Simulant 3	14	<3.42E-06	>5.5	<1.28E-11	>10.9	4.01E-10	9.4
	14	<3.35E-06	>5.5	<1.26E-11	>10.9	4.05E-10	9.4
	28	<1.35E-08	>7.9	1.58E-11	10.8	1.79E-10	9.7
	28	<1.32E-08	>7.9	6.45E-12	11.2	1.97E-10	9.7
	42	1.22E-07	6.9	2.09E-11	10.7	1.18E-10	9.9
	42	1.52E-07	6.8	1.17E-11	10.9	1.31E-10	9.9
	49	<3.02E-08	>7.5	<5.70E-11	>10.2	9.13E-11	10.0
	49	<2.96E-08	>7.5	<5.58E-11	>10.3	1.05E-10	10.0
	63	<9.22E-09	>8.0	<1.74E-11	>10.8	6.46E-11	10.2
	63	<9.05E-09	>8.0	<1.70E-11	>10.8	6.44E-11	10.2
	0.08	1.43E-08	7.8	1.27E-10	9.9	8.40E-09	8.1
	0.08	1.23E-08	7.9	9.66E-11	10.0	8.81E-09	8.1
	1	8.06E-09	8.1	2.56E-10	9.6	3.79E-09	8.4
	1	7.33E-09	8.1	1.80E-10	9.7	3.55E-09	8.5
	2	1.15E-08	7.9	1.68E-11	10.8	1.90E-09	8.7
	2	6.60E-09	8.2	1.12E-11	11.0	1.93E-09	8.7
Simulant 4	7	1.23E-09	8.9	2.45E-12	11.6	6.36E-10	9.2
	7	1.38E-09	8.9	2.36E-12	11.6	6.85E-10	9.2
	14	<1.02E-08	>8.0	1.27E-12	11.9	2.61E-10	9.6
	14	<1.02E-08	>8.0	1.00E-12	12.0	2.48E-10	9.6
	28	1.64E-10	9.8	6.67E-13	12.2	1.23E-10	9.9
	28	1.02E-10	10.0	5.50E-13	12.3	1.20E-10	9.9
	42	7.41E-10	9.1	5.55E-13	12.3	8.60E-11	10.1
	42	7.25E-10	9.1	4.40E-13	12.4	8.10E-11	10.1

A.6

Calculated Diffusivity and Leachability Index from EPA Method 1315

Waste Form	Cumulative Leaching Time (days)	I Diffusivity (cm²/s)	LI	Tc Diffusivity (cm²/s)	LI	Na Diffusivity (cm²/s)	LI
	49	<9.06E-11	>10.0	5.48E-13	12.3	7.40E-11	10.1
	49	<9.07E-11	>10.0	5.17E-13	12.3	7.61E-11	10.1
	63	5.33E-11	10.3	5.43E-13	12.3	5.23E-11	10.3
	63	4.78E-11	10.3	4.39E-13	12.4	4.98E-11	10.3
ND indicates "not detected" below quantification level. Because of low concentration of spiked I, leaching percentage of Iodide was calculated based on the instrumental MDL. For ND values, sample MDL was used to calculate diffusivity (in table with <).							

Appendix B

Simple Scaling and Interaction Model for Cast Stone Rheology

Appendix B: Simple Scaling and Interaction Model for Cast Stone Rheology

A simple scaling and interaction model (based on a pair of particles) of a pure cement slurry at an early stage is described here. While the major components of the Cast Stone are fly ash (typically ~45 wt%) and slag (typically ~47 wt%), the focus is on a pure cement slurry because 1) it is a reasonably well-defined material (note that the physical properties [e.g., size] of fly ash and slag vary with their processing conditions) and 2) it is the major component involved in the hydration reactions that lead to the hardened Cast Stone. This simplification can allow us to provide a simple and qualitative model as an initial framework, whereas more details would be needed for a complicated and extensive model. The proposed model provides characteristics of particle flocculation at the early stage of hydration as a function of parameters such as particle size, particle density, and shear rate. Stated in other terms, the model provides a tool to understand the nature of the hydration process as a function of particle interactions.

This model envisions that the cement slurry at an early stage of hydration is a dense suspension, and all the cement particles are surrounded by an aqueous medium (i.e., water). Taking w/c (water to cement ratio) = 0.4 (equivalently, 71 wt% cement particles) as a typical condition, one can calculate that the cement particles represent 0.44 of the volume fraction of cement slurry, φ, with the density of cement (3.15 g/cm^3) and water (1.0 g/cm^3) via the following equation:

$$\varphi = \frac{x\left(\dfrac{\rho_l}{\rho_s}\right)}{1 + x\left[\left(\dfrac{\rho_l}{\rho_s}\right) - 1\right]}$$

(B.1)

where x is a weight fraction of cement, ρ_l is the density of liquid (i.e., water), and ρ_s is the density of the solid (i.e., cement). An average separation between particles can be scaled as $a\phi^{-1/3}$ where a is the particle radius. Using d$_{50}$ (the 50th percentile diameter) of cement particles (~15 µm) obtained from particle-size analysis in Section 3.3, we can see that the average separation between particles is about 10 µm, which is comparable to the radius of median cement particles (~7.5 µm). Typically, colloidal interactions, such as repulsive electrostatic and attractive van der Waals interactions, become effective when particles are separated by distances around and below the mean particle radius as is the case for the Cast Stone. Therefore, colloidal interactions between cement particles are assumed to be important even at the beginning of the hydration process when the w/c = 0.4 or 71 wt% cement.

Focusing on the pair-interaction, simple, conceptual model to obtain a qualitative understanding of the dynamics of particles, one can calculate a typical flocculation time between two particles based on the following second-order rate description for flocculation:

$$-\frac{dn}{dt} = k_f n^2$$

(B.2)

where n is the number density of individual particles, and k_f is a flocculation rate coefficient (Chun and Koch 2005). Implementing appropriate scalings with the assumption that colloidal and hydrodynamic particle interactions are negligible, one can obtain typical flocculation times due to Brownian motion (t_B), shear (t_S) and gravity (t_G):

$$ t_B \sim \frac{6\pi\mu}{kTn} \; ; \; t_S \sim \frac{1}{\dot{\gamma}a^3 n} \; ; \; t_G \sim \frac{9\mu}{2a^4(\rho_s - \rho_l)gn} \tag{B.3} $$

where k, T, and μ denote the Boltzmann constant, temperature (Kelvin), and viscosity of the medium, respectively. Here g represents the gravitational constant, and $\dot{\gamma}$ is an applied shear rate. These scaling relationships can be used to obtain a flocculation time by a driving force (e.g., Brownian motion, shear, and gravity) as a function of physicochemical parameters. For example, using typical conditions (i.e., w/c=0.4 and $\dot{\gamma}$ =20 sec^{-1}) along with d$_{50}$ ~ 15 μm (a = 7.5 μm), one obtains that t_B ~ 5 hours, but t_S and t_G are less than one second, which clearly indicates that the w/c=0.4 condition will possibly be an unstable condition (flocculated from the beginning) by shear and gravity.

While the above scaling analysis would be appropriate for estimating the flocculation time to within an order of magnitude and for predicting the qualitative stability of a slurry, one must account for particle interactions to obtain semi-quantitative information on stability, especially with ongoing hydration. The Derjaguin-Landau-Verwey-Overbeek (DLVO) theory provides a useful and simple way to understand the interactions between cement particles. Applying the DLVO theory to cement particles implies that a cement particle at any situation can be modeled as a uniformly charged, rigid colloid with known dielectric properties. This appears to be reasonable based on previous studies (Lewis et al. 2000, Flat 2004). Therefore, we used the DLVO theory as another simple model to understand the interactions between cement particles during the early stage of hydration and to correlate changes in rheological properties.

Although different constituents, C$_3$S, C$_2$S, C$_3$A, and C$_4$AF, are known to exist in cement, and C$_3$S particles are a major ingredient in Portland cement (Mindess et al. 2003, Hewlett 1998, Taylor 1997). After mixing with water, C$_3$S particles begin to dissolve, and the surface of C$_3$S particles becomes negatively charged (Suzuki et al. 1981). As the hydration proceeds, Ca^{2+}, OH$^-$, and silicate ions are produced, and their concentrations increase with time. As a result, a very thin protective layer (most likely C-S-H [calcium-silicate-hydrate] layer) is initially formed on the surface of the C$_3$S particles (Taylor 1997). Note that concentrations of Ca^{2+} and OH$^-$ are much higher than that of silicate ions, so the concentration of silicate ions can be relatively negligible (Thomas and Double 1981). As the pH rises and the Ca^{2+} concentration exceeds the solubility limit, the precipitation of C-S-H vigorously takes place on the existing C$_3$S particles (with a very thin layer of C-S-H) and forms an appreciably thicker layer of C-S-H. This is often related to the initial setting of the cement paste. After setting, more dissolution of C$_3$S particles occurs, and another layer of C-S-H forms on the C$_3$S particles, but concentrations of Ca^{2+} and OH$^-$ are increasing very slowly (Thomas and Double 1981). Time scales of the overall process are dependent on w/c.

To explore changes in the particle interaction during the early stage of hydration, we examine particle interactions at four representative stages over time: 1) the very initial stage ($t=t_0=0$) where the concentration of ions in the fluid is considered very low, 2) a time when the fluid is close to the solubility limit for Ca^{2+}, but no appreciable C-S-H layer has formed ($t=t_1$), 3) the time when an appreciable C-S-H

layer starts to form on the C₃S particles ($t=t_2$), and 4) a time when a thicker C-S-H layer forms on the C₃S particles ($t=t_3$) as the hydration proceeds. Note that one can assume a "core (C₃S)-shell (C-S-H layer)" structure of the particle at both $t=t_2$ and $t=t_3$ based on previous studies on cement hydration (Jönsson et al. 2005). Following the DLVO theory (Russel et al. 1989), the interactions between two spherical particles in the case of a small Debye screening length (which is true for our case) are represented by a sum (V_total) of the following two interaction potentials:

$$V_\text{D} = 2\pi\varepsilon\varepsilon_0 a\psi^2 \ln(1 + \exp(-\kappa as))$$
(B.4)

$$V_\text{vdw} = -\frac{A}{6}\left[\frac{2}{s(s+4)} + \frac{2}{(s+2)^2} + \ln\left(\frac{s(s+4)}{(s+2)^2}\right)\right],$$
(B.5)

where V_D and V_vdw = electrostatic and van der Waals interaction potentials, respectively

ε_0 = permittivity of the vacuum

ε = dielectric constant of water (=79)

ψ = surface potential of the particle

A = Hamaker constant between particles in aqueous medium

κ^{-1} = Debye screening length.

Additionally, the normalized minimum separation s between two particles is defined as H/a, where H is the dimensional separation between the particles. Note that the expression for V_D is obtained using constant potential conditions with the Deryaguin approximation because any approximate formula for V_D based on the constant surface charge conditions is not relevant for small separations under large κa (i.e., $\kappa a > 2$). Note that the ε of the simulants will be different from that of water used in this simple model. The current model lays the foundation for understanding hydrating particles. The model can be appropriately modified for complex simulants.

To calculate the interaction between two particles using the DLVO model, one needs physicochemical parameters such as the Hamaker constant, the surface potential of a particle, and ionic strength, as well as particle size. We postulate that the surface potential of a C₃S particle is mainly determined by that of SiO₂ because SiO₂ provides the main charge-carrying groups in this calcium oxide-silica compound. Then, the surface potential of a C₃S particle at $t=t_0$ would be about -30 mV based on the zeta potential measurement of SiO₂ (Coreno et al. 2001), which is supported by the previous zeta potential measurement (~ -25 mV) of a C₃S particle (Suzuki et al. 1981). At $t=t_1$, [Ca²⁺] ≤ 20 mM and the C-S-H layer are not formed yet, which implies that the zeta potential of a C₃S particle simply becomes negligible because of the increase in Ca²⁺ concentration upon hydration. Previous studies show that the zeta potential is negligible (~ 0 ± 2 mV) in this situation (Suzuki et al. 1981, Lewis et al. 2000, Zhang 2001). Because of the structure, the surface potential of the core (C₃S)-shell (C-S-H layer) particle can be estimated from the sole contribution of C-S-H; the surface charge density of C-S-H is approximately 0.4 C/m² at pH~12 (Jönsson et al. 2005). The surface potential can be obtained from the surface charge density in the case of $\kappa a > 0.5$ at any ψ as follows:

$$q = \frac{\varepsilon \varepsilon_0 kT}{ez} \kappa \left[2\sinh\left(\frac{ez\psi}{2kT}\right) + \frac{4}{\kappa a} \tanh\left(\frac{ez\psi}{4kT}\right) \right]$$

(B.6)

where e is the magnitude of charge on an electron ($=1.6 \times 10^{-19}$ C), and z is the valence of ion (2 in our case due to the Ca^{2+} ion). Because the $[Ca^{2+}] \sim 20$ mM and the $[OH^-] \sim 40$ mM are in the solution after forming the C-S-H, owing to the solubility limit, the Debye screening length is about 1.3 nm, which gives rise to $\kappa a = 428$. Using these values, one obtains $\psi \sim -100$ mV for the core (C_3S)-shell (C-S-H layer) particle at $t=t_2$. As hydration proceeds, the C-S-H layer becomes thicker. Since there are abundant Ca^{2+} ions in solution during hydration, it has been shown that Ca^{2+} ions bind chemically to the C-S-H layer, and the surface potential of the core (C_3S)-shell (C-S-H layer) particle reverses (i.e., changes from negative to positive). The Ca^{2+} binding and surface charge reversal is supported by the zeta potential measurements (Suzuki et al. 1981). Therefore, at $t=t_3$, we assume that $\psi \sim 100$ mV from the previous zeta potential measurements during hydration, but $[Ca^{2+}] \sim 20$ mM and $[OH^-] \sim 40$ mM in the solution.

The dielectric properties (ε) of particles at different times are crucial in obtaining van der Waals interaction through the Hamaker constant. To obtain the dielectric property of a C_3S particle, we assumed that the C_3S particle is a homogenous mixture of $CaCO_3$ (calcite) and SiO_2 (quartz) (with ¾ and ¼ fractions) whose dielectric properties over the frequency range covering the optical to ultraviolet range of the electromagnetic spectrum can be calculated from the damping oscillator models shown elsewhere (Bergström 1997):

$$\varepsilon_{C_3S}(i\xi_n) \approx (3/4)\varepsilon_{CaCO_3}(i\xi_n) + (1/4)\varepsilon_{SiO_2(quartz)}(i\xi_n)$$

(B.7)

where $i = \sqrt{-1}$ and $\xi_n = 4\pi^2 nkT/h$ ($n=0,1,2,\ldots$). Here h is the Planck's constant. Using the dielectric property of water (ε_w) available elsewhere (Russel et al. 1989), we obtain the Hamaker constant (nonretarded) to represent an aqueous C_3S particle suspension by:

$$A_{C_3S-C_3S} = \frac{3}{2}kT\sum_{n=0}^{\infty}{}' \left(\frac{\varepsilon_w(i\xi_n) - \varepsilon_{C_3S}(i\xi_n)}{\varepsilon_w(i\xi_n) + \varepsilon_{C_3S}(i\xi_n)} \right)^2$$

(B.8)

where the prime in the summation indicates that the $n=0$ term is multiplied by $^1/_2$. Our calculation shows $A_{C_3S-C_3S} = 1.74\times10^{-20}$ J, which is close to the 1.68×10^{-20} J used in previous studies (Lewis et al. 2000, Zhang 2001). Considering the approximations and uncertainties in the measurement of key variables in Equation B.8, our calculated value for the Hamaker constant is fairly reasonable, which supports our assumptions. For the core (C_3S)-shell (C-S-H layer) particle, the structure of the particle needs to be taken into account. Using the analogous result for the diffusion problem for "core-shell" structure particles (Yu and Choi 2003), one can estimate the dielectric property for the core-shell particle as

$$\varepsilon_{core-shell}(i\xi_n) = \frac{\left(2(1-\gamma) + (1+\hat{\beta})^3(1+2\gamma)\right)\gamma}{-(1-\gamma) + (1+\hat{\beta})^3(1+2\gamma)}\varepsilon_{C_3S}(i\xi_n)$$

(B.9)

B.4

where $\varepsilon_{\text{core-shell}}$ is the dielectric function of the core-shell particle, which mimics the C-S-H layered C_3S particle, γ is the ratio of the dielectric property of the shell (C-S-H) to core (C_3S) and is given by $\varepsilon_{\text{C-S-H}} / \varepsilon_{C_3S}$, and $\hat{\beta}$ denotes the ratio of shell thickness to the core C_3S radius. We assume that the radius of the core-shell particle is approximately the same as that of the C_3S particle (i.e., 7.5 µm) over time while the shell becomes thicker. Estimating the dielectric property of $\varepsilon_{\text{C-S-H}}$ is based on a reasonable ratio of CaO: SiO_2: H_2O. A previous study (Young and Hansen 1987) showed that the ratio can be 1.7:1:4=CaO: SiO_2: H_2O in the C-S-H gel. Similar to the dielectric property of a C_3S particle, it is assumed that the C-S-H layer is a homogenous mixture of $CaCO_3$ (calcite), SiO_2 (fused silica), and water with a 1.7:1:4 ratio. From the known dielectric properties for the three components at an entire frequency electromagnetic radiation by the material, one obtains:

$$\varepsilon_{\text{C-S-H}}(i\xi_n) \approx (1.7/6.7)\varepsilon_{CaCO_3}(i\xi_n) + (1/6.7)\varepsilon_{SiO_2\text{(fused silica)}}(i\xi_n) + (4/6.7)\varepsilon_w(i\xi_n) \quad \text{(B.10)}$$

Note that the dielectric property of fused silica is used for the C-S-H whereas the dielectric property of quartz is used for the C_3S particle based on previous studies (Bergström 1997, Ferraris et al. 2006). The Hamaker constant to represent an aqueous core (C_3S)-shell (C-S-H layer) particle suspension can be obtained similarly to that for an aqueous C_3S particle suspension. Our choices for the values for key parameters follow: $\hat{\beta}$ =0.5 (used for $t=t_2$) and $\hat{\beta}$ =1.0 (used for $t=t_3$) give rise to 5.39×10^{-21} J and 3.46×10^{-21} J as the Hamaker constant for the C_3S core and the C-S-H shell portions of the particles, respectively.

Figure B.1 shows the calculated total interactions between two particles at four representative times of hydration ($t=t_0$, t_1, t_2, and t_3). Note that we assume that the concentration of ions at $t=t_0$ is very low (~ 0.1 mM) so that the Debye screening length is about 17.5 nm. As shown in Figure B.1, the cement suspension is initially very stable (highly repulsive potential at H/a ~10^{-2}) at $t=t_0$ but becomes unstable (highly attractive potential starting at H/a ~10^{-2}) because of hydration at $t=t_1$. Hydration produces Ca^{2+} ions in solution, which shields the surface charges of the C_3S particle. But as soon as the C-S-H layer forms on the C_3S particle, the interaction potential becomes less attractive at a moderate separation and repulsive at a small separation (at $t=t_2$). This strongly suggests that the formation of the C-S-H reduces the flocculation of the particles during this stage of hydration. This change originated from the decrease of the Hamaker constant, a measure of attractive van der Waals interaction, as well as the significant increase in the surface charges of the C-S-H. The decrease in the Hamaker constant is due to the change in the dielectric property of the particle (from the sole C_3S to the core [C_3S]-shell [C-S-H layer]). At $t=t_3$, further hydration produces more Ca^{2+} ions, and the charge reversal takes place (Jönsson et al. 2004, Jönsson et al. 2005). More importantly, as the C-S-H layer becomes thicker, the Hamaker constant becomes smaller, which is a major factor in being more repulsive at $t=t_3$ because the Debye length does not change significantly with a very slow increase in Ca^{2+} ions in the solution. Figure B.1 indicates that the tendency for flocculation of particles becomes less as hydration proceeds. Because the flocculation of particles is directly connected to the rheological properties of the cement, it can be deduced that the rheological properties may change very significantly at the beginning of hydration, but further changes become moderate as hydration proceeds.

While a simple and qualitative model based on pure cement slurry is presented in this section as an initial framework, some insights on our system can be obtained. The simple scaling suggested that the w/c=0.4 condition with pure cement slurry corresponds to an unstable slurry (i.e., flocculated by shear

and gravity from the beginning). Slag has a similar particle-size distribution and the 50th percentile diameter to cement, but the density of slag (~ 2.4 g/cm^3) is less than that of cement. Therefore, the volume fraction of Cast Stone slurry with the same w/c would be higher than that of cement slurry, which indicates that the Cast Stone would be a more unstable slurry at the beginning as to physical factors (i.e., without considering a chemical reactivity factor). The interaction the model based on two cement particles (Figure B.1) shows a close connection between the hydration and rheological properties (through changes in particle interactions) over time; the tendency for flocculation of particles becomes less as hydration proceeds. Because the flocculation of particles is directly connected to the rheological properties of the cement, it can be deduced that the rheological properties may change very significantly at the beginning of hydration, but further changes become moderate as hydration proceeds. For the Cast Stone, the connection is still valid, but the hydration would be less prominent for Cast Stone since cement (considered as a major component for hydration reaction) is only ~ 8 wt%.

In slurries and suspensions with small particles (typically d ~ 10 μm or less), colloidal interactions dominate the interactions between particles. Thus, the colloidal interactions dictate the rheological behavior of such slurries and suspensions as stated above. However, noncolloidal interactions (e.g., hydrodynamic interactions) become more important controls on the rheological properties as the particle size increases. The balance between colloidal and hydrodynamic forces can be estimated by two dimensionless numbers: the shear-repulsion number (N_{SR}) and the shear- attraction number (N_{SA}):

$$N_{SR} = \frac{\mu a^2 \dot{\gamma}}{\varepsilon \zeta^2} \; ; N_{SA} = \frac{\mu a^3 \dot{\gamma}}{A} \tag{B.11}$$

where ε_w, ζ, and μ denote the dielectric permittivity of the suspending medium (i.e., water), the zeta potential of the particle, and the viscosity of the medium, respectively, and the other symbols are as previously defined (Probstein 1994). Note that $N_{SR} << O(1)$ and $N_{SA} << O(1)$ imply that colloidal forces dominate over hydrodynamic forces and vice versa. While N_{SR} and N_{SA} scales as a^2 and a^3, implying that the role of colloidal interactions become rapidly negligible as the particle size increases, it really depends on the order of magnitude of electrostatic and van der Waals forces, i.e., $\varepsilon \zeta^2$ and A/a. In other words, larger particles can still play a role in the colloidal interactions as ζ and A increase.
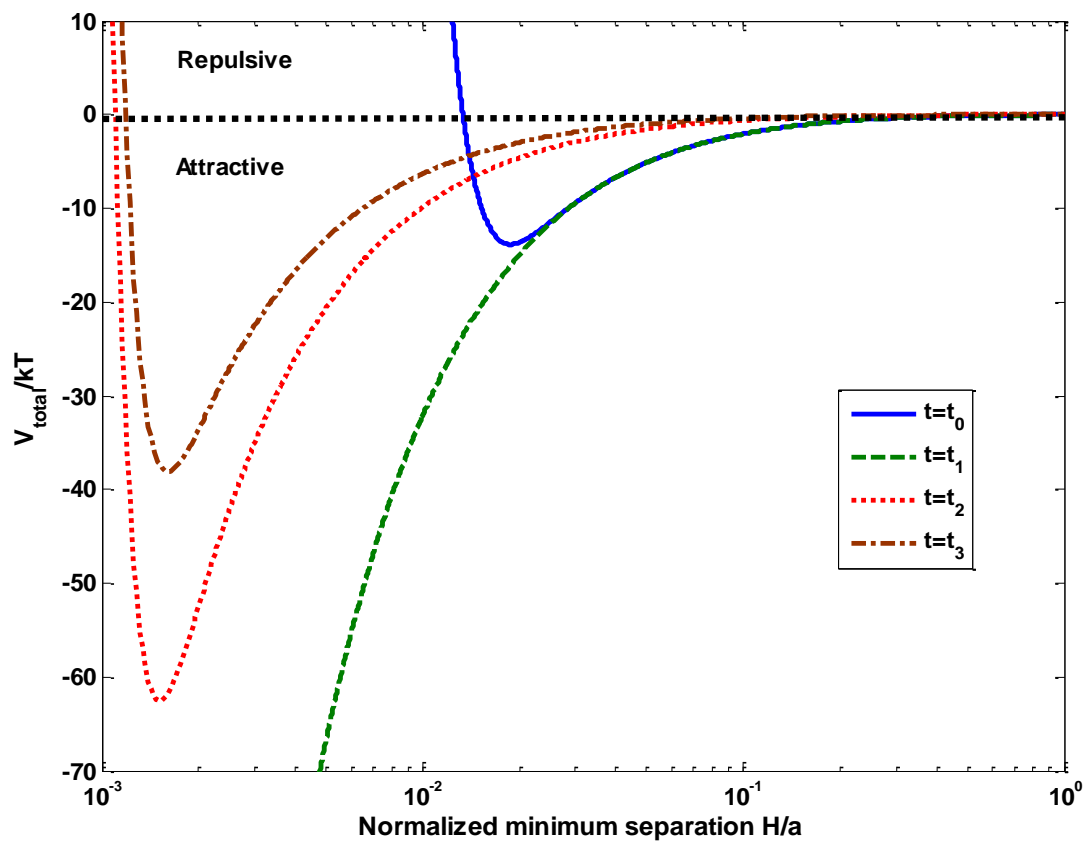
Figure B.1. Total Interactions Between Particles at Four Representative Times of Hydration ($t=t_0$, t_1, t_2, and t_3). See the text for detailed physical descriptions on four representative times.

Distribution

3   Civil & Environmental Engineering
Vanderbilt University
2301 Vanderbilt Place
Nashville, TN   37235-1831
     D. Kosson
     KG Brown
     AC Garrabrants

5   Savannah River National Laboratory
P.O. Box 616
Aiken, SC 29802
     D Kaplan
     G Flash
     J Harbour
     C Jantzen
     C Langton

1   SK Sundaram
Kazuo Inamori School of Engineering
The New York State College of Ceramics at Alfred University
2 Pine Street
Alfred, NY 14802

1   EM Pierce
Building 1505, MS 6038
Oak Ridge National Laboratory
P.O. Box 2008
Oak Ridge, TN 37831-6038

1   PC Suggs
Savannah River Operations Office
US Department of Energy
P. O. Box A
Aiken, SC 29802

6   U.S. Department of Energy

BM Mauss	H6-60
J Morse	A5-11
RD Hildebrand	A6-38
RW Lober	H6-60
DOE Public Reading Room (2)	

2   CH2MHill Plateau Remediation Company

LL Lehman	H8-51
MI Wood	H8-51

4   Washington River Protection Solutions

K Colosi	E6-20
T May	E6-20
MA Melvin	E6-30
KE Smith	E6-30

20   Pacific Northwest National Laboratory

PR Bredt	K6-50
CA Burns	P7-25
KJ Cantrell	K6-81
J Chun	K6-24
C-W Chung	K6-24
ML Kimura	K6-28
SV Mattigod	K3-62
KE Parker	K3-62
LM Peurrung	K9-09
SG Pitman	J4-55
N Qafoku	P7-54
RJ Serne	K6-81
MB Triplett	H6-61
MM Valenta	P7-54
W Um	P7-54
JH Westsik, Jr (5)	K7-15